



Department of Precision and Microsystems Engineering

ADVANCING IN-NOZZLE C-FRTP 3D PRINTING:  
Experimental Insights into Melt Impregnation Dynamics and  
Interface Adhesion Through Meso-Level FDM Printing

Danny de Grijff

Report no : 2024.008  
Supervisor : Dr. ir. J.F.L. Goosen  
Specialisation : Mechatronic System Design  
Type of report : Master Thesis  
Date : 29 January 2024

# Advancing In-Nozzle C-FRTP 3D Printing

Experimental Insights into Melt Impregnation  
Dynamics and Interface Adhesion through  
Meso-Level FDM printing

by

D. de Grijff

to obtain the degree of Master of Science  
at the Delft University of Technology,  
to be defended publicly on Monday January 29, 2024 at 10:00 AM.

Student number: 4384989  
Project duration: May 1, 2023 – January 29, 2024  
Thesis committee: Dr. ir. J.F.L. Goosen, TU Delft, supervisor  
Dr. ir. M. Tichem, TU Delft  
Dr. P. Fanzio, TU Delft

An electronic version of this thesis is available at <http://repository.tudelft.nl/>.

# Preface

”Hereby, I would like to present my Master Thesis, which I have worked on for the past year. My interest in 3D Printing has prompted me to start researching this engineering field. As a 3D printing hobbyist and mechatronics enthusiast, I own a desktop format FDM Printer and enjoy the process of 3d modeling and self-manufacturing functional parts. As I am experiencing the benefits of additive manufacturing technology, I am convinced that additive manufacturing will play an important role in the future of smart manufacturing.

Back in 2015, the executive chairman of the World Economic Forum (WEF), K. Schwab, first introduced the term fourth industrial revolution (: industry 4.0) to a broader audience in an article (Schwab, 2015) published by Foreign Affairs magazine. In this article, Schwab stated that society is on the brink of a technological revolution, subsequently changing industry and society. The essence of this so-called Fourth Industrial Revolution is the autonomation of production chains and the intensified data exchange between cyber and physical systems. However, additive manufacturing has many technological advantages for the manufacturing industry, such as the manufacturability of greater geometric complexity. The main motive for K. Schwab to label Additive Manufacturing as the vital ingredient for implementing Smart Manufacturing is the significant waste reduction and energy savings compared to other production technologies. However, it also has massive challenges before fully implementing this relatively new production technology and outperforming traditional manufacturing technologies. One of these challenges includes searching for more robust and lightweight materials with complex geometries. This opened up an entirely new section within additive manufacturing, namely multi-material additive manufacturing.

Special thanks go out to Dr. ir. J.F.L. (Hans) Goosen for providing feedback and supervising me throughout my research. The PME Lab supports employees in lab training, resources, and time.”

*D. de Grijff*  
*Delft, January 2024*

# Abstract

The ever-growing demand for high-performance materials and more functional 3D printing has raised tremendous interest in advancing Multi-Material Additive Manufacturing (MMAM). Developing C-FRTP 3D printing through FDM Technology opens new scalable FRP solutions. These components possess exceptional properties such as specific strength, recyclability, impact/chemical resistance, and geometrical complexity. Researchers have successfully exploited FDM technology to print C-FRTP composites but lack high interface bonding between the reinforcing fibers and thermoplastic polymer matrix. Moreover, C-FRTP is limited to weak frictional forces and mechanical interlocking. Besides, porosities are observed at the interface, which results in overall mechanical weakness.

Various Meso-level C-FRTP 3D printing methods and print heads have been developed and standardized, but more knowledge is needed of essential 'In-Nozzle' C-FRTP impregnation dynamics. During In-Nozzle impregnation, solid-dry fiber and molten Thermoplastic polymer matrix bond inside the print head before extrusion. This master thesis explores the challenges and potential solutions by conceptualizing a functional 'In-Nozzle' impregnation extruder capable of extruding proper C-FRTP composites using FDM printing.

Initially, a theoretical framework is presented on melt impregnation dynamics and Interface adhesion, followed by experiments as validation. Based on the melt impregnation analysis observations, a limited permeability of Thermoplastic polymer melt is observed. These are primarily from the high viscosity of the thermoplastic materials (PLA) and the dense fibers. Applying an overflow of melt with extensive external pressure achieves a smoother and faster melt flow around the interface. Tensile strength experiments underscored the dependency on the exposure time and encapsulation of fibers by matrix and showed an increase in IFSS compared to the neat thermoplastic polymer. Further research is recommended to augment contact surfaces between fibers and the matrix. This research highlights the current challenges and lays the foundation for future advancements in C-FRTP 3D printing through in-nozzle impregnation, offering insights into improving material compatibility, impregnation quality, and interfacial bonding.

# Contents

<b>Preface</b>	<b>i</b>
<b>Abstract</b>	<b>ii</b>
<b>Abbreviations</b>	<b>vi</b>
<b>1 Introduction</b>	<b>1</b>
1.1 Background . . . . .	1
1.2 Applications . . . . .	2
<b>2 State of the art</b>	<b>4</b>
2.1 C-FRP Composites . . . . .	4
2.1.1 Fabrication methods . . . . .	4
2.1.2 End product . . . . .	5
2.2 Additive manufacturing . . . . .	6
2.2.1 Multi Material Additive Manufacturing . . . . .	6
2.3 FDM Printing . . . . .	6
2.3.1 Printing process . . . . .	8
2.3.2 Printhead mechanics . . . . .	8
2.3.3 Printing parameters . . . . .	10
2.4 C-FRTP 3D Printing . . . . .	13
2.4.1 Pre-impregnation: Embedding in TP filament . . . . .	13
2.4.2 Ex-Nozzle impregnation: Embedding in the model . . . . .	14
2.4.3 In-Nozzle Impregnation: Embedding in the printhead . . . . .	14
2.5 “In-nozzle” Impregnation printhead designs . . . . .	15
2.5.1 Shared entrance . . . . .	15
2.5.2 Separate entrance . . . . .	15
2.5.3 Central fiber feed . . . . .	15
2.5.4 State of the art: 2022 CFP-500 . . . . .	16
2.6 Materials . . . . .	16
2.6.1 Thermoplastic polymers . . . . .	16
2.6.2 Continuous Fibers . . . . .	17
2.7 Research objective . . . . .	19
<b>3 Initiating C-FRTP Printing Experiments</b>	<b>21</b>
3.1 Research methodology . . . . .	21
3.1.1 Theoretical examination . . . . .	21
3.1.2 Microscopic analysis of melt impregnation . . . . .	21
3.1.3 Interfacial shear strength study . . . . .	22
3.1.4 Data evaluation and feasibility analysis . . . . .	22
3.2 Development of experiment setup . . . . .	22
3.2.1 Sample development . . . . .	22
3.2.2 Static mold design . . . . .	23
3.2.3 PID temperature controller . . . . .	23
3.2.4 Experiment procedure . . . . .	24

3.3	Material selection . . . . .	24
3.3.1	TP Matrix: PolyLactic Acid (PLA) . . . . .	25
3.3.2	Reinforcement Fiber: PAN-based CF . . . . .	25
<b>4</b>	<b>Melt impregnation</b> . . . . .	<b>27</b>
4.1	Melt impregnation process . . . . .	27
4.1.1	Melt flow dynamics . . . . .	27
4.1.2	CF Melt impregnation . . . . .	28
4.1.3	C-CFTP composite deposition . . . . .	28
4.2	Melt impregnation theory . . . . .	28
4.3	Experimental setup . . . . .	30
4.3.1	Static Setup . . . . .	30
4.3.2	Pressurized configuration . . . . .	30
4.4	Microscopic results . . . . .	32
<b>5</b>	<b>Interfacial shear strength</b> . . . . .	<b>37</b>
5.1	Modified rule of mixture . . . . .	37
5.2	Adhesion engineering . . . . .	37
5.3	Experimental Methodology . . . . .	39
5.3.1	Experiment 1: Single pull-through test . . . . .	40
5.3.2	Experiment 2: Dual pull-through test . . . . .	40
5.3.3	Experiment 3: Modified dual pull-through test . . . . .	41
5.4	Analysing stress-strain curves . . . . .	41
5.4.1	Polymer stress-strain curves . . . . .	41
5.4.2	Pull out debonding . . . . .	42
5.5	Test results . . . . .	42
5.5.1	Exposed Carbon Fiber . . . . .	43
5.5.2	Neat thermoplastic polymer . . . . .	43
5.5.3	Experiment 1: single pull-through test . . . . .	44
5.5.4	Experiment 2: Dual pull through . . . . .	44
5.5.5	Experiment 3: The modified dual pull-through test . . . . .	45
5.5.6	IFSS v Exposure Times . . . . .	45
<b>6</b>	<b>Discussion</b> . . . . .	<b>47</b>
6.1	Methodology . . . . .	47
6.2	Data evaluation . . . . .	47
6.2.1	Limited melt impregnation . . . . .	47
6.2.2	Reinforced thermoplastics . . . . .	48
6.2.3	In nozzle pressure advantage . . . . .	48
6.3	Design improvements . . . . .	49
6.3.1	Modifying nozzle shapes . . . . .	49
6.3.2	Adjusting fiber packing . . . . .	50
6.3.3	Pre-impregnation of fiber bundle . . . . .	50
<b>7</b>	<b>Recommendations</b> . . . . .	<b>51</b>
<b>8</b>	<b>Conclusion</b> . . . . .	<b>53</b>
	<b>References</b> . . . . .	<b>55</b>
<b>A</b>	<b>Tables and figures</b> . . . . .	<b>60</b>
A.1	Schematic representation of different AM technologies . . . . .	60
A.2	Overview of available thermoplastic polymers . . . . .	61

---

A.3	Thermoplastic Polymer rheology analysis . . . . .	62
A.4	Fiber selection criteria . . . . .	63
A.5	C-CF catalogue from supplier . . . . .	64
<b>B</b>	<b>Technical drawings and fabrication steps</b>	<b>65</b>
B.1	Technical drawing sample designs . . . . .	65
B.1.1	Experiment 1 & melt impregnation . . . . .	65
B.1.2	Experiment 2 . . . . .	66
B.1.3	Experiment 3 . . . . .	66
B.2	Step-by-step sample fabrication . . . . .	67
B.3	Step-by-step pressurized experiment . . . . .	68
B.4	Keyence© VHX-6000 Digital microscope . . . . .	69
B.5	Tensile testbench . . . . .	70
<b>C</b>	<b>Results</b>	<b>71</b>
C.1	Interfacial shear strength analysis . . . . .	71
C.1.1	Single fiber tensile test results . . . . .	71
C.1.2	Neat thermoplastic tensile test results . . . . .	72
C.1.3	C-FRTP tensile test results (Experiment 1) . . . . .	73
C.1.4	C-FRTP tensile test results (Experiment 2) . . . . .	73
C.1.5	C-FRTP tensile test results (Experiment 3) . . . . .	74

# Abbreviations

Here, an overview of all abbreviations used in this report is presented in alphabetical order:

<b>AM</b>	Additive manufacturing
<b>ASTM</b>	American Society for Testing and Materials
<b>CF</b>	Carbon Fiber
<b>C-FRP</b>	Continuous Fiber Reinforced Polymer
<b>C-(C)FRTP</b>	Continuous (Carbon) Fiber Reinforced Thermoplastic Polymer
<b>FDM</b>	Fused Deposition Modeling
<b>FRP</b>	Fiber Reinforced Polymer
<b>IFSS</b>	Interfacial Shear Strength
<b>ISO</b>	International Organization for Standardization
<b>IPA</b>	Isopropyl alcohol
<b>ME</b>	Material extrusion
<b>MJ</b>	Material Jetting
<b>MMAM</b>	Multi Material Additive Manufacturing
<b>MST</b>	Maximum Service Temperature
<b>PLA</b>	Poly Lactic Acid
<b>S-FRTP</b>	Short Fiber Reinforced Thermoplastic Polymer
<b>TP</b>	Thermoplastic polymer



# 1

## Introduction

### 1.1. Background

Over the years, researchers have found a significant increase in specific strength by melt-impregnating high-performance (long) continuous fibers with polymers. These kinds of meso-level composites are already widely adopted by various engineering industries such as the aerospace, military, sports, and automotive industries [27]. Continuous Fiber Reinforced Polymers (C-FRP) fabrication starts with the manufacturer laying out large woven mats of high performance fiber fabric in a specially made mold. A polymer resin, Thermoset, is then added together with a crosslinking agent to cure and harden the compound. Therefore, the orientation of the fiber is essential since the fiber only supports tensile loads over the longitudinal direction of the fibers. An optimal structural strength is obtained by layering the fiber mats with varying orientations.

The ever-growing demand for high-performance materials and more functional 3D printing has raised tremendous interest in using additive manufacturing (AM) technologies to advance Multi-Material Additive Manufacturing (MMAM). Such developments could facilitate the creation of macro-level structures with enhanced specific strength, reduced production costs, waste reduction, and greater geometrical complexity. In addition, material extrusion AM technology allows for precise control over fiber orientation and makes C-FRP fabrication scalable.

The adaptability of AM material extrusion technology, fused deposition modeling (FDM), as a highly versatile additive manufacturing process, has proven the most potential for Meso-level multi-material 3D printing. Although AM technology has been around for quite some time, use was minimal due to the expiration of many patents in 2009 Kabir, Mathur, and Seyam [22]. In the last decade, FDM has benefited from affordability, accessibility, and open-source knowledge. In the past decade, FDM has become increasingly well-known in the industry for its easy-to-use character, inexpensive machinery, and wide variety of printable thermoplastics and composites. FDM can be utilized for Multi-Material Additive Manufacturing (MMAM) applications. Although FDM 3D Printing is limited to thermoplastics, there are advantages compared to currently used thermoset polymers. Thermoplastic materials are recyclable, ductile, and impact & chemical resistant. Researchers try to improve the mechanical characteristics of the composition using FDM technology by exploring various fabrication strategies such as Short Fiber Reinforcement (S-FRTP), Continuous Fiber Reinforced polymer (C-FRTP), Powder Addition Reinforcement, Vibration-Assisted FDM, and annealing [38]. However, the development of C-FRP increases, as can be seen in Figure 1.1 [9]. According to Fedor Antonov, CEO of Anisoprint, C-FRTPs can have up to 30 times more strength than neat thermoplastics [43].

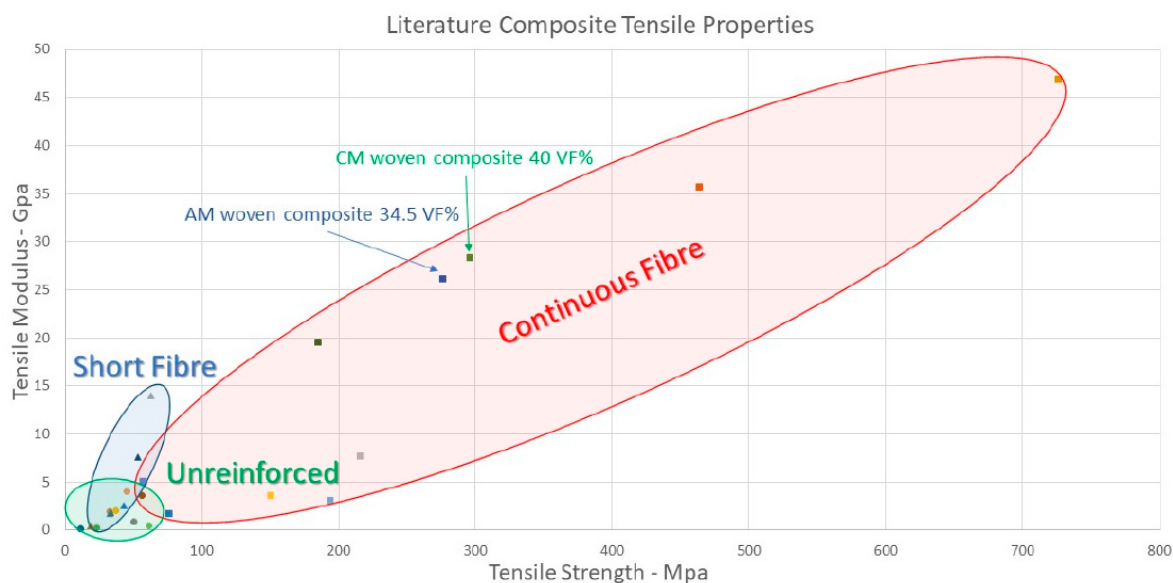


**Figure 1.1:** Bubble chart highlighting similar PA66/CF composites fabricated using AM or Compression moulding (CM), adapted from [9].

The development of C-FRTP AM fabrication methods opens up new scalable FRP solutions to fabricate high-performance components. These components possess exceptional properties such as specific strength-to-weight, recyclability, impact/chemical resistance, and geometrical complexity. This triggers academic researchers and the industry by reducing production costs and providing greater precision, accuracy, and the capability to control the fiber orientation in components. Moreover, this method is scalable and can be implemented in the electrical and semiconductor industries.

## 1.2. Applications

### Parts reduction for electrical components

The electrical conductivity of Carbon Fiber (CF), in combination with scalability and controlled fiber orientation, makes it possible to lay tiny traces of conductive wire through printed components. Pushing the limits in terms of scaling and reducing production costs by reducing assembly time.

### Wind energy, Aerospace, Automotive industries

C-FRTPs are commonly applied to multiple industries. The relatively high strength-to-weight ratio makes them reasonably applicable for the blades of large wind turbines, the body of an airplane, and automotive vehicles. However, these parts are fabricated from FRP using epoxy resins, which are not recyclable and end up in substantial waste piles. Thermoplastics solve this issue.

### Protective gear

C-FRTP composites also demonstrated impressive results when subjected to impact tests compared to C-FRP composites using epoxy resins. For example, Protective face guards manufactured with C-FRTP composites were thinner and lighter than conventional Protective face guards while maintaining adequate shock absorption ability. This enables more complex and stronger components [55]

**ATALANTA; THE ROBOT FLY**

The final noteworthy application involves scalability and controlled fiber orientation within Meso-level FDM printing technology. Discussions with Professor Goosen (TU Delft) highlighted an application: the creation of miniature membrane wings resembling insect-like structures for a resonating (high frequency  $\tilde{g}$ ) flapping wing micro-air vehicle. A key challenge in this scenario is reinforcing these membrane wings with lightweight material, as current thermoplastics struggle to withstand the necessary tensile forces. The high tensile resistance and low weight of C-FRTP composites could provide a reliable solution to this problem.

# 2

## State of the art

In this chapter, a literature survey that investigates the state of the art of C-FRTP 3D printing is presented. This includes current FRP production methods, developments in the field of C-FRTP printing, and limitations in heading forward. Eventually, this leads to the research question.

### 2.1. C-FRP Composites

Numerous industries have revolutionized the integration of high-performance fibers in polymeric materials. These excellent mechanical properties of high-performance Fibers are due to the Incredibly strong interaction on atomic level [17]. The combination of excellent tensile strength and the ability to manufacture it precisely and lightweight makes fiber composites a precious asset for the industry. Much research has already found a considerable increase in strength and stiffness in meso-level compositions. These compositions are made from polymeric materials reinforced with high-performance fibers, such as fiberglass, CF, and aramid fiber [18]. Compositions containing high-performance fibers are already widely used in various engineering industries, such as aviation and automotive. Embedding high-tensile strength CFs in thermoset or thermoplastics polymer significantly increases strength-over-weight (specific strength), corrosion resistance, chemical resistance, high fatigue strength, and impact resistance. Moreover, by applying thermoplastics instead of thermosets, recyclability can be added to the list of more robust, lightweight, and more durable engineering properties. Fiber-reinforced polymers (FRP) are three times stronger than aluminium and 40% lighter depending on the composition.

#### 2.1.1. Fabrication methods

Three commonly used methods for fabricating C-FRP compounds are schematically shown in Figure 2.1.

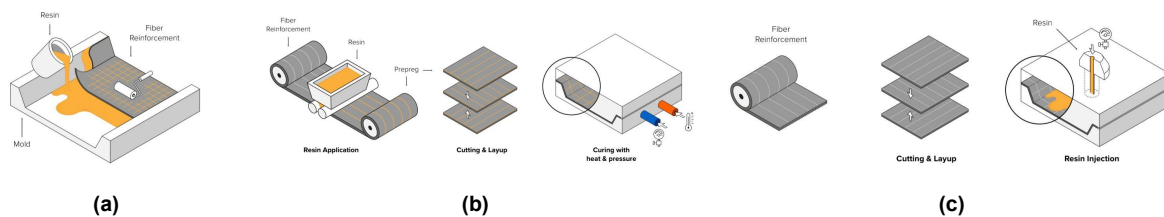


**Figure 2.1:** Schematic overview of three commonly used C-FRP composite fabrication methods: (a) Wet layup, (b) Prepreg lamination, and (c) Resin transfer molding. Adapted from [18]

In general, the fabrication of C-FRP composites consists of a set of crucial fabrication steps. Below is a step-by-step overview of this fabrication process [18].

1. Design generations and mold preparation. In this step, the object is designed using CAD software. A mold, typically made from Aluminium, is prepared when finished.
2. Pre-preg material selection. Sheets of fiber (Prepreg material) are chosen based on specific requirements. Prepreg material consists of fibers pre-impregnated with epoxy. After it is stored at a cool temperature to prevent curing. Commonly used fibers are Aramid Fiber, Fiberglass, and CF.
3. The layering phase. Woven CF sheets are cut into desired shapes and carefully stacked by laying sheets inside the prepared mold. The orientation of the sheets must be carefully picked since this influences the mechanical properties.
4. Vacuum bagging. Once the layering phase is complete, the mold is placed in a vacuum bag to compress the laminate. Apply pressure and ensure tight packing on the mold so air bubbles are removed. This is done until the epoxy resin is cured. The clamp pressure of the vacuum bag is the difference between the atmospheric pressure  $P_{atm}$  (101.4 kPa = 1.014 bar ) and the envelope pressure  $P_{env}$  ranging between the minimum required 84.7 kPa (0.847 bar) [20] and 41.4 kPa (0.414 bar) [54]. The last value may vary depending on the available vacuum bags. The minimum clamping pressure required by the atmosphere  $\Delta P=16$  kPa.
5. Autoclave curing. The assembled CF stacking is placed in an autoclave. This apparatus comprises a high-pressure and high-temperature chamber that subjects the mold to a specifically controlled heat and pressure cycle profile. The epoxy interfacing the fiber sheets is then cured.
6. Cooling and post-curing. The mold is now cooled inside the autoclave to prevent thermal stresses.
7. Demolding and Finishing. The cured CF composition is removed from the vacuum bag and mold. Excess material is trimmed. The process ends with quality control and strength testing. After the successful completion of quality checks, the end product is ready.

### 2.1.2. End product

In Figure 2.2, three pictures of C-FRP end product using CF as reinforcement and Epoxy resin (matrix) are shown. The researchers cut a cross-section of a 250×130×3.8mm sheet; This exposed the CF laminates with the epoxy resin surrounding it. This composite was made using 12 plies of 3k CF thread woven in a cross-shaped pattern, having a density of  $0.200\text{kgm}^{-3}$  and a thickness of 0.25 mm. The matrix comprised commercial epoxy resin 1050 and hardener 1056. The material's fiber volume fraction was determined to be 48% [31].

The C-FRP composite recovers its strength from the epoxy resin that holds the sheet laminates together. Any disturbance in the matrix affects the overall mechanical properties of the composite. Figure 2.2 shows that the epoxy permeates through the cross-woven sheets of CF nicely. However, generally speaking, the fabrications of C-FRP composites are relatively expensive if one considers material and energy costs, labor intensity, tooling and equipment, waste, and production efficiency. Technically, this process lacks repeatability due to inaccurate stacking of CF sheets, scalability, and complexity. This means that these kinds of compositions are only used for simple and large specialized applications.

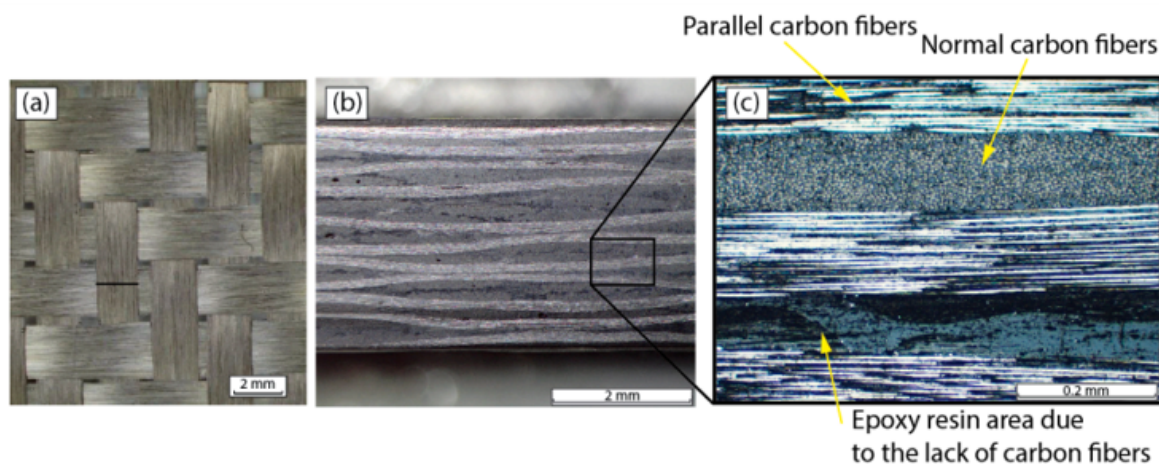


**Figure 2.2:** (a) Enlarged top view of 3k woven CF structure ; (b) Cross section of the CF reinforced polymer using epoxy (Thermosets), laminated and manufactured; and (c) detail of 0/90° oriented fibers [31].

## 2.2. Additive manufacturing

Additive manufacturing (AM), or simply 3D printing, is an advanced type of manufacturing process that involves the construction of three-dimensional (3D) models by joining layers of 3D elements (voxels). The process differs from traditional manufacturing technologies because the material is added to the building volume rather than subtracted or injected into an expensive prefabricated mold. As shown in Table 2.1, the American Society for Testing and Materials (ASTM) Group 'ASTM F42 - AM' standardized a set of 7 AM categories. (1) VAT photopolymerizations, (2) Material Jetting, (3) Binder Jetting, (4) Material Extrusion (including FDM), (5) Powder Bed Fusion, (6) Sheet lamination, and (7) Direct Energy Deposition.








Generally, all categories rely on a similar build sequence: CAD data generation, slicing, layering, and consolidation, but differ in feedstock, power source, and specific layering and consolidation methods. This gives them unique advantages and limitations in different characteristics. Think about reliability, scalability, resolution, design flexibility, production speed, and the capability of MMAM.

### 2.2.1. Multi Material Additive Manufacturing

From the overview given in Table 2.1 material jetting and material extrusion have the ability to exploit their methods for MMAM applications. Over the years, increasing demand for higher functional performance materials has raised tremendous interest in the development of processes capable of fabricating stronger, more complex, and lightweight compositions. Composite fabrication through AM, better known as Multimaterial Additive Manufacturing (MMAM), is a relatively new section of the AM industry. The ability to print reinforced structures with more complex geometries at greater precision, accuracy, and speed triggers the industry. Moreover, MMAM enables the possibility of exploiting different desired properties and reducing the effects of its weaknesses. For conventional manufacturing, this is only feasible with the use of multiple parts and the need for additional assembly. MMAM technology can reduce production and assembly time without extra cost for complex morphology. [9]

## 2.3. FDM Printing

In theory, utilizing the strength of C-FRP components printed with AM technology will give the following strengths: precise fiber orientation, (semi) autonomous manufacturing that reduces labor, producing more complex geometries, and the possibilities of scaling objects. The pro-

Categories	Technologies	Materials	Power source	Advantageous/ Limitations
 Material Extrusion	<ul style="list-style-type: none"> <li>FDM</li> <li>FFF</li> <li>ADAM</li> </ul>	Thermoplastics, Ceramics, Metal, pastes	<ul style="list-style-type: none"> <li>Thermal energy</li> </ul>	<ul style="list-style-type: none"> <li>Inexpensive extrusion machines</li> <li>Multi material printing</li> <li>Limited part resolution</li> <li>Poor surface finish</li> </ul>
 Powder Bed Fusion (PBF)	<ul style="list-style-type: none"> <li>SLS</li> <li>SLM</li> <li>DMLS</li> <li>EBM</li> </ul>	Polyamides, polymer, metal, powder Ceramic powder	<ul style="list-style-type: none"> <li>High power laser beam</li> <li>Electron beam</li> </ul>	<ul style="list-style-type: none"> <li>High accuracy and detail</li> <li>Fully dense parts</li> <li>High specific strengths &amp; stiffness</li> <li>Powder handling &amp; recycling</li> <li>Support and anchoring structure</li> </ul>
 Vat Photo-Polymerization	<ul style="list-style-type: none"> <li>SLA</li> <li>DLP</li> <li>CLIP</li> </ul>	Photo-polymer Ceramics, Alumina, Zirconia, PZT	<ul style="list-style-type: none"> <li>Ultra-violet laser</li> </ul>	<ul style="list-style-type: none"> <li>High building speed</li> <li>Good part resolution</li> <li>Overcuring, scanned line shape</li> <li>High cost for supplies and materials</li> </ul>
 Material Jetting	<ul style="list-style-type: none"> <li>Polyjet</li> <li>MJP</li> </ul>	Photo-polymer wax	<ul style="list-style-type: none"> <li>Thermal energy</li> <li>Photo-curing</li> </ul>	<ul style="list-style-type: none"> <li>Multi material printing</li> <li>High surface finish</li> <li>Low strength material</li> </ul>
 Binder jetting	<ul style="list-style-type: none"> <li>MJF</li> <li>SPJ</li> </ul>	Polymer powder, Plaster, Resin, Ceramic powder, Metal powder	<ul style="list-style-type: none"> <li>Thermal energy</li> </ul>	<ul style="list-style-type: none"> <li>Full color objects printing</li> <li>Require infiltration during post processing</li> <li>Wide material selection</li> <li>High porosities on finishes parts</li> </ul>
 Direct energy	<ul style="list-style-type: none"> <li>LENS</li> <li>EBAM</li> <li>LMD-w</li> <li>WAAM</li> </ul>	metal, powder	<ul style="list-style-type: none"> <li>Laser beam</li> </ul>	<ul style="list-style-type: none"> <li>High deposition rate compared to PBF</li> <li>Repair of damaged/ worn parts</li> <li>Functionally graded material printing</li> <li>Require post processing</li> </ul>
 Sheet lamination	<ul style="list-style-type: none"> <li>LOM</li> <li>UAM</li> </ul>	Plastic film, Metallic sheet, Ceramic tape	<ul style="list-style-type: none"> <li>Laser beam</li> </ul>	<ul style="list-style-type: none"> <li>High surface finish</li> <li>Low material, machine, process cost</li> <li>Decubing issues</li> </ul>

**Table 2.1:** Classification of different AM technologies. Standardized by ASTM International [8], partly adapted from [6]

duction method described in Section 2.2 only involves continuous fiber woven in cross-woven fabrics. Therefore, in this report, only continuous fibers are analyzed.

Two categories could be used for MMAM applications, namely Material Extrusion (ME) and Material Jetting (MJ). However, MJ machines are not capable to jet solid fibers leaving that the ME is far more suitable for long FRP printing. ME is a 3D printing technology that works with multiple classes of polymers, thermoplastics, and thermoset polymer material. The main distinction is how the materials behave when heated. Typically, thermosets cure and become permanently rigid when heated, while thermoplastic polymer (TP) softens and becomes hard when cooled, making the process reversible. Most Materials Extrusion machines utilize TP as filament for Fused Deposition Modelling (FDM). The main reasons for choosing thermoplastic

materials over thermosets are the unlimited storage, reusability, and recyclability of thermoplastic, short fabrication time, good flexibility, fracture resistance, and toughness, giving high impact resistance and flexibility, while thermosets are more brittle, and lower energy consumption compared to curing of thermosets, and the ability of part repair, modifications, or welding of existing parts. [40]

### 2.3.1. Printing process

FDM is classified as an ME process that uses TP as base material to build structures layer by layer. Typically, the printing process of thermoplastic material consists of three main steps. These occur in the following order. Initially, material is fed to the extruder by the drive mechanism. It arrives in the heating chamber, where the material is melted to a certain process temperature. When the drive mechanism is overfed, the overpressure causes the material to be extruded through the nozzle. The printer head applies the molten thermoplastic material to the build volume. The printhead moves from position A to position B in the xy plane to deposit strands of molten filament on the build volume. This is called the layering process. The FDM layering process differs from other AM technologies, such as sintering, chemical binding, or light curing, which comes with the advantage that FDM has a continuous deposition of thermoplastic strands. This makes it more suitable for the integration of continuous fibers. When layering is done, the printhead shifts in the z direction and starts the process again. The newly laid layer consolidates with the previous layer. The consolidation process is based on polymer sintering adjacent thermoplastic strands followed by polymer crystallization. After deposition, each TP extruded through the nozzle solidifies in the building volume. However, the TP forms a cross-bond with neighboring material between extrusion and full solidification. Layers extruded previously are solidified but still have a high temperature close to the glass temperature. When a new strand of thermoplastic material is extruded into the building volume, a bond formation is formed in the shape of the so-called 'necks,' a bridge between two successive strands. This process of bridge formation is called polymer sintering and is subject to the temperature, compatibility of the material, and amount of material. Proper bonding between the adjacent strands (intralayer bonding) and the bottom layer (interlayer bonding) enhances the overall strength of the 3D Macro structure. The FDM process is highly suitable for printing amorphous polymers because they quickly solidify with lower shrinkage. This behavior of the printed layer is essential to stick to the upcoming layer. [37] [51]

### 2.3.2. Printhead mechanics

The print head is an essential component in an FDM 3D printer and ensures filament is deposited on the build volume. It consists of an assembly of several parts. The filament supplied by the feed mechanism enters through the upper section of the printhead, reaching the cold end. The cold end contains the printhead cooling and filament guide. The use of a supply tube is optional and determined by the method by which the filament is fed into the 3D Printer, either by direct drive or Bowden. The lower section of the print head contains the hot end consisting of a Heat block (liquefier) that houses the heating element, heat sensor, and Nozzle. The hot end heats the filament until softened. A so-called heat break separates the hold-end and cold-end sections. Figure 2.3 shows a simplified schematic representation of a standard printer head.

#### Heatsink & HEAT BREAK

The heat breaks are part of the interfaces between the hot and cold ends, or the heat sink and heat block. This component has a tube-like structure with a connection option at both ends. The heat break consists of a material part with low thermal conductivity, titanium, and a material part with high conductivity, copper. Heat must be trapped in the heat block as much as



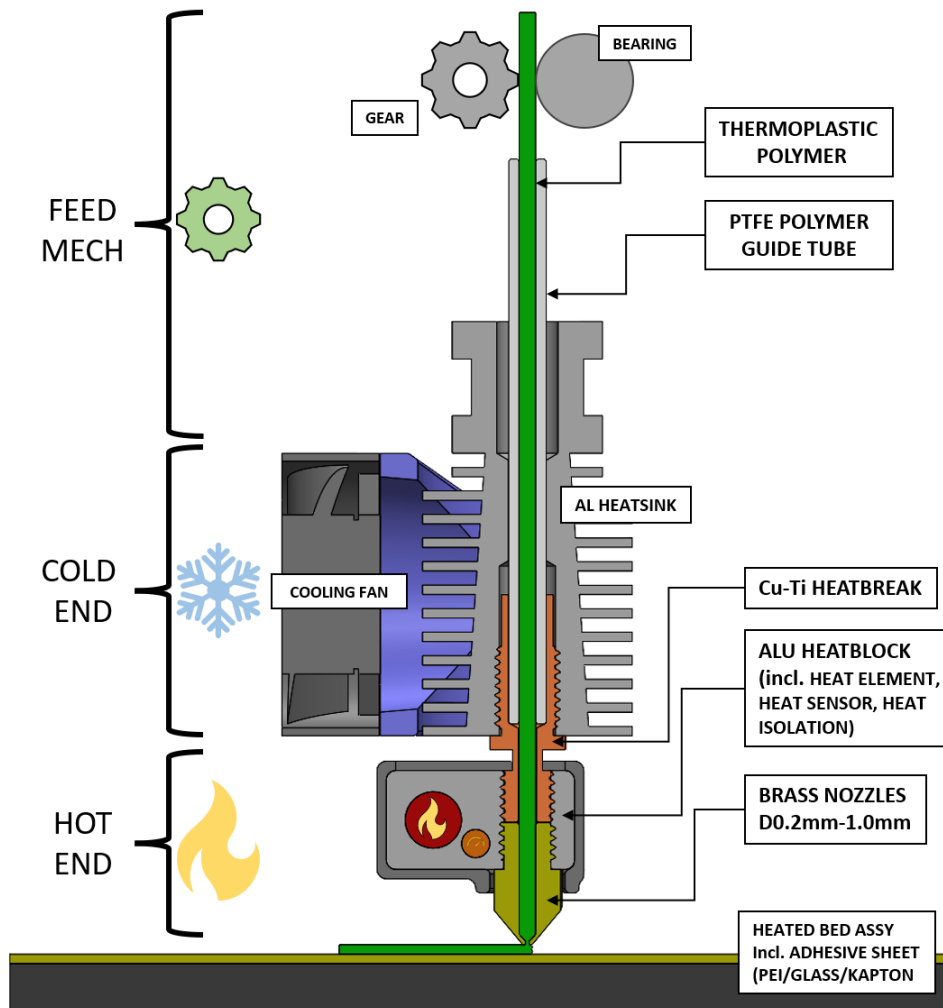


**Figure 2.3:** Schematic overview of a FDM Printhead used for plain TP printing

possible for a homogeneous heat distribution over the polymer filament. Eventually, heat starts to flow over the heat break to the cold part and needs to be distributed quickly over the heat sink. The aluminum heatsink cools the cold end with circular cooling ribbons supported by an active ventilator. This component has two main tasks. Namely (1) cooling and (2) suspension.

### Nozzles

The nozzle, located at the hot end of the printhead assembly, acts as the link between the heat block and the building platform in 3D printing. Typically made of brass, the nozzle withstands temperatures up to 300°C but is less durable with highly abrasive materials. Its narrow opening controls the flow of the polymer, shaping it into thin threads deposited onto the print area. Nozzles are available in various diameters. However, the 0.4mm nozzle is commonly utilized to balance print speed, resolution, and usability on most printing machines. The nozzle's size directly affects the layer's height and the strand's width. In general, the height of the layer should not exceed 75% or fall below 25% of the exit diameter. Small nozzles (0.1, 0.2mm) enhance print quality but increase print time due to lower material deposition. In addition, these nozzles easily clog, limiting the use of particle-infused filaments. Conversely, larger nozzles, like 0.8mm or 1.0mm, sacrifice print quality and complexity but significantly reduce print time. Besides, sizes are more suitable for C-FRTP printing since there exists a smaller risk of jamming. Successful C-FRTP print tests were performed using 0.8mm [61] and 1.0mm nozzles

[56]. The choice of nozzle diameter often relies on empirical testing due to limited literature guidance. The nozzle can be easily serviced since this part is the threaded attachment to the heat block.

### 2.3.3. Printing parameters

Processing parameters used in the FDM technology are adjustable direct settings with the slicing software. The print speed and specific design features can be set before printing the applied process and heat bed temperatures. These settings significantly affect the printability and reliability of the printed model.

#### Print speed, feed rate and exposure

Print speed is defined as the speed at which the printer head moves over the build volume in the XY plane and the height Z while extruding filament through the nozzle to produce mono parts. This parameter setting is measured in micrometers per second and is affected by the hardware and firmware of the 3D printer. The print speed is a 3D printer setting controlled by the slicing software and can be adjusted by the user. Together with settings such as layer thickness (resolution) and nozzle diameter, this eventually determines the printing time. Usually, the printing speed set for common 3D printers varies between 40 and 60 mm/s as medium part quality. However, this fact is subject to multiple influences, and the user requires some tests. In some machines, the print speed is the feed rate, given as a percentage. The feed rate that has not changed is 100% print speed. Adjusting this percentage impacts the behavior of the machine actuators and, thus, XYZ movement and flow rate. The temperature remains untouched. Increasing the print speed severely affects the quality and, thus, mechanical properties of the model. More and more capacity is required from the 3D printer. This results in a heavier load on the mechanics, and the print head will have to provide more thermal power to melt more filament in a shorter period. If this exceeds the printer's capabilities, it may result in filament jamming, skipping, and poor fusion of layers [21]. Commonly, lowering the print speed results in better precision and finer details. [32] [10]

In fluid dynamics, the fundamental principle of mass conservation states that mass cannot be created or destroyed within a closed system. This means the mass remains constant over time as an incompressible fluid flows steadily through a tube or nozzle. From the continuity equations, this leads to the equations for mass flow rate  $\dot{M}$ :

$$\dot{M}_{in} = \dot{M}_{out}, \quad (2.1)$$

and

$$\dot{M} = \rho_1 A_1 V_1 = \rho_2 A_2 V_2. \quad (2.2)$$

The applied equation 2.1 states that the mass flow rate of the solid thermoplastic at the input equals the mass flow rate of the extruded filament through the nozzle.  $\rho$  denotes the density  $kgm^{-3}$ , A the cross-sectional area  $[mm^2]$  and V the velocity of the fluid  $[ms^{-1}]$ . The printer's capacity to supply molten filament to the build volume is termed the flow rate and is directly related to the print speed. The slicing software automatically calculates this by means of a multiplier A. Multiplier A defines the ratio between the print speed and feed rate. Solving the equation for the mass flow (see Equation 2.2), assuming that  $\rho_1 = \rho_2 = \rho$  gives the following:

$$\frac{1}{4}\rho_1 V_1 \pi D_1^2 = \frac{1}{4}\rho_1 V_1 \pi D_1^2, \rightarrow V_2 = \frac{D_1^2}{D_2^2} V_1 \rightarrow A = \frac{D_1^2}{D_2^2} \quad (2.3)$$

Here  $D_1$  is the diameter of the supplied filament  $D_f$  and  $D_2$  the diameter of the nozzle  $D_n$ . FDM material is typically supplied on spools with filament having a diameter  $D_f = 1.75 \pm$

$0.05\text{mm}$  or  $D_f = 2.85 \pm 0.10\text{mm}$ . Furthermore, according to the venturi effect described by Bernoulli's principle, the fluid's velocity at the nozzle's tip increases, reducing pressure locally. [3]

Summarized, the fluid velocity profiles have been roughly estimated according to the conservation of flow. Three zones separate the deposition of TP by the nozzle (see Figure 2.4).

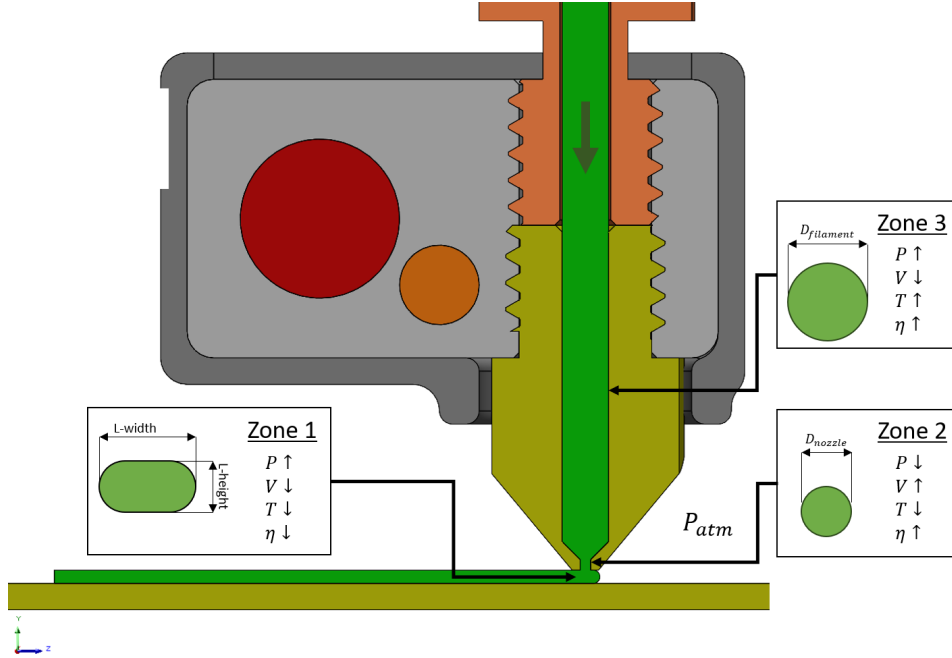


**Figure 2.4:** Schematic representation of pressure, velocity, and temperature profiles

The TP flow deposited on the build volume (zone 1), the flow at the exit of the nozzle with different nozzle sizes (zone 2,  $D_n = [0.2 \ 0.4 \ 0.6 \ 0.8 \ 1.0]\text{mm}$ ) and the flow at the inlet of the nozzle (zone 3,  $D_f = 1.75\text{mm}$ ). Theoretically, Zone 1 is defined as the print speed  $V_p = [10 \ 30 \ 50 \ 70 \ 90]\text{mm}\text{s}^{-1}$  of the nozzle tip laying a simplified cross section  $A_1 = 0.5D_n * 1.25D_n$  over a distance per second. The rule of thumb is that the layer height is  $0.5D_n$ , and the strand width is  $1.25D_n$ . The TP mass flow must flow through the exit of the nozzle (zone 2) and the input of the nozzle (zone 3). Mathematically, this states that:

$$Q_f = Q_1 = Q_2 = Q_3, \quad (2.4)$$

with the flow rate defined as

$$Q_f = V_f A [\text{mm}^3 \text{S}^{-1}]. \quad (2.5)$$

In practise, defining the velocity in a specific zone is subdued to frictional losses and, thus, a complex process. However, it can be certainly said that the flow rate in zone 1 must be equal to:

$$Q_1 = V_p A_1 = 0.625 V_p D_n^2 \quad (2.6)$$

So, the flow rate over different nozzle zones can be defined as:

$$V_2 = \frac{Q_1}{A_2} = \frac{0.625 V_p D_n^2}{0.25 \pi D_n^2} = \frac{5}{2\pi} V_p = 0.796 V_p, \quad (2.7)$$

and,

$$V_3 = \frac{Q_1}{A_3} = \frac{0.625V_p D_n^2}{0.25\pi D_f^2} = 0.816 D_n^2 V_p. \quad (2.8)$$

This shows the correlation between the fluid velocity  $V_f$  in zone 1 and zone 2 in [mm/s] and the print speed  $V_p$  [mm/s]. However, the feed rate of the delivered filament differs. Feed velocity  $V_1$  must be increased when print speed increases and / or nozzle diameter increases. [42]

### Pressure

The feed mechanism pushes the filament supply through the nozzle. This requires a driving force from the motor  $F_m$  that originates from the torque of the motor  $T_m = 0.5 F_m d_{gear}$ . The motor needs to overcome the frictional forces of solid TP and the pressure drop by the molten TP in the cylindrical-shaped nozzle. Both have been neglected during this investigation, since it is assumed that the TP is in solid state when flowing through the PTFE tube and the heat break.

The pressure P is calculated by the following equation:

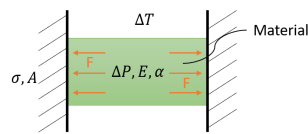
$$P = \frac{F_m}{A_3} = \frac{2T_m}{A_3 d_{gear}}. \quad (2.9)$$

The pressure exerted by the motor drops over the length L of the nozzle. This pressure drop can be estimated by the Hagen-Poiseuille equation:

$$\Delta P = \frac{128\mu L Q}{\pi D^4}. \quad (2.10)$$

$\Delta P$  in [MPa] is the pressure drop on the nozzle with length L [mm] and the corresponding diameter D [mm] of the nozzle in that zone (in zone 1  $D = D_f$  and in zone 2  $D = D_n$ ).  $\mu$  is the dynamic viscosity of the molten TP and Q is the volumetric flow in [ $mm^3 s^{-1}$ ]. Theoretically, the pressure drop over nozzles with a small exit diameter  $D_n$  has a smaller pressure drop than nozzles with a larger exit diameter [44].

In practise, swelling behavior of the TP is noticed when the temperature is increased. The pressure increase (pressure difference  $\Delta P$ ) due to the thermal expansion of TP can be estimated using the equation for thermal stress caused by a change in temperature [52]. From Hooke's law, the following can be said:



$$\begin{aligned} \varepsilon &= \alpha \Delta T, \sigma = E \varepsilon \\ \sigma &= \Delta P = \frac{F}{A} = E \alpha \Delta T \end{aligned} \quad (2.11)$$

### Print temperature and rate of cooling

Precise temperature control of the extruder temperature is crucial to achieve high-quality prints and avoid poor interlayer bonding. This setting is an essential process parameter that helps temporarily manipulate the thermoplastic filament during printing. Each thermoplastic has their own recommended temperature that properly melts material, accomplishing good polymer sintering, and optimizing printing properties without causing degradation or clogging. The required temperature setting is influenced by feed rate, resolution, ambient temperature, and extruder design. The heat sensor and heating element regulate the extruder temperature. According to [50], raising the printing temperature resulted in a significant increase in viscosity, improving the polymer impregnation and a reduction in porosities. Also, it was found that the increase in temperature enhances the interlayer bonding, and thus increases flexural strength and flexural modulus.

### Polymer rheology

Viscosity is a measure of the resistance of a fluid to flow. In the context of thermoplastics used in FDM, viscosity plays a crucial role in the 3D printing process. Viscosity is often quantified in units of Pascal-seconds (Pa·s). The viscosity of a thermoplastic in FDM affects several aspects of the printing process: (1) Extrusion: Higher-viscosity thermoplastics require more force to be extruded through the printer nozzle, which can affect the accuracy and speed of the printing process. (2) Layer adhesion: Viscosity can affect the bonding between the printed layers. Lower-viscosity materials may flow together more easily, leading to better layer adhesion. (3) Surface finish: Viscosity can influence the smoothness of the printed surface. Materials with lower viscosity may produce smoother surfaces. [53] The viscosity of thermoplastics represents a complex non-Newtonian nature and depends on temperature, shear rate (flow speed), and shear stress (pressure difference) [30]. In general, the viscosity of TP drops dramatically when the temperature increases and a shear rate is applied but remains relatively high, 0-500 Pa.s at FDM processing temperature (see Appendix A). In comparison, thermosets have a viscosity range of 0.1-50 Pa.s. and water 0.001 Pa.s. at 20 °C). [23]

## 2.4. C-FRTP 3D Printing

C-FRTP printing involves embedding continuous fibers directly into the thermoplastic material as the part is printed. This means the fibers are incorporated during the 3D printing, resulting in a single-step fabrication. In 2019, a standardization attempt by A. Matschinski, a research associate and expert at TU Munich chair, presented a standardization attempt. Recently, concepts within the 3D printing C-FTP methods landscape have been categorized. In Figure 2.5, the five conceptual standards for C-FRTP printing are shown. [28].

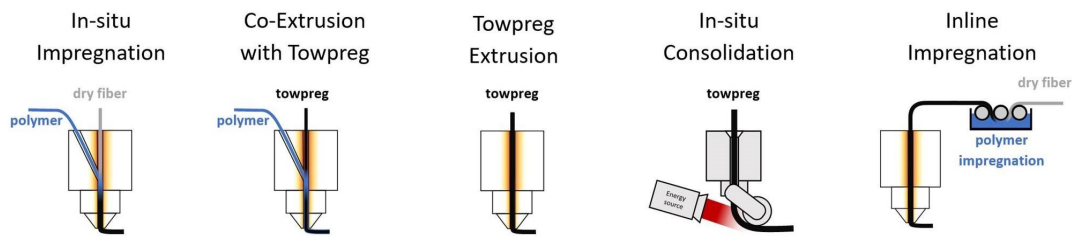


**Figure 2.5:** Standardisation attempt by A. Matschinski of 3D printing with continuous fibers. Adapted from [28]

However, printing C-FRTP can be approached by three methods: Pre-impregnation, In-Nozzle and Ex-Nozzle impregnation. Three approaches are listed below.

### 2.4.1. Pre-impregnation: Embedding in TP filament

This method is the most straightforward and does not require modifications to the original 3D printheads or machinery. Regular single-material printheads and feed mechanisms can be utilized because only one input is necessary. The fiber-embedded filament is often labeled as "prepreg." This method falls partly under the "in-nozzle" and "ex-nozzle" impregnation because adhesion is already formed outside the nozzle. Theoretically, the fiber is already soaked in polymer before entering the printhead. Fiber-impregnated filament is introduced to the heat block of the printhead together. When the prepreg passes through the hot end, the composite melts again, debonds, and reflows around the solid Fiber, cools, and forms again. The advantage is that the TP and fibers are inserted in a more packed form, which reduces the risk of air bubbles, but this requires an extra fabrication step in the fabrication process. Subsequently, molten thermoplastic and solid fiber composition are deposited to the build volume with a constant volume fraction. Currently, there are few commercially available pre-impregnated fila-

ments containing long fibers. Many pre-impregnated filaments are produced in-house, making them inaccessible for this research [21].

### 2.4.2. Ex-Nozzle impregnation: Embedding in the model

The second ex-nozzle method approaches the embedding of the fiber in the component as shown in Figure 2.7 (b). This involves the deposition of fiber and matrix through separate extruders. First, the matrix material layer is deposited, and then the second extruder is pressed into solid fiber. Ex-nozzle impregnation is often used in cases where particular fiber orientations are required. However, this method carries a high risk of defects due to the limited amount of heat applied to fuse the fiber matrix bond. Markforged, Mark two [19] introduces a commercially available machine.

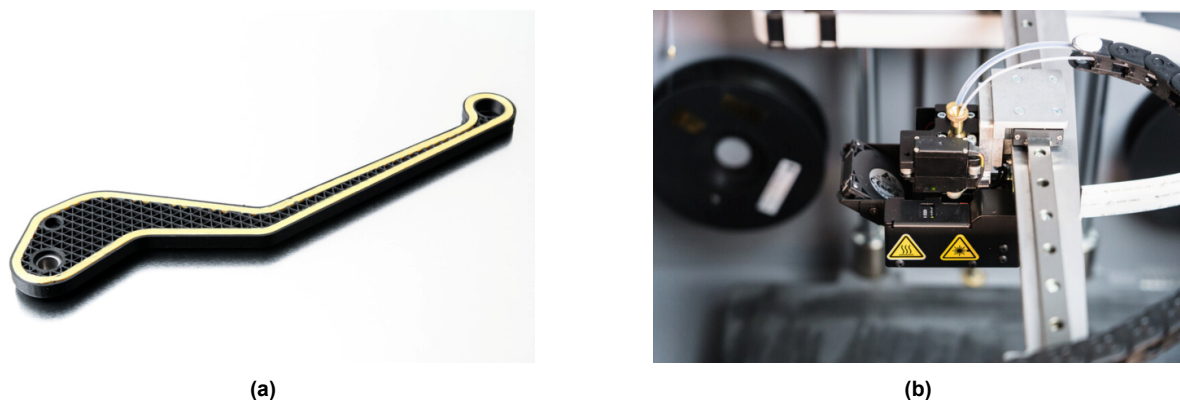


**Figure 2.6:** (a) This brake lever (paused mid-print to reveal the cross-section) shows black Onyx matrix with triangular infill pattern and two rings of concentric Kevlar fiber around the perimeter; (b) Plastic and Fiber tubes entering the top of the Mark Two print head. Adapted from [19]

### 2.4.3. In-Nozzle Impregnation: Embedding in the printhead

Alternatively, 'In-nozzle' impregnation describes the process of introducing fiber reinforcement into the matrix inside the extruder. This means that the two constituents are supplied to the heat chamber simultaneously through a separate or common entrance [35]. This method is closely related to embedding in a filament. However, the constituents are now supplied separately. The TP filament melts while the Fiber remains in the solid state. Then the constituents are deposited in the building volume together. Fibers are integrated into each layer as they are printed; this method can achieve more uniform and consistent fiber distribution. Compared to embedding in a filament, this method enables the possibility of adjusting the type of material and volume fraction, which gives the designer the freedom of design.

The "in-nozzle" approach benefits over the 'ex-nozzle' approach, as it involves only one manufacturing step and uses commercially available low-cost feedstocks. Ex-nozzle impregnation requires a separate post-processing step, adding time, labor, and cost to the manufacturing process. In addition, it provides the ability to adjust the flow rate of polymer, enabling real-time control over the local volume fraction and density of the component while opting for the ideal fiber orientation. However, infiltrating dry fiber yarn without forming air inclusions can be difficult due to the high viscous TP. In practice, pre-impregnated filaments are used in combination with the 'in-nozzle' and 'ex nozzle' impregnation methods. Basically, the fiber is soaked prior to the printing process, which has a positive effect on the shear bonding strength. An increased and consisted distributed interfacial shear bonding strength distributed the load more evenly over the composition and improves the in-plane mechanical properties. [60]

## 2.5. "In-nozzle" Impregnation printhead designs

The idea of feeding fiber and matrix to the printer head has been interpreted differently for 'in-nozzle' impregnation. Below As illustrated in Figure 2.7, various methods have been explored [35]. Ideally, a strong interface bond must be formed between the fiber and the matrix, which gives an extreme boost to the strength of the composite. This must be done in a very short printing time between feeding and extruding. Possible design options are described below. The print head is an attachment designed to work with standard FDM 3D printing machines. It allows the simultaneous extrusion of TP melt and continuous reinforcing fibers.

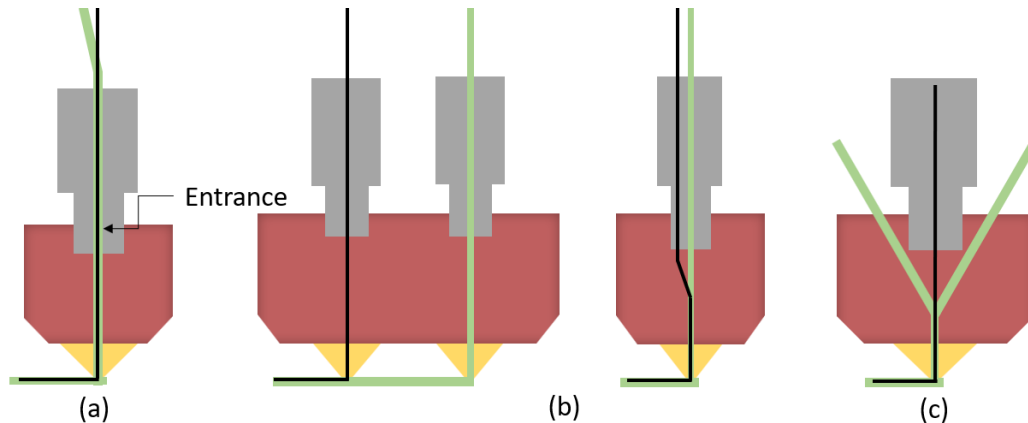


**Figure 2.7:** Different printheads; (a) shared entrance, (b) separate entrance, (c) Central fiber feed

### 2.5.1. Shared entrance

This straightforward method requires almost no modification of the original printheads and basically feeds both constituents using a common entrance approach. This involves introducing both materials through a single entrance. Researchers observed many malfunctions and unsuccessful attempts to extrude FRTP using a common entrance. It was stated that the effectiveness of this system relies significantly on the fiber-matrix interface since fiber bundles got trapped easily during extrusion. Another error occurred with an uneven distribution of the TP material around the fiber and fiber breakage arising from the lack of tension and the inadequately controlled extrusion rate [35].

### 2.5.2. Separate entrance

Deviation in feed rates between the two constituents and the inability of the fiber to withstand push forces highlighted that it was important to introduce fiber into the matrix in the smallest section of the nozzle. This led to the introduction of a separate entrance approach of [29]. modified a commercial 3D printer and introduced preheated reinforcement fibers to improve fiber permeability and fiber matrix bonding. However, their study found that fibers tended to cluster at the edges of printed filaments, leading to failures caused by fiber pull-out. This suggested that preheating alone was not sufficient and recommended additional measures such as proper fiber sizing to improve bonding [35].

### 2.5.3. Central fiber feed

Positioning the fiber bundle at the center of the polymer flow has the potential to resolve issues like uneven placement of the fibers, challenge to eccentric location, poor impregnation of fiber within the deposited filament [pandelidi 129]. Initially, Prüß and Vietor developed and built a prototype C-FRTP printhead in 2015 [39]. As shown in Figure 2.8, the design is mainly depicted from off-the-shelf FDM components supplied by E3D and RepRap technology. The

central feed serves as an entry point for the fiber to the extruder block. In the extruder block the fiber engages two feeds of thermoplastic filament from both sides. This approach ensures a consistent infusion of fibers through the molten thermoplastic material. Angled thermoplastic entrances drive the thermoplastics to the nozzle by downward force. [56] performed a permeability analysis based on such an extruder design.

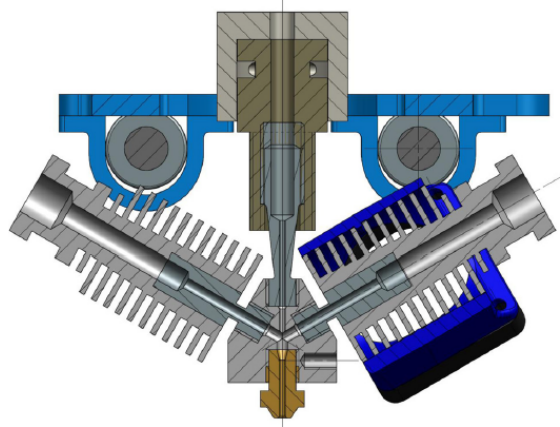


**Figure 2.8:** Central feed printer head modified built from regular 3D printer head components [39]

Commercially, there is no solution available to print the C-FRTP combination. Fiber is introduced into the heating system through a central entrance on top of the heating block. The literature shows that this type of printing head is the most promising concept with a high probability of a successful test result. The print head uses a central supply of fiber and two separate supplies of TP. In theory, the thermoplastic material can form more consistently around the CF bundle. It is important that the thermoplastic material flows as much as possible in the same direction as the fiber for optimal adhesion and flow towards the nozzle. This means that the angle between the vertical plane and the inlet line should be as small as possible. Several variants are possible for the heat block. Several variants are possible for the heat block, but due to time limitations, it is not possible to analyze aspects such as the attack angle or thermoplastic.

#### 2.5.4. State of the art: 2022 CFP-500

At the University of Calgary, Engineers showcased an innovative project, focusing on the development of a C-FRTP 3D printhead. This project aims to revolutionize AM by optimizing the deposition of C-Fibers within the TP matrix. The key emphasis of this project was to enhance the mechanical attributes and structural robustness of printed composites by precisely controlling the distribution and impregnation of fibers within the material. By addressing these aspects, the project highlighted the potential applications of advanced AM techniques in various industries that seek high-performance materials with customizable properties. [1]

## 2.6. Materials

### 2.6.1. Thermoplastic polymers

TP define as a class of materials that are very suitable for FDM printing because of their significant reduction in viscosity when heated. The weak van der Waals forces give these materials the ability to easily behave as a fluid when heated above their glass transition temperature or melt temperature  $T_m$  and solidify very rapidly when cooled beyond the crystallization temperature  $T_c$ . During this heating and cooling cycle no chemical bond is formed, only particles chains rearrange which makes this process reversible and suitable for rejoining, reshaping,



recycling and the fusion of 3 micro elements during the layering and consolidation process. [50]

TP are organic compounds that consist of sequences of identical cross-linked chains of one or more unbranched monomers. Thermoplastics are classified into two primary groups defined by their molecular chain structures. (1) Semi-crystalline (or semi-organized). Typically, these TP's characterize as stronger, harder, more stiff, opaque, chemical and heat resistant. (2) Amorphous (randomly organized) TPs are more relatively brittle, transparent, and impact resistant. Amorphous materials can already be extruded after passing the glass transition temperature, while semicrystalline TP need to surpass the melt temperature. Important to know is that by increasing the cooling rate after printing, more amorphous regions appear due to the lack of time to settle a crystalline structure. However, when the cooling rate decreases, more crystals are formed, but this also increases the shrinkage of the overall part. These groups exhibit distinct deformation characteristics. Semicrystalline thermoplastics have molecular chains that create arranged structures. On the contrary, amorphous thermoplastics consist of chaotic, linear, unbranched, and irregular molecular configurations.

In C-FRTP fabrication through FDM printing TPs form the base material (Matrix) of the composite surrounding the fiber bundle. Besides commonly 3D printing functions as layering and consolidation, TP matrices serve as:

- Bonding agent so that individual fibers are held together and load is evenly distributed over the interface. This functions as fundamental aspect in the overall strength definition;
- Support for the Fiber in compression, shear and impact loads. (The ultra-thin ( $< \emptyset 0.5mm$ ) Fiber bundle is only extremely strong in resisting tensile loads.
- Mantle that shields the fiber from external elements, such as ultraviolet and chemicals.

Despite their advantages, TPs have relatively high viscosity making the impregnation of fibers and penetration in between fiber bundles very difficult, in addition some TP's are prone to shrinkage which distort the interface (warping) . These results in poor fiber-matrix adhesion and lack interfacial shear strength [56].

In table A.1 found at Appendix A a brief overview of the TP materials commonly used in AM through FDM printing is shown. Materials are separated by primary group over three classifications, commodity, engineering and high-performance TP materials [46].

### 2.6.2. Continuous Fibers

As introduced in Section 2.1, multiple fibers are available for commercial use. Mainly used fibers in high-performance C-FRTP engineering applications are natural fibers, aramid fibers (Kevlar-29), fiberglass' (E-grade, C-grade), and CF. However, only a handful of different fibers have the potential to be selected for high-performance applications to be extruded by FDM printheads. FDM printing requires a high process temperature that can vary between 200-350°C exceeding the MST of most fibers that potentially influences the composition in an unexplainable way. Based on the requirements:

- High specific strengths over price per kg with material index:  $\frac{\sigma_f}{\rho C_p}$ ,
- High specific stiffness over price per kg with material index:  $\frac{E_f}{C_p}$ ,
- and Maximum Service Temperature (MST) to be higher than 350°C. Most of the FDM process temperatures require a temperature of around 200-350°C.

A selection of materials is found from the relevant bubble charts found in Appendix A. For this investigation, the Granta Edupack 2022 software package is used. Followed by this, a list

of potential fibers for C-FRTP printing through FDM technology is given. Potential materials are silica, basalt, CF, fiberglass (grade C and E) and natural fibers (sisol, kenaf and jute fibers).

Fibers are strategically aligned in line with the load in order to absorb this load in the tensile direction as efficiently as possible. However, in modern day engineering HPF fibers, when combined with a resin or matrix, exploit their full potential when the mutual friction between the microfilaments is increased. Therefore, HPF do not occur in isolation in high-performance engineering. The fibers can be ordered in different shapes and sizes, for example, chopped fibers, cross-woven fabrics (textile-like), continuous fiber threads and sheets/films [15].

#### PAN-based CF

CF is usually made from precursor materials, polyacrylonitrile (PAN) but also from a Rayon or petroleum pitch. Note: 90% of commercially available CF is a PAN-based precursor. That's why this investigation is limited to only 'polymer-based' CF. The precursor material is subject to multistep fabrication process. The first step intervenes in polymerization of polyacrylonitrile (semi-crystalline), meaning that atoms arrange in a continuous hexagonal lattice structure. Followed by a carbonization process in an oxygen-free environment that applies extreme heat to remove noncarbon atoms. The filaments are then spun into extremely thin filaments ( $<10\mu\text{m}$ ) and combined in "tows" containing a number of filaments (usually 1K, 3K, 6K, etc.). Fibers are classified on linear density "tex" (grams/kilometer or  $(10^{-6}\text{kgm}^{-1})$ ). Increasing the text number also increases the diameter of the bundle. Optionally, the CF is then coated with a bonding agent that helps facilitate the shape and provides extra strength. [4]

#### Fiberglass

Fiberglass is a high performance fiber that is made from tiny glass threads that are drawn from molten glass through a platinum bushing, coated with sizing agent, and spun on a drum under an extremely high temperature. A bundle of glass filaments is then combined in a roving. In the industry, three types of fiberglass are commonly used in FRP, namely E-glass, S-glass, and C-glass. S-glass has the highest strength, but has a very high fabrication cost. E-glass has the lowest manufacturing costs and is used mainly. C-glass is used in chemical applications because of its greater resistance to corrosion. Also, it can be woven into fabrics or used in the form of mats, roving, or chopped strands. Fiberglass possesses high tensile strength, excellent resistance to impact, corrosion and temperature variations, and good compressive strength, but is very brittle. [27]

#### Natural Fiber

Natural Fibers (NF), as the name suggests, are derived from plants or animal sources. Examples include banana, cotton, flax (linen), hemp, and wool. NFs have gained attention as an environmentally sustainable replacement for certain synthetic and mineral fibers in FRP composites. NF shows potential for FRP composites. However, concerning these kinds of fibers, various issues regarding their mechanical strength (which varies), environmental performance, and technical feasibility need to limit the use of widespread industrial implementation. For example, flax and hemp fibers have good tensile strength, while cotton is softer and less robust. In addition, NFs are biodegradable, have relatively low maximum service temperatures (which makes it hard to process with FDM technology), typically around  $160\text{-}400^{\circ}\text{C}$ , and are sensitive to environmental conditions, such as moisture, pests, and UV exposure. Industrial implementation of the natural fiber-reinforced TPs (NFRTPs) requires a successful melt impregnation method to encapsulate the fiber compound fully. [27] [48]

## 2.7. Research objective

From the literature, C-FRTP 3D printed composites appear to be a feasible solution for industrial applications due to their incredible added tensile strength to the neat TP. Researchers successfully used FDM technology to 3D print C-FRTP composites but still face significant challenges in extruding compositions exhibiting high interface bonding strength between fibers and TP, achieving repeatable and reliable parts that have fiber concentrically aligned internally. C-FRTP 3D printing is limited not only by the common macro-level limitations known to material extrusion challenges within FDM technology, such as infill voids, improper polymer sintering between layers, and shrinkage that disrupts the printed part but also by Meso-level Low-force interface bonding interaction between the fiber and the TP matrix has been recorded. This is observed as porosities in the interface, resulting in overall mechanical weakness.

Over time, various manufacturing processes have been developed to manufacture 3D-printed C-FRTP composites. Two primary C-FRTP 3d printing methods can be distinguished: “in-nozzle impregnation” and “ex-nozzle impregnation” of fiber reinforcement. The reason for investigating the feasibility of ‘in-nozzle impregnation’ is that ‘in-nozzle’ impregnation offers advantages over ‘ex-nozzle impregnation’ because it involves a single manufacturing step, increases applied pressures, and uses commercially available cost-effective feedstocks. Furthermore, it allows for adjusting polymer flow rates, better heat distribution, and real-time control over the local volume fraction. However, despite the many advantages of this 3d printing method for academic researchers, In-nozzle impregnation needs further research to determine whether a strong interface bond between the two constituents with a short fusion time can be achieved.

In-nozzle impregnation is described as a method where the fiber is introduced to the TP within the heat chamber of the extruder or vice versa. However, because of the low compression resistance of dry CF threads, CF cannot be punctured into the high-viscosity TP matrix. Thus, the permeability of the dry fiber through the melt pool represents a significant challenge in the “in-nozzle” impregnation process. The TP must perform traction on the CF wire from the CF bundle to the TP matrix to ensure that CF is impregnated and extruded. To achieve and maintain the concentricity of the dry continuous fiber thread the nozzle exit must be very close to the inlet where fiber enters the fusion area. This will ensure precise alignment and positioning of the fiber within the printed structure without deviations or misalignments, which is crucial to improving the final composite’s mechanical properties and structural integrity [21]. However, shortening the length of the fusion area may affect the efficiency of the melt impregnation process and the interface bonding strength.

Therefore, a conceptual C-FRTP print head is proposed but requires further investigation into the effects of melt impregnation and the impact that this has on the interfacial shear strength (Fiber-matrix adhesion). Therefore, this research aims to address the following research question.

### Research objective:

Conceptualize a functional ‘In-Nozzle’ impregnation extruder capable of extruding proper Continuous Fiber Reinforcement Thermoplastic compositions using FDM printing.

This main challenge is posed by the limitations of dry fiber to penetrate the thick TP melt. The analysis highlighted the need for the fiber to exit the fiber guide tube closely to the nozzle exit, limiting its exposure time in the fusion area with the TP melt. Evaluating the feasibility of dry fiber impregnation using FDM technology and finally conceptualizing a print head solution requires a series of sub-questions that guide the systematical addressing of various aspects. The sub-question breaks down the research objective into manageable components. The following sub-question holds:

**Sub question 1:**

How does molten TP flow affect the distribution in and around the continuous fibers during melt impregnation with varying process parameters (pressure, temperature, and time)?

**Sub question 2:**

How does the melt impregnation in terms of heat exposure time affect the mechanical adhesion of the fiber matrix, defined as the interfacial shear strength?

**Sub question 3:**

Evaluating the feasibility of in-nozzle impregnation printing involves comparing its benefits, cost-effectiveness, and overall performance against current technologies in similar industry applications.

Understanding how this innovative approach compares with established methods is essential to determine its potential as a pioneering solution within the field. Analyzing efficiency, material properties, production costs, and scalability will illuminate whether 'In-nozzle' impregnation printing is a promising innovation that deserves further attention and development.

# 3

## Initiating C-FRTP Printing Experiments

### 3.1. Research methodology

The following experimental methodology is proposed to investigate the melt impregnation and the related interface strength to give a clear answer to the objectives of Section 2.7. Experimental research is preferred over numerical models to initiate a feasibility study on C-FRTP 3D printing. Conduct experiments to replicate real-world conditions more accurately and achieve a smaller chance of overlooking or oversimplifying complexities and variables. Experiments can also uncover unexpected results or new phenomena, offering insights beyond the predictive scope of numerical analysis. Additionally, they serve as valuable educational tools, providing hands-on experience and deepening theoretical understanding. Also, considering the available equipment at the laboratory makes experimental research more cost-effective and thus a practical choice in resource-limited situations.

#### 3.1.1. Theoretical examination

In this investigation, each subquestion begins with a comprehensive theoretical investigation involving mathematical formulas and early research results. It delves into the theoretical aspects of the melt impregnation process of thermoplastic polymers into CF bundles. It creates an interfacial shear strength that defines the load-bearing strength of the composite. First, a brief indication is approached by the influence of process parameters such as pressure, temperature, and time. The exploration focuses on fundamental theories, mathematical models, and initial research that provides insight into the melt impregnation mechanism, adhesion engineering, and factors influencing that efficiency.

#### 3.1.2. Microscopic analysis of melt impregnation

Following the theoretical examination, this phase transitions to an empirical analysis conducted by "in-nozzle" impregnation, offering a microscopic perspective of what happens within the nozzle during the impregnation process. Utilizing microscopy equipment, the actual interaction between the thermoplastic polymer and the CF bundles at the microscopic level. Again, the effect of different process parameters is analyzed. This analysis aims to validate theoretical assumptions and provides real-time insights into impregnation phenomena, including wetting, spreading, and distributing the polymer matrix around the CF bundles.

### 3.1.3. Interfacial shear strength study

Transitioning to a preview of Chapter 5, this segment introduces the planned research on the evaluation of the interfacial shear strength of the composite material. The study involves testing the interfacial strength between the thermoplastic polymer and the composition of the CF. Using a tensile bench, the interfacial shear strength will be evaluated, providing crucial information on the composite material's mechanical integrity and bonding properties.

### 3.1.4. Data evaluation and feasibility analysis

Data evaluation begins by analyzing the data obtained from microscopic observations. The images and data collected are examined to understand the distribution and estimate the percentage of polymer melt allowed inside the CF bundle. Identify any patterns or correlations observed between the impregnation quality and the microscopic characteristics of the composite material. Evaluate the results obtained from the tensile tests conducted to determine the interfacial shear strength of the composite material. Data analysis assessed mechanical properties and bond strength between TP and CF composition. Synthesize the findings of the microscopic analysis and the results of the tensile test to establish a correlation between the impregnation quality and the mechanical properties of the composite material. Use statistical analysis or correlation techniques to identify any significant relationships or trends between the quality of melt impregnation (permeability) and the composite material's mechanical performance (interfacial shear strength). Draw conclusions based on correlated data, highlighting the significance of permeability achieved during impregnation in influencing the resulting interfacial shear strength. The implications of these findings on optimizing the impregnation process to enhance the mechanical integrity and performance of thermoplastic polymer-CF composites. Based on this, a statement can be made about the feasibility of in-nozzle impregnation methods for the fusion between Continuous fibers and Thermoplastic polymers.

## 3.2. Development of experiment setup

This approach aims to allow for a controlled and focused investigation of the melt impregnation process, ensuring accuracy, precision, and repeatability in the experimental procedures while minimizing the need for significant modifications to standard FDM equipment and the utilization of major preprocessing steps before printing.

To Investigate the melt impregnation process and fiber-matrix adhesion, an experimental method is developed for more accurate imitation, thermal stability, repeatability, and limit the external influences. A brief description is given of the precise fabrication of C-FRTP composite samples, the modified static mold, and the implementation of the PID controller. Emphasizing an encapsulation technique on the samples rather than in the mold ensures the repeatability and scalability of the experiment in generating large amounts of data. The sample development process is explained by interpreting the strategic integration of carbon fibers into the thermoplastic polymer matrix.

### 3.2.1. Sample development

The sample designs adopted for this study involve a fabrication process to mimic the 'in-nozzle' impregnation of TP accurately melted in CF reinforcement. The methodology involves integrating the CFs into the TP matrix effectively using a secondary FDM 3D printer that prints the matrix in the desired shape layer by layer. During this printing process, a strategic pause is used to allow for the precise laying of the CF bundle in the center of the cylindrical polymer matrix. Note that this process is similar across different experiments to enhance similarities in the results. Geometrical aspects may vary depending on the unique requirement of that specific study. After the continuous carbon fibers are placed, the printing process resumes,

ensuring the completion of the composite structure by applying the remaining PLA material over the laid CFs. This approach is impossibly close-packed composite samples, where the CF is encapsulated in the polymer matrix, forming a sealed package of reinforced material. This tailor-made sample fabrication process serves as a basic basis for subsequent analyses of the printed composite materials' impregnation quality, mechanical performance, and interfacial properties. In Fig 3.1, a schematical representation of the sample in the mold is shown. From the outside in, the sample consists of an aluminum packing and a polymer matrix with a cavity in the core where the CF bundle is located. The CF is very densely laid in the cavity but spreads out when released. In theory, The CF bundle is laid over the centreline of the cylindrical-shaped polymer printer matrix. The challenge in manufacturing these types of samples using dry CF bundles is to keep the air gap between the polymer matrix and CF bundle as small as possible. When cutting the end of the fiber bundle, the microfilaments start to fray. This problem was solved by greasing the bundle using wax as the sizing agent. However, this affected the samples in a later phase since the wax created cavities around the interface. It has been decided to remove the sizing agent. Options for sizing agents are available but not included in this investigation to limit influences [24].

### 3.2.2. Static mold design

Critical components of this experiment set-up are the modified aluminum heat block, heat element, and heat sensor derived from a regular FDM printer to facilitate controlled heat distribution. Heat blocks (20x18x12mm) are widely available, including attachments and heat insulation. These heat blocks house the heat cartridges, thermocouples, or thermistors—the bore where the nozzle is typically used as a heated cavity. A tiny air gap exists between the heated sample and the heat block, filling it with aluminum foil. It has been chosen to reduce the heat block's volume to improve the heating element's and the sensor's ability to maintain stable and controlled temperatures. The heating element comprises a 24V 70W heater element (cylindrical  $\varnothing$  6x20mm), and the heat sensor is a thermocouple type K

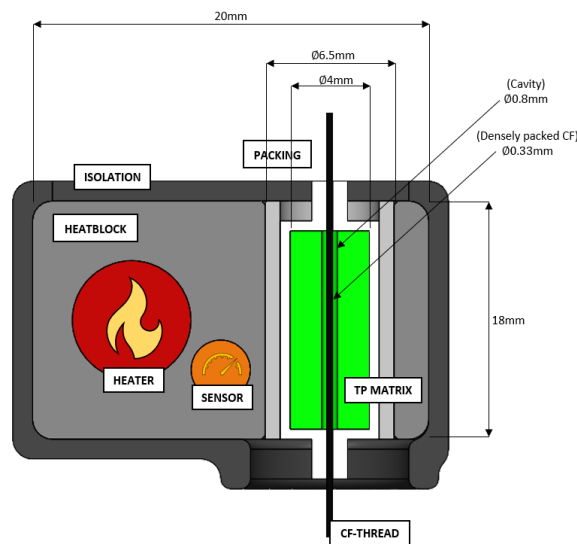


**Figure 3.1:** Schematic representation of the static heat mold with sample

### 3.2.3. PID temperature controller

Precise temperature control is essential to improve a reliable and stable heat distribution over the sample when placed in the static mold. Therefore, the use of a PID controller is preferred. A

Delta Electronics DTK Panel mount controller is employed as a temperature controller, which comprises a PID (Proportional-Integral-Derivative) thermal control system. To regulate and stabilize the heating system, the PID values have been autotuned by the controller and slightly adjusted by the user for optimized heat control of the aluminum heat block. The deviation in heat is  $\pm 2.5^{\circ}\text{C}$  around the temperature setting. The PID thermal controller ensures consistent and accurate temperature profiles throughout the experiment. A 24V switching power supply is used to power the 24V 70W heat cartridge and is switched with a breakout MOSFET. The controller is calibrated using a secondary measuring device from the PME laboratory.

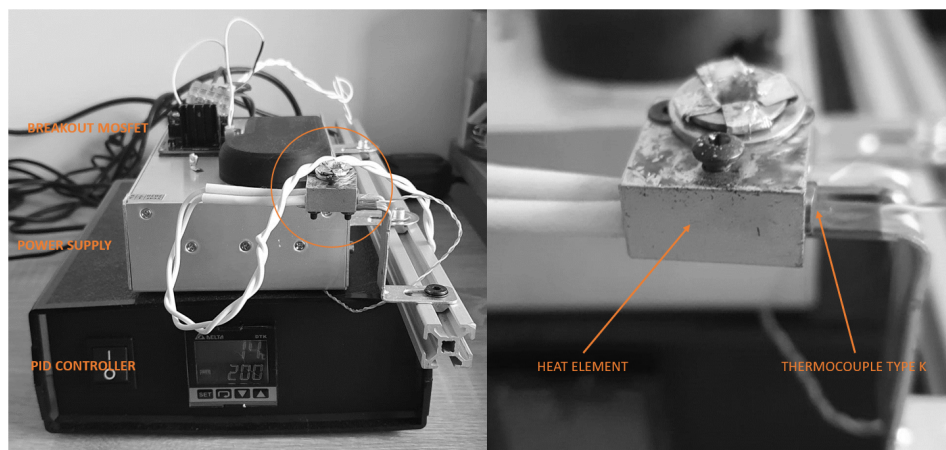


**Figure 3.2:** (Left) Picture showing the PID Heat controller (Black), Switching power supply breakout Mosfet and user interface with Thermal control settings; (Right) The static mold

#### 3.2.4. Experiment procedure

The procedure for the experiment is described below. The aluminum heat block is heated to a processing temperature of approximately  $210\text{--}220^{\circ}\text{C}$ . It was decided to apply the maximum allowable processing temperature to PLA to ensure the complete flow of the PLA. The resistance to flow or viscosity of PLA decreases at a higher temperature. This cannot be done indefinitely because the decomposition of PLA occurs at a temperature above  $250^{\circ}\text{C}$ . The manufacturer indicates a temperature range of  $190\text{--}215^{\circ}\text{C}$ . The experiment is conducted in an environment with an average room temperature of  $21^{\circ}\text{C}$ . The different samples are then placed in the heating block and heated for a certain period to mimic the exposure time inside the nozzle. After the elapsed heat exposure time, the package is removed from the heat block to cool. The sample is then stored in a sealed zip bag and marked with the relevant research group.

### 3.3. Material selection

Selecting Fiber and thermoplastic matrix materials with relatively good material compatibility is crucial in establishing a good interface bonding. Materials are more likely to adhere when compatibility is high [12]. However, adhesion is a complex phenomenon and depends on several factors. Tian et al. mentioned that the interface area of the thermoplastic composition relies on relatively weak physical interactions such as mechanical interlocking, surface wetting, surface tension, surface energy, and diffusion of molecular chains [50]. However, recent research has found that materials with similar properties, such as melting temperature, thermal expansion coefficient, and viscosity, are more likely to be compatible with each other [56].



### 3.3.1. TP Matrix: PolyLactic Acid (PLA)

The choice of material for this study is based on using a standard 1.75mm polylactic acid (PLA) filament surrounded by the 123-3d Jupiter series. PLA emerges as the primary candidate due to its potent properties that match the experimental goals. The low thermal resistance, wide availability, and minimal emission of hazardous gases during heating make PLA a preferred choice for this research. Regarding mechanical properties, PLA has lower shear resistance than other thermoplastics, allowing smoother flow around the fiber wire [2019 Fidan]. Choosing a light-colored PLA variant improves the visibility of the (darker) fibers within the composite structure. However, it is essential to recognize that while PLA is suitable for this study, it may not represent the behavior of other thermoplastic polymers. Therefore, further comparative research with alternative materials is recommended to understand the impregnation behavior [11] fully.

Preliminary, PLA filament underwent a 24-hour drying process at approximately 42°C before being used in the experiments. Exposure to a humid environment leads to moisture absorption by the filament. When the polymer is heated, trapped moisture evaporates, creating tiny cavities and swells. The result is a decreased printability and an improper deposition of the polymer melt, affecting the layering and consolidation process. The filaments are dried, cleaned, and stored in a sealed back to ensure reliable samples. This will provide an optimal condition for studying the melt impregnation process of continuous fibers using FDM technology.

### 3.3.2. Reinforcement Fiber: PAN-based CF

In this study, the high-tensile resistant 3K-CF, derived from the precursor PolyAcryloNitrile (PAN) material, is obtained from the supplier. Except for the extraordinary tensile resistance that plays a crucial role in strengthening the PLA matrix, this specific type of carbon fiber was chosen to fit the exit of a regular FDM extrusion nozzle. The diameter of the CF bundle is approximately  $D_{CF} = 0.3mm$  and has a cross section of  $A_{CF} = \frac{1}{4}\pi D_{CF}^2 = 0.07mm^2$ . In Fig. 3.3, an SEM image of the carbon figure is shown. The side note is that the surface of the CF bundle is very smooth, which may cause issues clamping the bundle on the tensile bench. Before the experiment, the CFs were cleaned with 99% isopropyl alcohol (IPA) and dry cleaned.

The selection of CF as a reinforcing agent is due to its outstanding mechanical attributes, notably its high tensile strength, stiffness, and impressive weight-to-strength ratio. In addition, its compatibility with the PLA matrix ensures an effective melt impregnation and robust interfacial bonding. CF threads are carefully wound onto spools to avoid entanglement. As seen in Figure 3.3 the CF bundle consists of microfibers placed in parallel and gains its strength from mutual friction offered mainly by polymer packing. The composition of these bundles is based on the number of microfibers present, indicated with prefixes such as 1K for 1000 microfibers and 3K for 3000 microfibers in a bundle. Each microfiber has a diameter that varies between 0.005 and 0.007 mm. The density of the CF bundle is measured in Tex (grams/kilometer or  $10^{-6}kg/meter$ ). For this experiment, the smallest CF by Tex is selected to fit the exit of the nozzle, which ranges around 0.6-1.0 mm. [15]

In Table 3.1, the mechanical properties of the PLA matrix and the 3K CF are detailed for reference, allowing a comprehensive comparison. This comparative analysis highlights the practical components' intrinsic strengths and provides insight into their synergistic potential when combined into the composite structure. By mapping these mechanical properties, this study will clarify how the properties of CF and PLA matrix interact and contribute to the tremendous performance and behavior of printed composite materials.

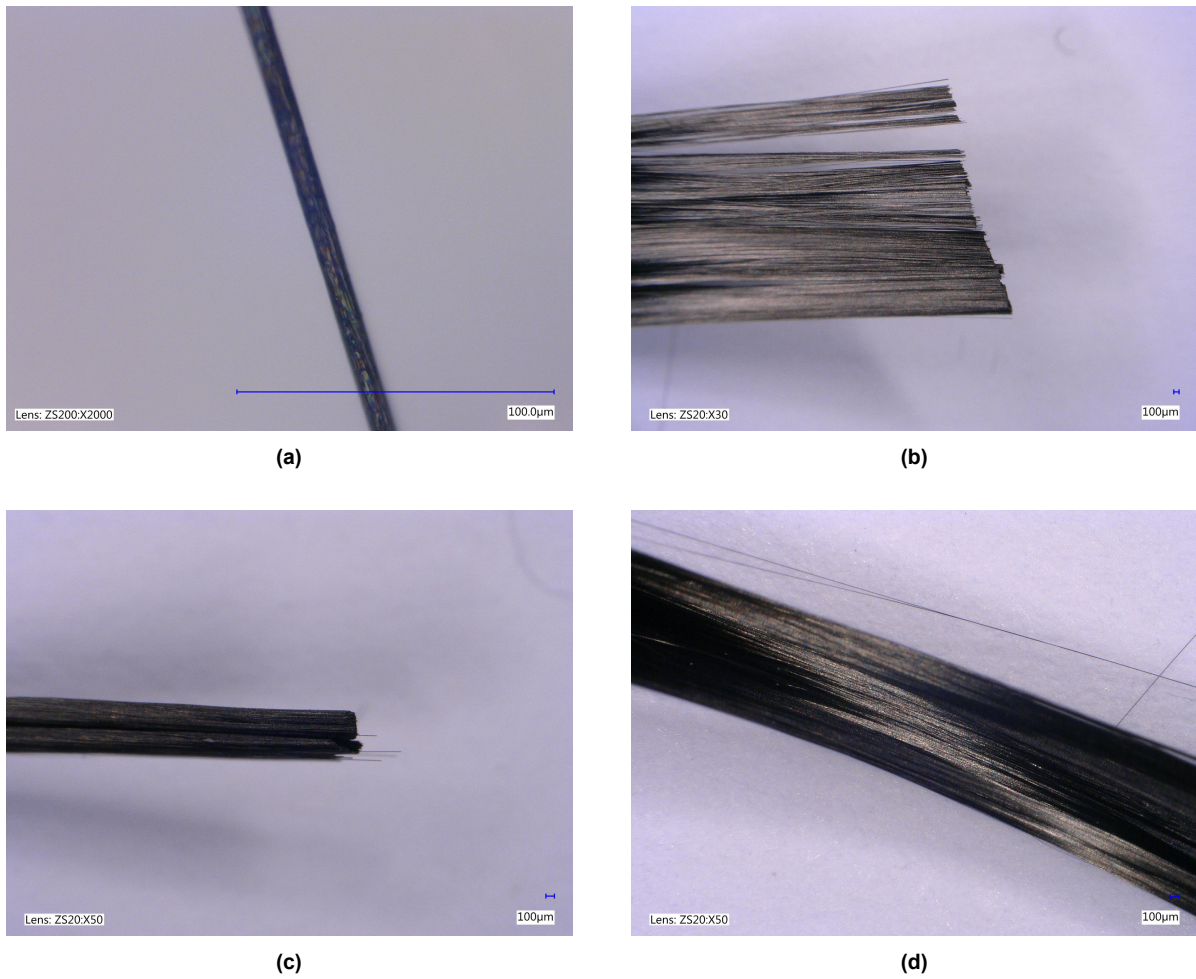


**Figure 3.3:** Microscopic images of an CF bundle taken by Keyence®; (a) Full bundle section (M50x); (b) Single microfilament (M2000x); (c) Cutt CF (M2000x); (d) Straighten bundle of CF (Magnitude 50x)

	PLA	CF (PAN BASED)
Density (Solid) $kgm^{-3}$	1.252	1.850 (200 Tex; $gkm^{-1}$ )
Density (molten) $kgm^{-3}$	1.073	
Tensile Strength [MPa]	39.9-59	3500
Elastic Modulus [GPa]	3.5	230
Melt point [ $^{\circ}C$ ]	55 ( $T_g$ 165 $T_m$ )	3650
Coefficient of thermal expansion [ $10^{-6}K^{-1}$ ]	135.5	16
Diameter [mm]	1.75 ± 0.05mm	0.33 (3K*7µ m)

**Table 3.1:** Mechanical properties of PLA and 3K-CF. adapted from [11] & Granta edupack software package

# 4

## Melt impregnation

The primary objective of this chapter is to explore the behavior of melt impregnation through reinforcement within the domain of FDM technology. The research starts with a theoretical exploration based on established laws of nature, and early practical models, followed by an empirical microscopic investigation. This investigation aims to document the precise interaction and permeability that occur between the TP matrix and the continuous CF after their entry into the hot end and their subsequent “fusion” somewhere in between entry and extrusion. Understanding and optimizing the melt impregnation process are crucial for achieving desirable mechanical properties and ensuring the quality of printed composite materials.

### 4.1. Melt impregnation process

Melt Impregnation describes the fusion process between thermoplastic polymers and continuous fibers within the hot end. The degree of melt impregnation is described by the ratio between encapsulated or impregnated fibers over the total number of Fibers [36]. Mathematically, the following holds:

$$R_{impreg} = \frac{\text{number of impregnated fibers}}{\text{total number of fibers}} = \frac{A_{impreg}}{A_{CFbundle}}. \quad (4.1)$$

The implementation of a specialized C-FRTP printhead design, with dedicated inlets for polymers and fibers, is a critical aspect underlying this investigation. The design incorporates a solid polymer flow and controlled introduction of polymer into continuous fibers. In this investigation, the central feed printhead from Section 2.5 is used as a baseline. The use of two 45° degrees angles side entrances that meet the central feed of aligned Fibers is designed to improve the flow dynamics around the Fiber. The aim is to provide an effective impregnation through the Fiber bundle. As the thermoplastic polymer enters the printhead through entrances, its journey unfolds in several stages.

#### 4.1.1. Melt flow dynamics

Initiating the formation of the composite, solid-state TP enters the hot end of the C-FRTP printhead, marking the beginning of the fusion process. Under controlled heating, the solid polymer undergoes transitions to a liquid molten state when it progresses through the printhead. The temperature profile gradually rises along the polymer pathway, reaching a predefined level suitable for efficient impregnation. It is assumed that the polymer is fully molten when it enters the melt impregnation (fusion) area.

### 4.1.2. CF Melt impregnation

Continuing along the pathway, the polymer material approaches the point where it encounters the central feed allocated for C-CF. TP PLA is now fully molten, and the fusion phase marks the subsequent stage, where the polymer material and C-CF interact within the hot end of the printhead. The time from the first interaction to extrusion and thus the last interaction with the hot end is called the TP-CF exposure time  $t_{exp}$  in [s].

### 4.1.3. C-CFTP composite deposition

From Equations 2.3 found in Section 2.3.3 it is indicated that the flow rate must be reduced when the volume fraction is increased [3]. High flow rates cause accumulation of thermoplastics that increases pressure at the nozzle. Fiber damage or rupture is expected. Furthermore, porosity of C-FRTP samples was observed when produced under low pressure. This also relates to an increase in interlaminar shear strength (ILSS) [33]. In addition, increasing the pressure to much could cause avoiding leakage from the inlet and outlet. To gain a longer exposure time inside the heating element, two methods are proposed. The length of the heating chamber is increased or the feed rate is reduced drastically [23].

However, in the contrary Rivero-romero et al found that decreasing the printing speed causes excessive porosity growth around the fiber surface [41]. Increasing the print speed immediately also decreases the flow rate, increasing the exposure time between the molten filament and the fiber. The relationship between exposure time and interfacial shear strength is unknown.

## 4.2. Melt impregnation theory

Achieving rapid and full impregnation of a dry fiber bundles with thermoplastic polymer as a matrix is hindered by the flow properties of thermoplastic polymer melts which remain highly viscous and exhibits non-Newtonian fluid characteristics within a porous medium.

Theoretically, modeling the infusion of thermoplastic polymer melt into a porous reinforcement is approached with Darcy's law. Darcy's law formulates the one-dimensional flow rate (Q) of a fluid through a porous medium, the law is expressed as follows:

$$Q = vA = A \frac{dx}{dt} = \frac{KA}{\eta} \frac{dP}{dx}. \quad (4.2)$$

Through the integration of Darcy's law over time  $t$ , the penetration depth  $x$  in a porous medium along a single direction. Restructuring Equation 4.2, the penetration depth  $x$  is defined by:

$$x = \sqrt{\frac{2K\Delta P}{\eta}} (t)^{0.5}, \quad (4.3)$$

where the permeability coefficient  $K$  of a continuous unidirectional fiber bundle can be predicted using the Gebert formula. Hence, the permeability along the radial direction of the fiber bundle, denoted as  $K_r$ , can be expressed as follows:

$$K_r = C_1 R^2 \left( \sqrt{\frac{V_{fm}}{V_f}} - 1 \right)^{\frac{5}{2}}, \quad (4.4)$$

where,  $C_1$  and  $V_{fm}$  represent the characteristic coefficients associated with the fiber arrangement. These values are numerical constants. The volume fraction  $V_f$  is the ratio of fiber volume to total volume. Here it is assumed that the fiber array is densely packed in a hexagonal oriented manor (see Figure 4.1).

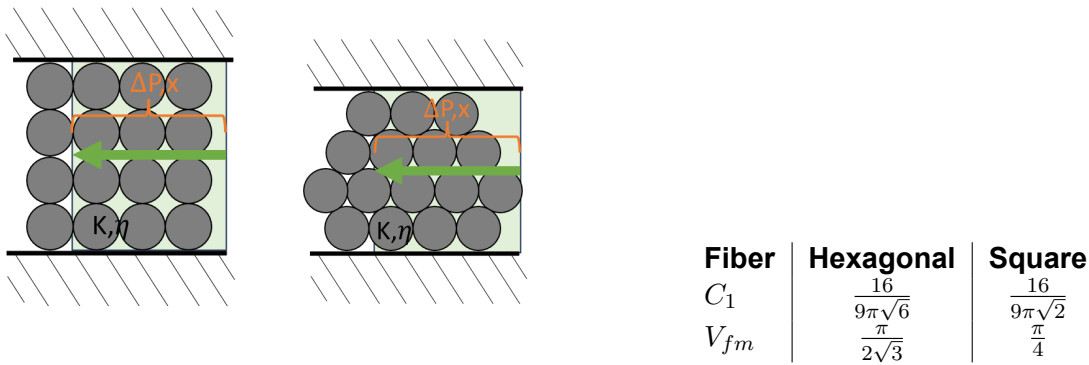


**Figure 4.1:** Theoretical difference in cross sectional alignment of Micro-Fiber filaments; (a) Square array; (b) Hexagonal array; (c) Table with Gebart's constants [56],[23].

Substituting the formula for  $K_r$  in Darcy's law and completing the value for  $x$  provides the following theoretical insight into the various parameters and how they influence the melt impregnation in the fiber bundles (see Eq. 5).

$$x_r = \sqrt{\frac{9\pi R^2}{8\eta} \left( \sqrt{\frac{\pi}{2\sqrt{3}V_f}} - 1 \right)^{\frac{5}{2}} \Delta P t} \quad (4.5)$$

Figure 4.1 shows a simplified schematic representation of the penetration profile. Simply put, the samples were rolled out with a fiber bundle on the left and an excess of TP melt on the right. These parameters collectively contribute to the determination of the permeability of a material. Modifying these parameters can significantly affect the ability of a matrix to flow through a porous medium, influencing the overall permeability of the composite. Based on Equation 4.2, adjustments in these parameters could satisfy the melt impregnation process of composite materials to achieve the desired permeability characteristics for specific applications. [14] [58] [23] [56]

- Time  $t$  represents the impregnation time of the melt pool. Having a longer impregnation time increases the permeability of the polymer melt proportional to the root over time. Increasing the flow path or lowering the print speed increases melt impregnation. [2021 Wang]
- $\Delta P$  denotes the pressure difference in the flow direction. Higher pressure differentials usually lead to higher permeability  $x$  as the force driving the polymer matrix flows more readily through the medium. Like with the time variant, the pressure has root progression.
- $\eta$  Signifies the viscosity of the polymer melt. Decreasing the viscosity increases the permeability of the melt. Lowering viscosity increases the impregnation that is achieved by increasing the temperature. (This parameter is deemed constant throughout this report.)
- The permeability coefficient  $K$  depends on factors such as fiber diameter, fiber packing density, and flow direction. Tensioning the fibers aligns the bundle but results in a smaller penetration depth  $x$ . (This parameter is deemed constant throughout this report.)
- Volume fraction  $V_f$  of the reinforcement fibers in the composite material. The melt impregnation benefits from a lower volume fraction of fibers, gaining a higher permeability as there is an excess of available matrix to flow through the bundle. (This parameter is deemed constant throughout this report.)

### 4.3. Experimental setup

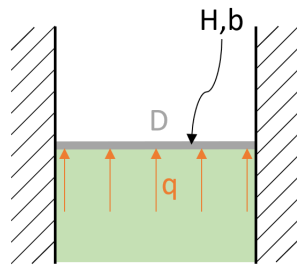
From Equation 4.2 it has been derived that mainly two variables achieve the impregnation of the melt, the difference in pressure  $\Delta P$  and the exposure time  $t$ . Both have a root progression over the crawling displacement  $x_r$  of polymer through a porous medium. The other parameters are assumed constant. Different samples were prepared using the experimental method described in Section 3.2. Basically, the aim is to closely investigate with a microscopic lens whether melt impregnation has actually occurred and if porosities along the interface occur. This will be used as validation of whether the polymer melt is able to permeate through the relatively packed bundle of fibers.

#### 4.3.1. Static Setup

The 'non-pressurized' setup involves an investigation that focuses on the influence of exposure time under heat, excluding the application of pressure differentials. This setup aims to comprehend the singular effect of exposure duration under controlled thermal conditions on melt impregnation. By insulating the exposure time as the driving parameter, this experimental arrangement seeks to discern the impact of extended or reduced exposure periods on infiltration and/or bonding and distribution of TP over the interface. In this setup, the melt pool flows through the fiber driven by thermal expansion, gravitational, and capillary forces. These three forces must be greater than the surface tension of the relatively dense CF bundle. It is expected that the gravitational forces are neglectable and that capillary forces are too weak. The driving force is the thermal expansion pressing against the interface. Based on Equation 4.6 an estimation of the pressure difference by thermal expansion is calculated below:

$$\Delta P = E\alpha\Delta T = 3500 * 10^6 * 135.5 * 10^{-6} * (215 - 20) = 92.5 \text{ MPa} \quad (4.6)$$

The sample is simplified so that an approximation can be made with the beam theory. The TP exerts pressure on the top and bottom of the sample pack when expanding. Suppose that the sides are supported by the static mold. The packing will first break at the top and bottom. The thickness of the packing is 200 microns and the aluminum foil has a UTS of: 310 MPa. If  $I_z = bh^3/12$  and the diameter  $D=4\text{mm}$ , then the pressure is derived by:



$$\sigma = \frac{FLu}{I_z} \rightarrow F_m = \frac{\sigma_{max} I_z}{Lu} \quad (4.7)$$

$$P = \frac{F_m}{A} = \frac{\frac{\sigma_{uts} I_z}{0.5Lh}}{0.25\pi D^2} = 160 \text{ kPa}$$

In theory, the absolute maximum pressure is calculated but will never be reached since the pressure is limited by the strength of the sample packing. This gives a rough idea of the pressure in the packing. Depending on the wall thickness. It can be said that the pressure will never be higher than 1 MPa.

During the experiment, 7 groups with variable exposure times and temperatures were evaluated. Group 1:  $t = 15 \text{ s}$  at  $215^\circ \text{C}$ , Group 2:  $t = 30 \text{ s}$  at  $215^\circ \text{C}$ , Group 3:  $t = 60 \text{ s}$  at  $215^\circ \text{C}$ , Group 4:  $t = 120 \text{ s}$  at  $215^\circ \text{C}$ , Group 5:  $t = 300 \text{ s}$  at  $215^\circ \text{C}$ . In addition, similar groups were investigated under lower  $190^\circ \text{C}$ . In Figure 4.2 a schematic representation is shown.

#### 4.3.2. Pressurized configuration

In contrast, the pressurized configuration and the experimental configuration are tailored to examine the influence of the pressure difference on the impregnation of the melt. The setup

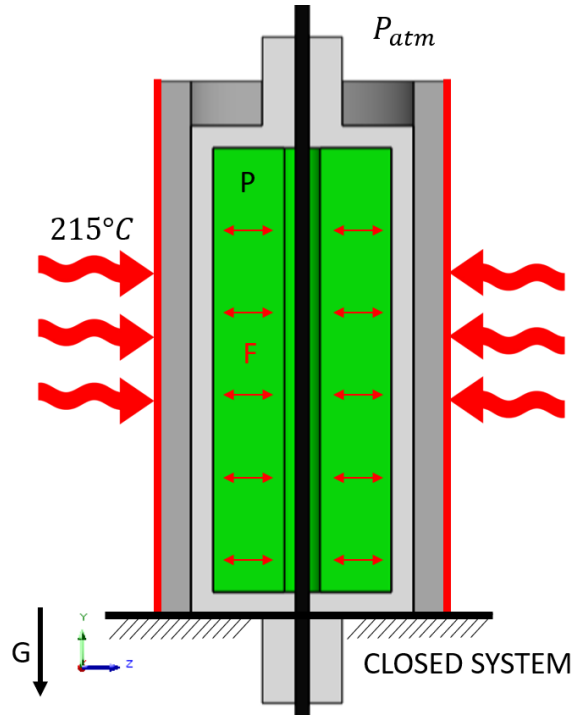


**Figure 4.2:** Cross sectional schematic representing the Static Mold

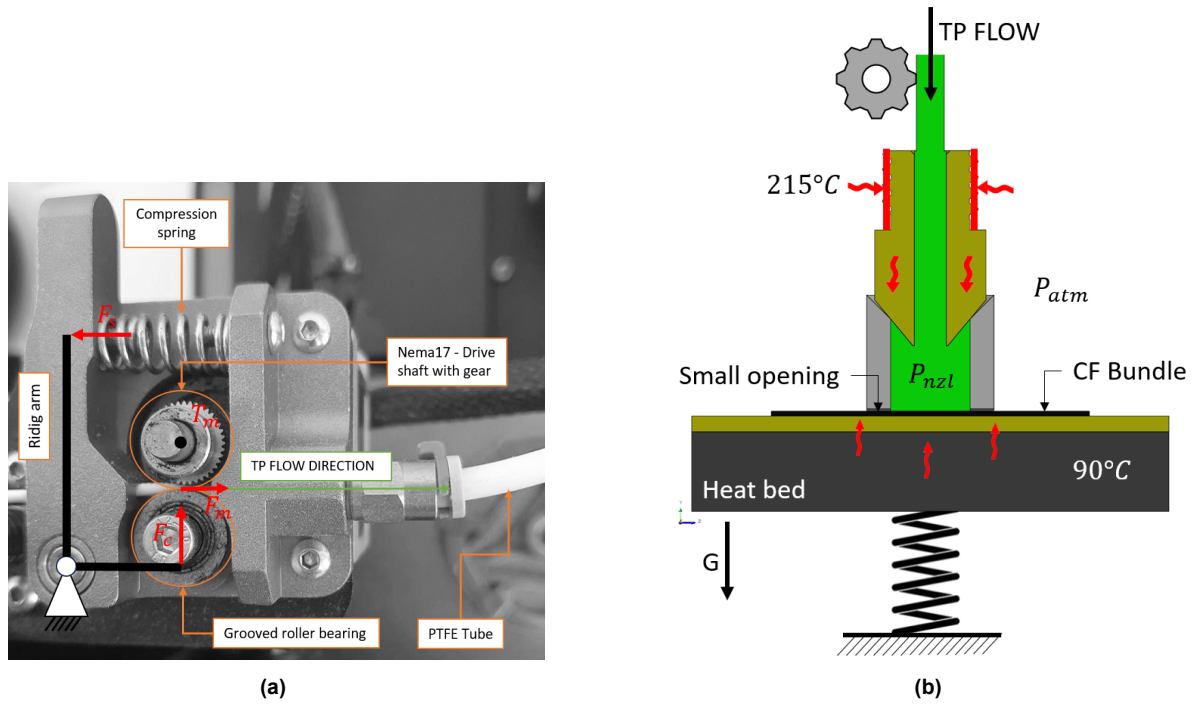
involves the controlled application of pressure differentials across the CF bundle as close as possible to the printer nozzle. This system applies constant pressure within predefined ranges to explore its impact on impregnation efficiency. This setup aims to elucidate how a higher initial pressure affects the flow dynamics. In addition to the constant pressure impregnation and distribution of the TP. The feed Mechanism can exert a force  $F_m$  of 0.4 Nm torque  $T_m$  with the gear having a diameter  $D_{gear} = 10.95mm$ , according to the specifications of the 3D printer manufacturer. In the event of a certain overpressure in the mold, the motor starts skipping which means that the maximum torque is reached. Friction in the PTFE tube is then assumed to be zero and the compression force on the mold is equal to:

$$F_m = \frac{T_m}{r} = \frac{0.4 [Nm]}{0.5 * 0.01095 [m]} = 73.06N \quad (4.8)$$

This corresponds to 7.4 kg of force exerted on the mold that causes an overpressure calculated in Equation 4.8. The opening of the nozzle  $A_{in}$  is drilled with a  $\emptyset 2.0mm$  drill.

$$p = \frac{F_m}{A_{in}} \frac{73.06}{\frac{1}{4}\pi 0.002^2} = 23.3MPa \quad (4.9)$$

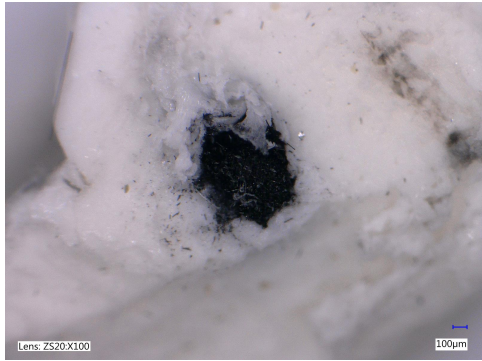
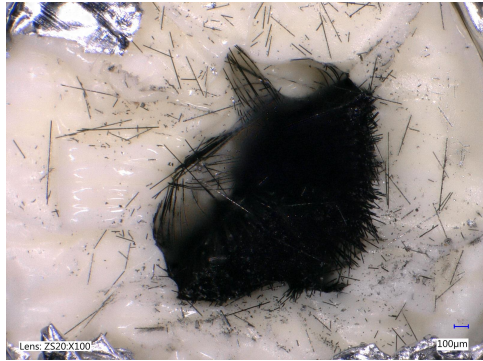
Therefore, in addition to the increase in pressure caused by the expansion of the material caused by heat, an additional pressure of 23.3 MPa is applied. The pressure drop due to fluid velocity can be neglected. However, this calculation is roughly as TP PLA managed to escape. Empirically, it was measured that by extruding 10 mm of feed filament the motor is active for approximately. 5 seconds, so this leaves an exposure time of 30 s that requires 60mm of extrusion, 60s 120mm, and so on. This measurement starts when the mold is full and starts to poring through the small opening. In Figure 4.3 a schematic representation of the configuration is shown.



**Figure 4.3:** (a) Feed mechanism of an Creaality© Ender 3 V2; (b) Cross sectional schematic representing the Pressurised Mold

### 4.4. Microscopic results

Moving beyond the experimental setups, the subsequent section employs advanced microscopic analysis using a Keyence VHX-6000 digital microscope (see Figure B.6 in Appendix B). This analysis details the microscopic examination of the impregnation process imitating the "in-nozzle" impregnation. Two experiments, described in Section 4.3, have been performed. In table 4.1 & 4.2, figures from the microscopic analysis are shown. Five different time-measurement points have been chosen to determine the progression of melt impregnation. After the heat treatment, the samples are removed from the setup and carefully grinded to make the CF bundle internally visible. To ensure that the polymer does not melt and re-solidify disrupting the experiment, grinding was performed in a bowl of water.

Time (s)	Static mold (Temp = 215°C)	Static mold (Temp = 215°C)
15		



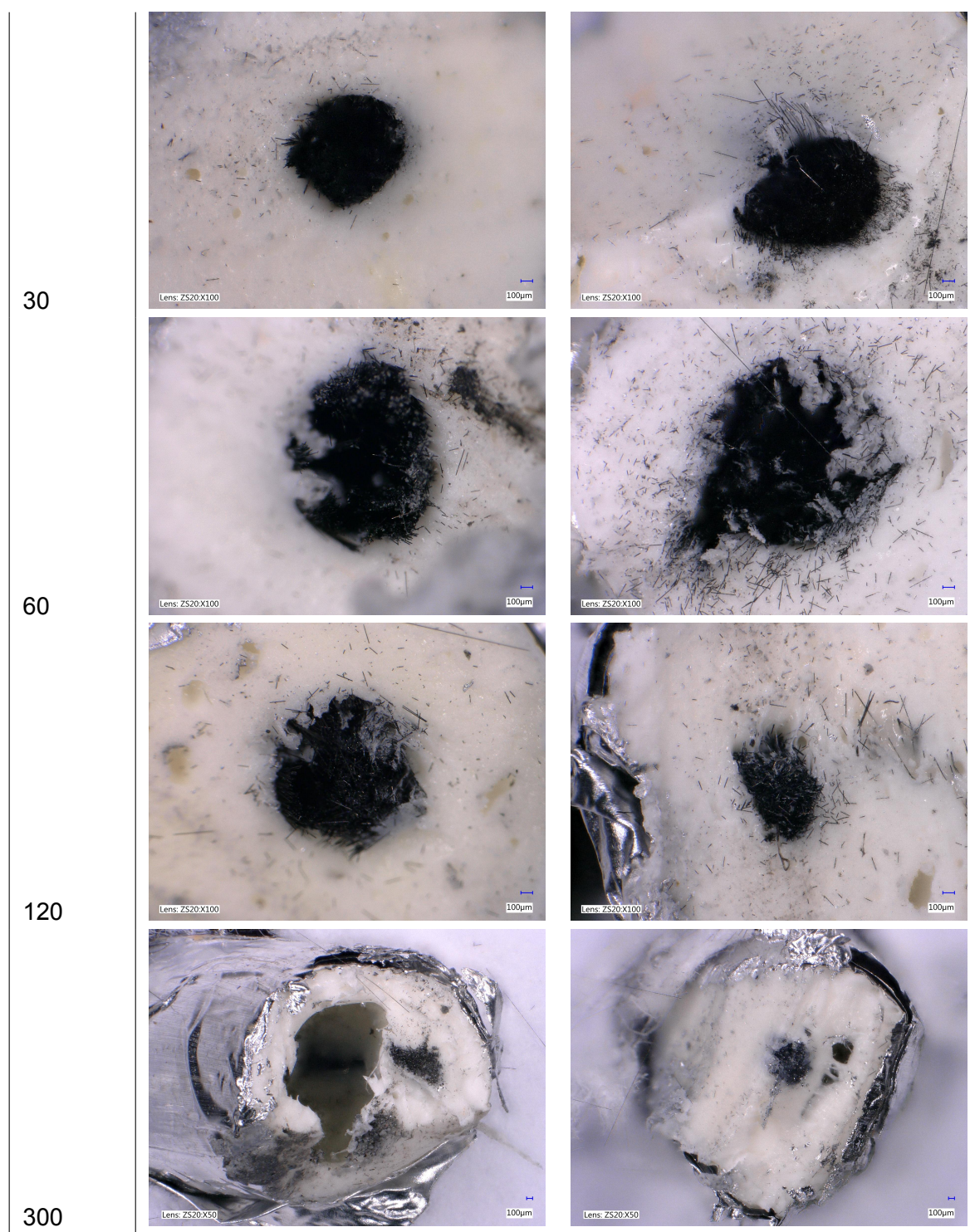


**Table 4.1:** Microscopic analysis by the Keyence© VHX-6000 Digital microscope of C-C-FRTP composites, produced by the experimental static setup described in Section 4.3

Microscopic observations, presented in Table 4.1 show interesting characteristics. In the figures, the black dot is the fiber encapsulated by PLA melt (white). The compound is packed in (silver) aluminum thin foil.

It is observed that samples exposed to heat for 15 seconds show inadequate heat diffusion and that the matrix did not have the time to flow around the fiber. The existing air gap between

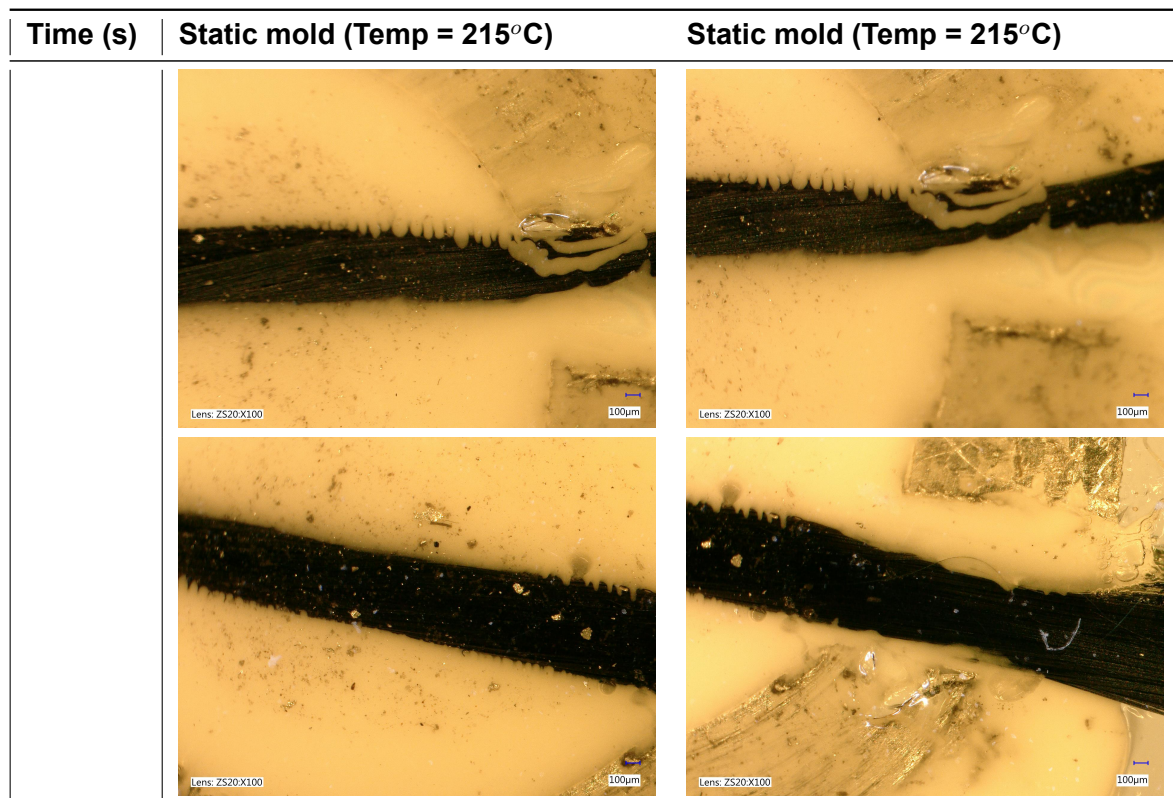
bulk fiber and bulk matrix is not filled. Subsequently, samples exposed for 30 seconds showed a more compact and cleaner interface between matrix bulk caused by enough heat diffusion, melt flow, and thermal expansion. This means that the matrix started to flow towards the bulk fiber and started to exert pressure on the fiber.

Around 120 seconds aluminum foil fracture is observed. TP melt starts to flow out of the boundary of the closed system. This means that the internal pressure is high, pushing the TP melt outward. In the microscopic images small cavities appear in the PLA. These cavities are caused by the expansion and withdrawal of melt. TP melt flows away and is unable to flow back. In addition, the rate of cooling was low, allowing for more semicrystalline regions to be formed with a higher density.

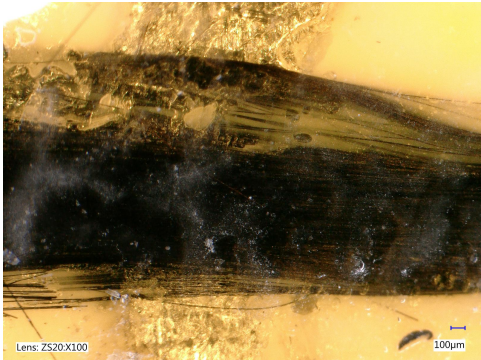
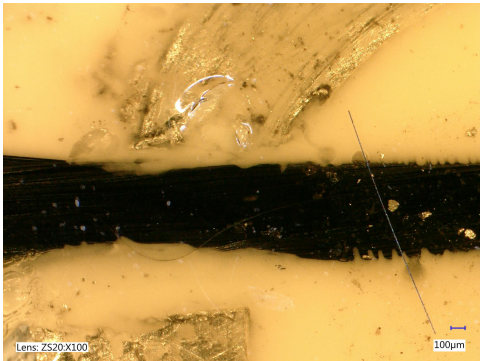
Further increasing the exposure time towards 180 and 300 seconds shows expansion of cavities. By forming the large cavities around 300 seconds. Despite the emergence of larger cavities in the 300-second exposure group, remnants of PLA were still observed adhering to the fiber surface.

A discussion can be raised about the origin of the cavities. In addition to melt expansion and flow out of the boundary. Air bubbles in the air gap could be trapped expand.

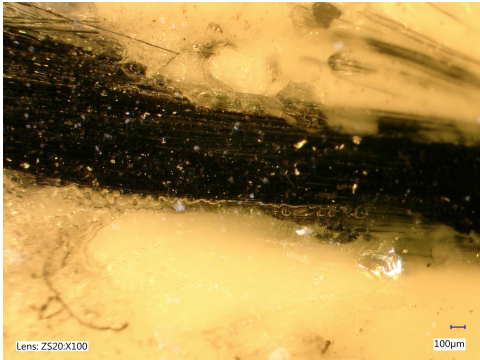
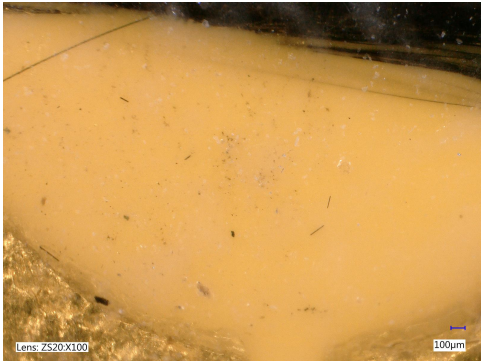
These findings suggest a positive correlation between exposure time and interface characteristics when exposure time is short, highlighting the critical role of time duration in achieving optimal impregnation without compromising the integrity of the matrix interface.



15-30



30-60



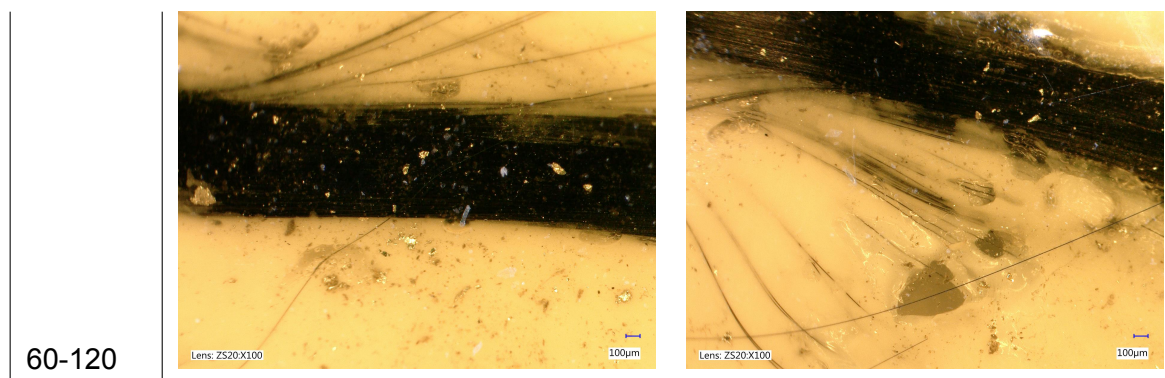


**Table 4.2:** Microscopic analysis of C-FRTP composites under the Keyence© VHX-6000 Digital microscope. Samples were manufactured using a dynamic mold that adds additional pressure and PLA overflow by a modified 3D printer

Observations from the dynamic mold experiment reveal different phases during the impregnation process. Initially, for the duration between unrestricted PLA overflow and pressure application up to 30-60 seconds, a notable occurrence was the matrix around the fibers. There was no formation of air bubbles and a very fast interface formation.

As the experiment progressed from 60 to 120 seconds, a transition was observed, showcasing a remarkably smooth interface between the polymer and the fibers. However, after reaching the 300-second mark, smaller bubbles began to appear within the matrix. It is noteworthy that while bubbles did emerge, their overall size remained relatively small. It seems that the pressure of the PLA pushes these bubbles away. This observation contrasts with the static experiment phases, where larger cavities were prominent.

This delineates a dynamic process, indicating distinct phases in impregnation dynamics, with initial overflow, transition to a smooth interface, and the eventual appearance of smaller bubbles/cavities. The presence of these smaller bubbles after extended timeframes suggests the complexity of impregnation dynamics and the impact of prolonged exposure times on bubble formation during the impregnation process.

# 5

## Interfacial shear strength

From Chapter 4 it is observed that the TP is too thick and treachy to penetrate the fiber. This means that the C-CFRTP strength must come from the interfacial shear strength (IFSS) or simply adhesion between the two constituents. First, a theoretical framework at the mechanical properties of C-CFRTP and their adhesion strength are researched. Then a tensile test is performed to identify the bonding strength. Finalizing a visual analysis has been performed using a microscopic apparatus.

### 5.1. Modified rule of mixture

Straightforward the rule of mixture gives an insight in overall strength at the composite level. However, with C-CFRTP printing through FDM technology, this mixture rule is modified involving aspects such as 'porosity correction factor  $(1 - \varphi)^2$ ' quantifying the effect of porosity that results in stress concentration in the material. and 'Fiber orientation  $\eta_0$ '. In single unidirectional fibers, these terms can be simplified to  $\eta_0 = 1$  and  $\varphi \neq 0$  (Chapter 4, porosities appear and limited impregnation) [26]. Given the elastic modulus and tensile strength of C-CFRTP as follows, in equations 5.1 and 5.2 [25]

$$E_c = (\eta_0 E_f V_f + E_m V_m) (1 - \varphi)^2 = (E_f V_f + E_m V_m) (1 - \varphi)^2 \quad (5.1)$$

$$\sigma_c = (\eta_0 \sigma_f V_f + \sigma_m V_m) (1 - \varphi)^2 = (\sigma_f V_f + \sigma_m V_m) (1 - \varphi)^2 \quad (5.2)$$

And with  $V_f$  and  $V_m$  being the volume fraction of fiber and matrix volume fraction. In the case of cylindrical samples with a cylindrical-shaped fiber thread internally, The following holds:

$$V_f = \frac{V_{fiber}}{V_{composite}} = \frac{\frac{1}{4}\pi L D_f^2}{\frac{1}{4}\pi L D_c^2} \quad (5.3)$$

$$V_m = \frac{V_{matrix}}{V_{composite}} = \frac{\frac{1}{4}\pi L (D_{m.out}^2 - D_{m.in}^2)}{\frac{1}{4}\pi L D_c^2} \quad (5.4)$$

### 5.2. Adhesion engineering

The effectiveness of the load-bearing capacity of the composition C-CFRTP depends mainly on the adhesive strength of the bond between the CF and the TP. This fiber-matrix bond, known as Interfacial Shear Bond Strength (IFSS), or referred to as "pull-out" resistance to shear, significantly influences the overall mechanical efficiency of the composition. However,

characterization of the FRTP interface is a challenging process since this is subject to multiple variables in which different mechanisms affect the bond. This phenomenon is extremely complex since it not only involves the 2D interface between the two constituents but also diffuses bulk material around the interface. Any weakness in this zone may result in premature failure of the composite during external loading. The mixing of materials during printing can also affect the quality of the print, and pre-processing techniques, such as heating or chemical treatment, can improve the compatibility of the material [56]. Due to the complexity of the area of the interfacial bond, research is conducted at three distinct levels [7].

- Molecular interaction level research aims at identifying molecular interaction at the interface. The main mechanics of adhesion are investigated.
- Micro-level research tries to characterize the interfacial mechanical properties and provides information about the fiber matrix failure modes at the interface.
- Composite level - Aims to identify the overall mechanical properties of the composition and tries to find the effect of interfacial properties.

In this study, mechanical properties are identified in micro-level research according to the above classifications. This means that the relation between melt impregnation and tensile strength influenced by the exposure time in the heat block and the pressure that prevails is investigated. This is analyzed by testing the fracture mode related to the 'pull-out' resistance of the attachment. Subsequently, the four main adhesion mechanics at the interface are recognized as follows. These mechanical properties govern the strength of the interfacial shear strength (IFSS) and define the strength of the bond. However, it is nearly impossible to identify which adhesion mechanics play a key role at a particular moment since this will bring about a more detailed study of multiple engineering branches. According to Carnavale, the following mechanics of adhesion affect the overall strength of the bond [7]:

- Chemical bonding (adhesives, sizing agents)
- Molecular interaction (London forces, Vander Waals forces, acid-base interaction)
- Mechanical interlocking
- Residual stresses

It's been pointed out that a composite material will not reach its best performance unless the connection between the Fiber and matrix is strong enough to transfer loads from the matrix to the Fiber without breaking too soon. The general mechanical properties of the C-CFRTP load bearing structure are defined by the stress transfer between soft thermoplastic and hard fiber through the interface [45]. Wang et al. [56] investigated the impact of the percentage of melt impregnation on the tensile strength of a single composite strand. Higher impregnation percentages, particularly, result in increased tensile strength, reaching the highest mean value of 221.78 MPa for Nylon/CF. The research concludes that optimizing process parameters, including low transverse movement speed, high nozzle temperature, and small layer thickness, improves impregnation percentage and improves the tensile strength of a single composite strand.

Conflicting here is that [56] observed melt impregnation through the Fiber, while in Chapter 4 shows almost no impregnation. This could have been caused by differences in the packing and the number of microfilament packing. Wang et al. modified a printhead to extrude C-CFRTP through it causing some difference in the observations.

However, it is observed that processing methods also affect fiber-to-matrix interface bonding. The curing conditions, such as temperature and pressure, can affect the cross-link density

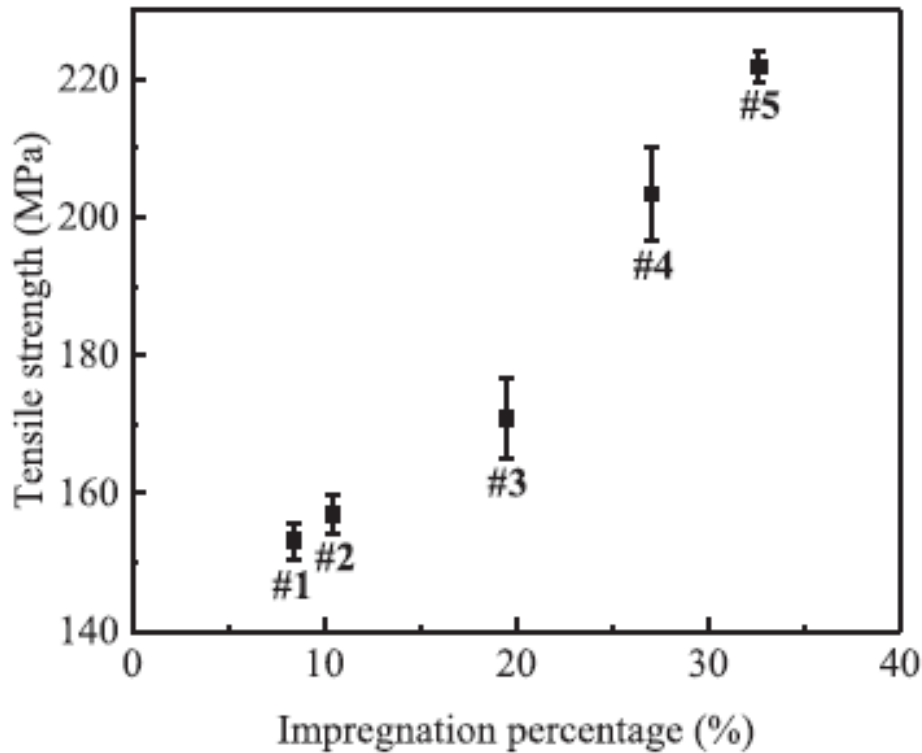


**Figure 5.1:** Effect of impregnation percentage on the tensile strength of a single composite strand. Adapted from [wang 2022]

of the matrix material and its interaction with the CFs. High temperatures and pressures can enhance the interfacial bonding by increasing the cross-link density of the matrix and promoting diffusion of the matrix material into the fiber surface. However, excessive curing temperatures and pressures can also cause degradation of the fibers and reduce the interfacial bonding.

Typically, TP have significantly higher thermal expansion coefficients ( $130 * 10^{-6} K^{-1}$ ) compared to CF reinforcement ( $15 * 10^{-6} K^{-1}$ ). During the cooling process, compressive radial stress  $\sigma_r$  arises at the interface [48]. This is influenced by the cooling rate, which affects the crystallization process. If assuming that the coefficient of static friction  $\mu_s$  exists at the interface, Coulomb's friction law ( $f = \mu N$ ) suggests that these compressive stresses contribute a frictional component,  $\tau_f = \mu_s \sigma_R$ , to the shear strength of the interface.

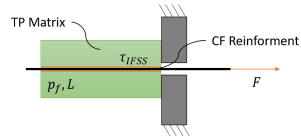
### 5.3. Experimental Methodology

In this section the experimental methodology for evaluating the IFSS of C-CFRTPs is described. Unfortunately, due to insufficient knowledge provided in the literature and the lack of a standardized test method to test C-CFRTP samples, various approaches have been employed to assess the bonding strength accurately. Therefore, this experiment is described chronologically to support future research in specific design choices and test analysis.

To analyze the pull-out strength of the composition, samples have been prepared and tested on a tensile test bench provided by the TU Delft PME laboratory. Unfortunately, no standardized tensile test bench is prescribed to experiment with the IFSS of a single fiber. Therefore, modified single fiber samples have been developed to be further investigated based on early single fiber research reports and the available heat treatment equipment described in Section 3.2. However, in the literature, multiple pull-out techniques have been utilized [57] and described [2], [49]. Five different techniques are (1) Pull-out test, (2) Fragmentation test, (3)

Push-out test, (4) Pull-through (microdroplet) Test & (5) Compression test. However, considering the extreme resistance to a tensile load of single fiber bundles and the weak resistance to compression and shear. The test of individual fibers is limited to the tensile test (1), (2) & (4).

From the pull-out experiment, a force curve ( $F$  in [N]) and a displacement curve (mm) are generated as output. The maximum force  $F_{max}$  [N] exerted by the tensile bench is used to calculate the IFSS or bond  $\tau_{IFSS}$  using the following formula (see Equation 5.5 [13]).



$$\tau_{IFSS} = \frac{F_{max}}{P_f L_e}, \quad (5.5)$$

Where  $L_e$  [mm] describes the embedded length of fiber in the matrix. The perimeter in the plane  $P_f$  is defined as a circular-shaped ( $\pi D^2$ ) interface. However, this is a very rough assumption, but it is reliable for this calculation proven by [47].

Two typical methods for fiber testing were employed: the pull-out technique and the microdroplet or pull-through technique. However, the microdroplet technique was selected since the other technique requires clamping on the relatively weak TP PLA, which could preliminarily deform and damage the interface by squeezing, which could disrupt the results. The observations from Chapter 4 revealed an issue where the polymer began to seep from the sample due to inadequate strength in the mold walls. To rectify this, the samples were reinforced with thicker pieces of aluminum foil to reinforce the structural integrity of the molds. This is crucial to maintain the samples' shape and prevent poor structural integrity along the interface.

Besides, to prevent a random error, each sample group contains three tests. The results of distorted samples are removed but evaluated to avoid further mistakes. The tensile test bench from the TU DELFT laboratory was utilized for the experiments. This machine has two clamping jaws. The test bench was extended with modified equipment to perform the tests. The machine preloads the samples at 0.2 N before applying an excessive tensile load at a 10mm/min rate.

### 5.3.1. Experiment 1: Single pull-through test

Evaluating the tensile bench, the samples are clamped. Clamping may deform the interface, and thus, the pull-through technique was chosen for the first experiment. This involves securing one end of the fiber within the beaks of the tensile bench while the opposing beak holds a tight gap through which the sample was pulled. The primary samples, described in Section 3.2, were pulled through a small opening in a specially made bracket (see Figure 5.2). This approach allowed the evaluation of the shear resistance  $\tau_{IFSS}$  of the fiber in the TP matrix. The jaws holding the fiber did not apply enough friction to apply full load on the interface. By trial and error, an attachment was added, and increased friction force was noted. CF interfacing a jaw material has a more significant friction coefficient than the mutual friction between the fiber sitting in the middle.

### 5.3.2. Experiment 2: Dual pull-through test

Since the test results of the experiment gave a relatively unreliable fluctuating result, in Experiment 2, a modified form of the pull-through technique was executed. As illustrated in Figure 5.4, the samples underwent a dual pull-through test using a different setup than Experiment 1. Rather than employing a single-ended clamping and pulling through a tiny slit, two modified L-shaped brackets were utilized in this test. These brackets were designed to hook in the sam-



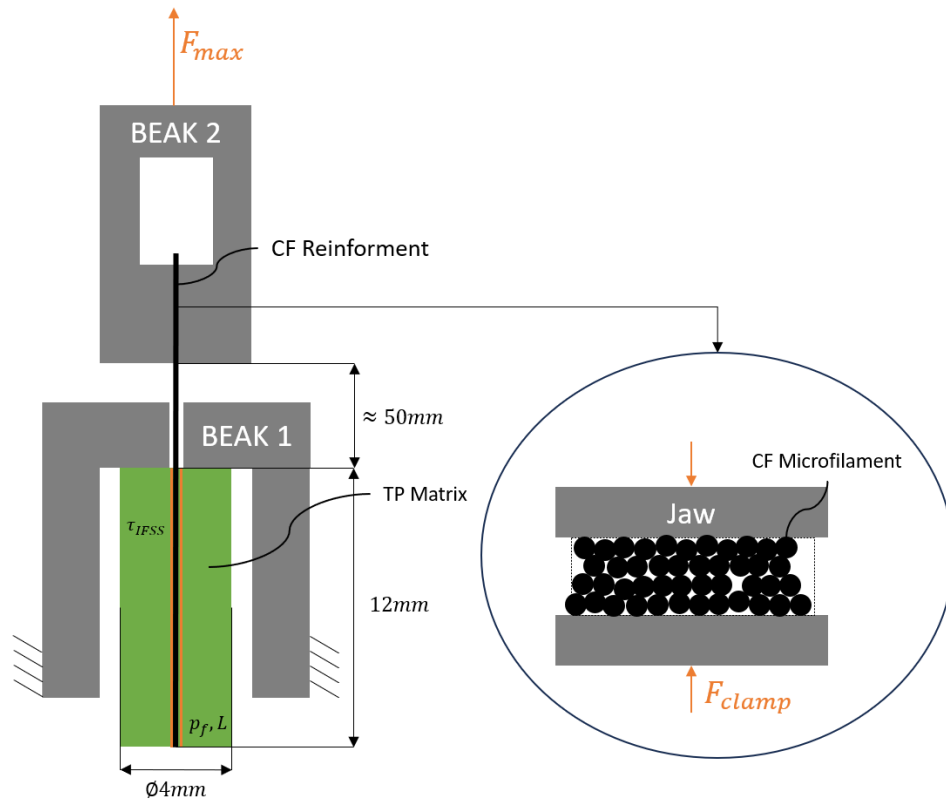


**Figure 5.2:** Schematic representation of test setup used for experiment 1. A cross-sectional breakout is sketched of fiber alignment in the beaks

ple, leaving the CF reinforcement exposed. The samples were secured within the modified L-shaped brackets, ensuring a minimal distance between the pulling ends to limit the effect of microfilament peeling. Subsequently, the tensile bench was used to pull the samples apart, facilitating the assessment of interfacial adhesion and resistance to pull-out forces.

### 5.3.3. Experiment 3: Modified dual pull-through test

The exposed fiber clearly showed an unreliable behavior. The weakness of the exposed fibers dominated the samples. Thus, in experiment 3, a modified dual pull-through method was utilized. Therefore, a third experiment was performed where the exposed reinforcement was now enclosed with polymer.

## 5.4. Analysing stress-strain curves

### 5.4.1. Polymer stress-strain curves

In general, the following holds for the stress-strain curves of different materials. This preliminary investigation on thermoplastic stress-strain behavior and debonding curves will help analyze the results later.

#### Thermoset polymers:

Behave like Brittle materials exhibit high strength, enduring substantial stress but allow for minimal stretching and sudden fracture upon reaching its breaking point.

#### Thermoplastics polymers:

Behave as Ductile materials with a larger elastic region, characterized by a linear stress-strain relationship. The elastic limit (at tensile yield strength) indicates that linearity disappears and

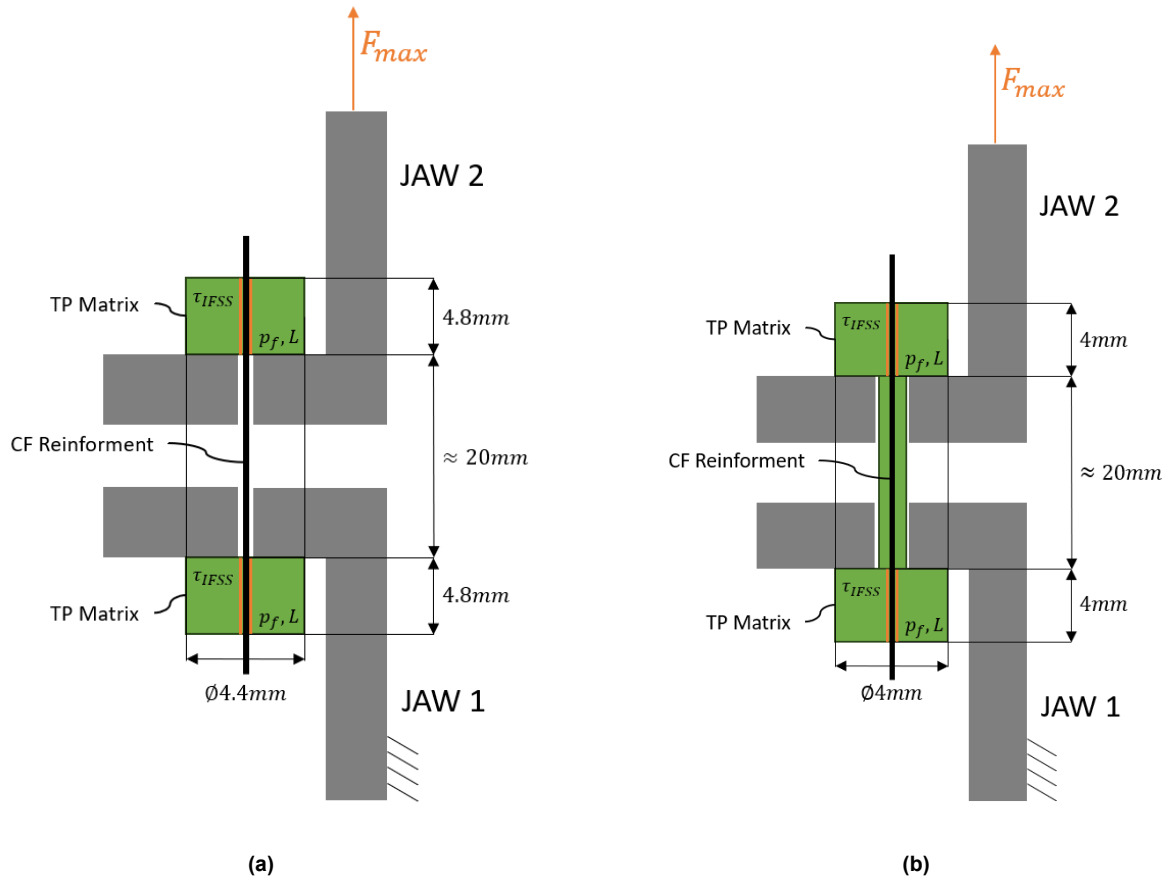


**Figure 5.3:** Schematic representation of the different test setup using the pull-through tensile approach for (a) Experiment 2 and (b) Experiment 3.

the material loses its ability to recover to its original shape. The ultimate tensile strength, observed at the second peak, represents the maximum stress a material can withstand before fracturing.

#### 5.4.2. Pull out debonding

Figure 5.6 shows a schematic representation of a load-displacement curve of a single fiber pull-out test. The area origin to point A shows an elastic region. From A to C, the debonding progresses until complete debonding. At point C, fiber pullout occurs. This means that static friction has been overcome. The load drops, and the fiber is pulled out [5].

### 5.5. Test results

In this section, the tensile test results from experiments 1, 2, and 3 are discussed (see appendix C). Load [N] - strain [mm] curves have been generated from the tensile bench. The raw data can be found in the (a) force-displacement curves. On the Y-axis, the Force  $F_m$  on [N] is plotted against the displacement  $X$  on [mm] on the x-axis. The plots are evaluated, and the (b) shear stress-strain curves are calculated. Detailed analysis and interpretation of the obtained stress-strain curves are conducted to explain observed behaviors. These curves are important for understanding the mechanical properties of the interface between TP and CF. The analysis utilizes previously explained formulas to determine the stiffness of the interface, breaking it down to elucidate multiple regions of stiffness observed. The shear stress is evaluated using Equation 5.5. The strain is derived from the perimeter of the fiber multiplied by the length of

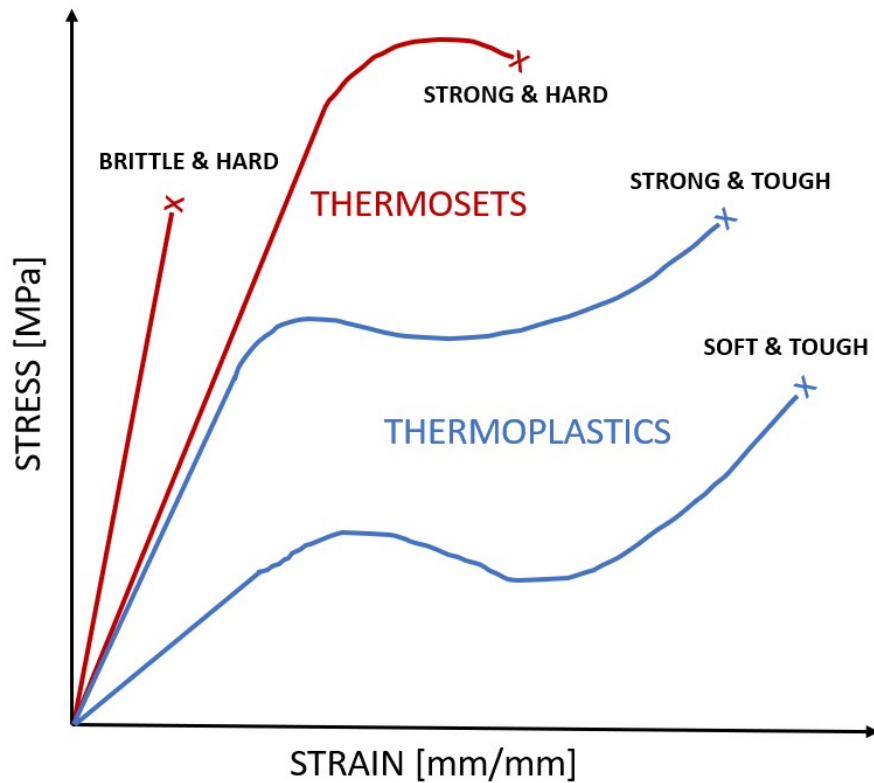


**Figure 5.4:** Schematic representation of characteristic stress-strain curves for Thermoset & Thermoplastic polymers. partly adopted from [16]

the sheared section. The following observations have been made during analysis using the tensile test bench:

### 5.5.1. Exposed Carbon Fiber

Single CF test (see Appendix C) was evaluated. Single CF threads have been tested to investigate the behavior of CF under tensile load. Understanding the behavior of the carbon fiber was imperative to distinguish specific characteristics within the IFSS test curves at the C-CFRTP sample. From this plot, the fiber's elastic modulus, determined within the elastic region, was lower than the datasheet's suggested value when evaluated using Hooke's law.

$$\sigma = E\varepsilon \longleftrightarrow E = \frac{\Delta\sigma}{\Delta\varepsilon} = \frac{342.465 - 231.767}{0.00262 - 0.00196} = 168000 \text{ MPa} \quad (5.6)$$

The maximum tensile load experienced by the fiber has an average around  $\sigma_{UTS} = 510 \text{ MPa}$ , which is lower than the value indicated on the datasheet. The rounded top of the stress-strain curve clarifies this. During the testing, it was observed that the microfilament of the CF started to break.

### 5.5.2. Neat thermoplastic polymer

Also, neat TP PLA has been evaluated to distinguish the behavior. From the analysis, the PLA exerted an average tensile strength  $\sigma_{UTS} = 30.4 \text{ MPa}$ . Note that the same sample has been used and that the PLA is heated up for 60 seconds to make sure that the PLA fully distributes over the neck. The experiments were carried out in chronological order (1), (2) & (3).

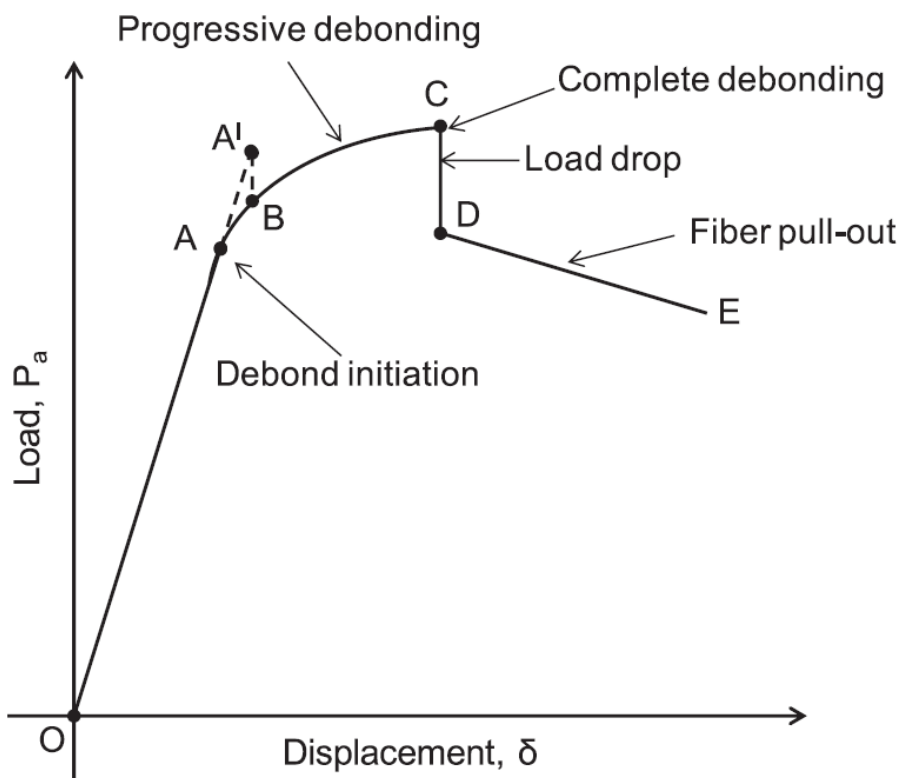


**Figure 5.5:** Load-displacement curve of a (single) Fiber pull-out process. Adapted from [2013, Bheemreddy]

### 5.5.3. Experiment 1: single pull-through test

- In a particular research group, heat was applied for 15 seconds, yet there were no observable adhesive results. Consequently, no strength outcomes were obtained.
- When processing the test results, a noticeable trend indicates an increase in the maximum shear strength. This trend is characterized by a clear upward movement or increase in the values representing the maximum shear strength in these plots.
- The rounded behavior observed at the tops of the force-displacement curves suggests a specific characteristic. Indicates that the fiber reaches a certain limit. The sample observation clarified that the microfilament that does not interfere with the matrix failed. Beyond that peak, the fiber is slowly pulled out and cannot sustain additional force.
- At 120 seconds, little load drops develop moving beyond the peak; these load drops increase when the exposure time is increased also
- The curves start with increased stiffness as more load is applied. At around 0.5mm of displacement, the stress-strain curve follows a linear elastic pattern. All results show the same linear elastic behavior except for the green and blue plots from plot 5a.

### 5.5.4. Experiment 2: Dual pull through

- The extended period observed before reaching the ultimate maximum tensile force primarily results from the initial compression of the aluminum foil situated between the sample and the jaws of the testing apparatus. This compression phase introduces a delay in achieving the maximum pulling force during the tensile test.

### 5.5.5. Experiment 3: The modified dual pull-through test

experiment shows a more reliable outcome. The curves are very close to each other, and the behavior of the curves looks similar. It can be said that this experiment gives a reliable result.

### 5.5.6. IFSS v Exposure Times

An investigation is presented into the relationship between exposure time under heat and maximum interfacial shear stress. The graphical representation indicates an upward trend in strength up to 200 s of exposure time, followed by a decline. The observed trend is explained on the basis of the findings discussed in Chapter 4.

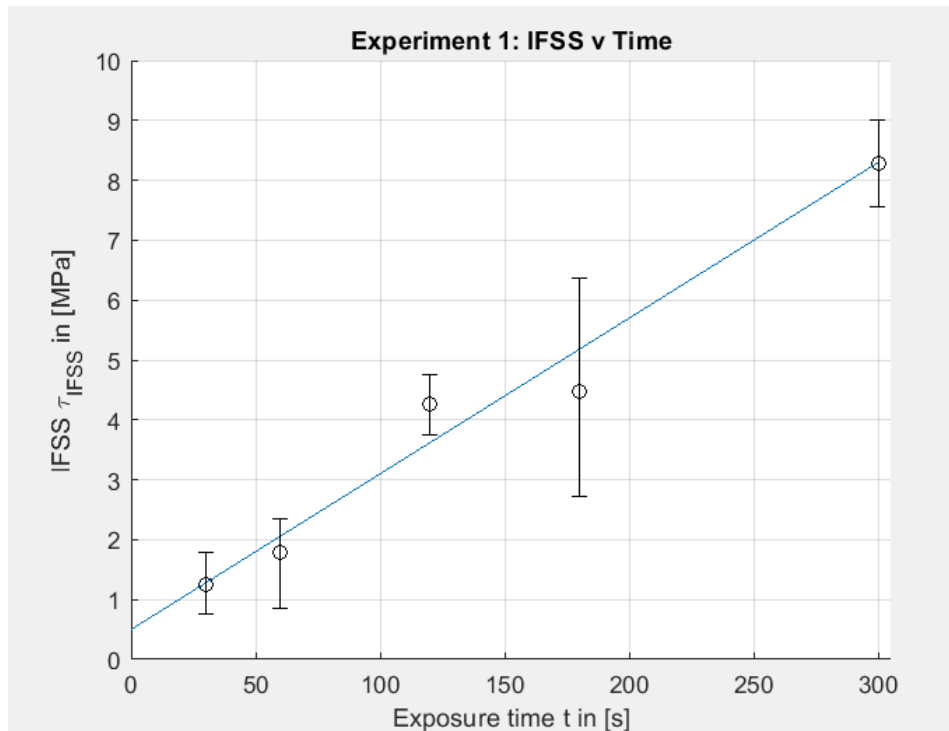


**Figure 5.6:** Evaluated test results showing the exposure time t in [s] against the IFSS  $\tau_{IFSS}$  for experiment 1

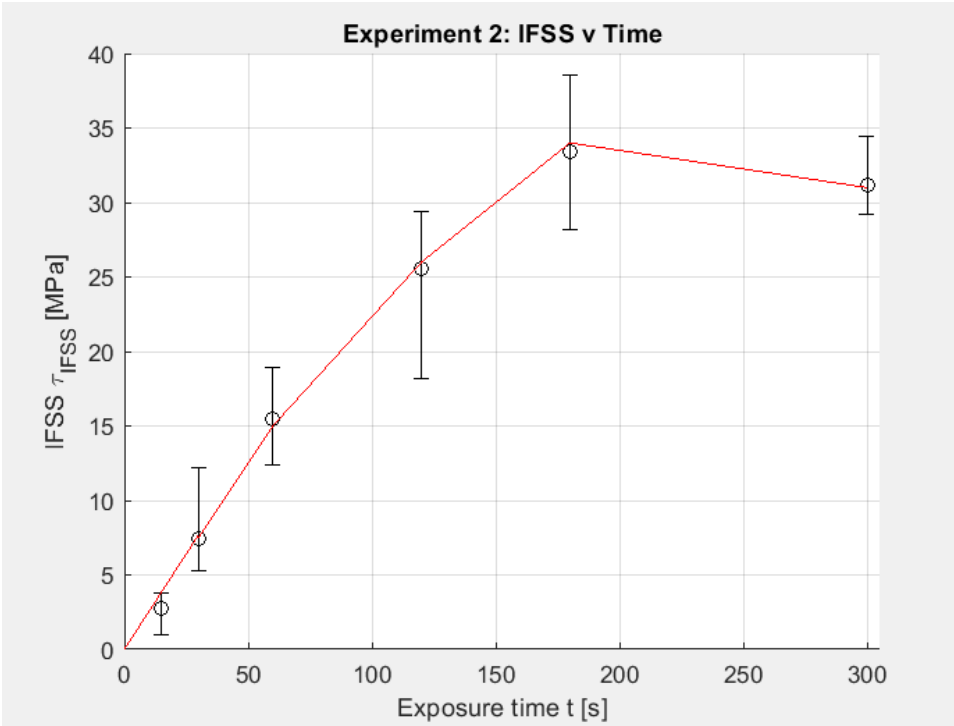


Figure 5.7: Evaluated test results showing the exposure time t in [s] against the IFSS  $\tau_{IFSS}$  for experiment 2

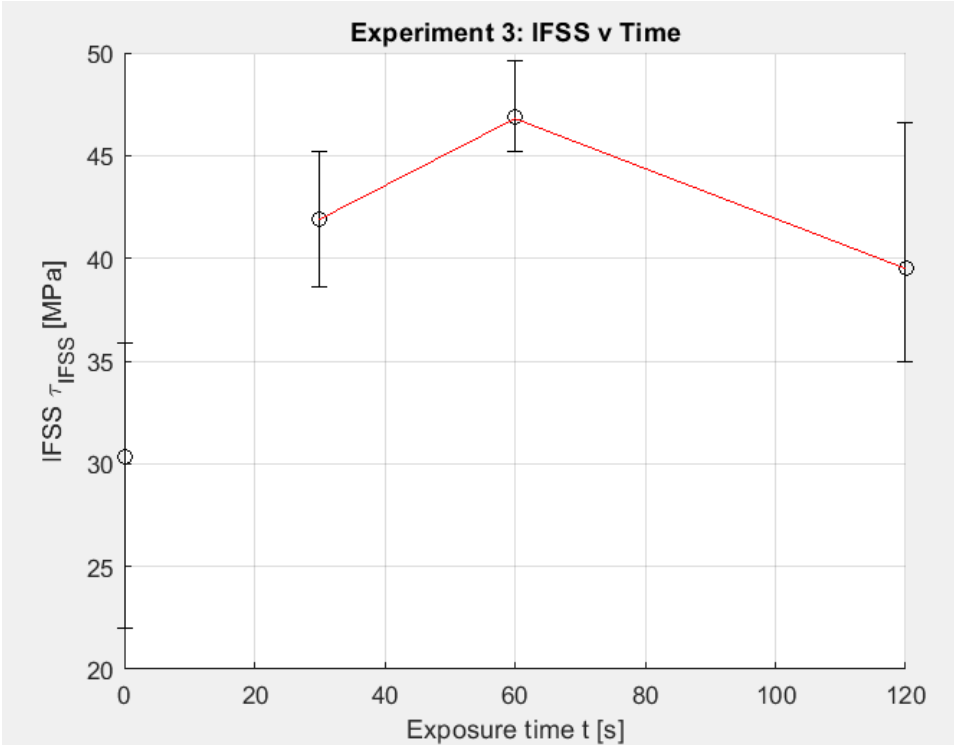


Figure 5.8: Evaluated test results showing the exposure time t in [s] against the IFSS  $\tau_{IFSS}$  for experiment 3

# 6

## Discussion

### 6.1. Methodology

In the discussion of our research methodology, a critical aspect relates to the samples that were fabricated and analyzed. Challenges encountered was the need to maintain a small volume due to the testing of single fibers with minimal diameters. Looking ahead, expanding the work volume would be beneficial. A larger mold could help stabilize temperatures more effectively, producing more consistent results.

In this study, it has been chosen to perform an experimental investigation using a real sample. In the future, it can be investigated to perform a numerical analysis on C-FRTP printing. The availability of equipment made it easy to perform simple experiments to verify the feasibility of this approach to fabricate composites.

Another significant point concerns the packaging of the sample. The swelling behavior of TP requires a very tight packing of the samples. During the experimentation, the removal of the packaging faced difficulty with the aluminum foil adhering firmly to the TP PLA. This adhesion made it challenging to remove the foil without risking damage to the matrix or reinforcement. However, in section 5.5.5, modifying the sample successfully addressed this issue. Future studies might explore alternative materials or methods for sample packaging to avoid such challenges and potential damage to the samples during handling. The drawback is the exposed fiber.

### 6.2. Data evaluation

From chapter 2, the literature survey suggests that C-FRTP composites are high in strength, flexibility, impact resistance, and a lightweight solution for the industry. However, from the experimental research performed in this study, research states otherwise:

#### 6.2.1. Limited melt impregnation

In Chapter 4, it is observed that C-FRTP printing through FDM technology is limited by the challenges related to the melt impregnation of fibers with the TP matrix. This limitation stems primarily from the high viscosity of the thermoplastic materials (PLA) and the dense fibers. The TP matrix is obstructed from penetrating in between the fiber and limits to envelop the CF perimeter. In this scenario, The interface significantly relies on pressure by the TP matrix against the interface with the fiber. This concludes that the adhesion and interlocking largely depend on the frictional force. Moreover, it should be noted that pressing the molten TP against the fiber's perimeter contributes to a decrease in permeability, further hindering its ability to infiltrate the spaces between individual fibers. Notably, the permeability of thermoplastics through

fiber is low but not fully obstructed, and some fiber has been successfully encapsulated within short exposure times. However, this incomplete penetration may compromise the effective reinforcement of the composite material and potentially affect the mechanical properties of the printed parts. In Figure 6.1, a schematic representation of the deposited C-FRTP composite is sketched at the exit.

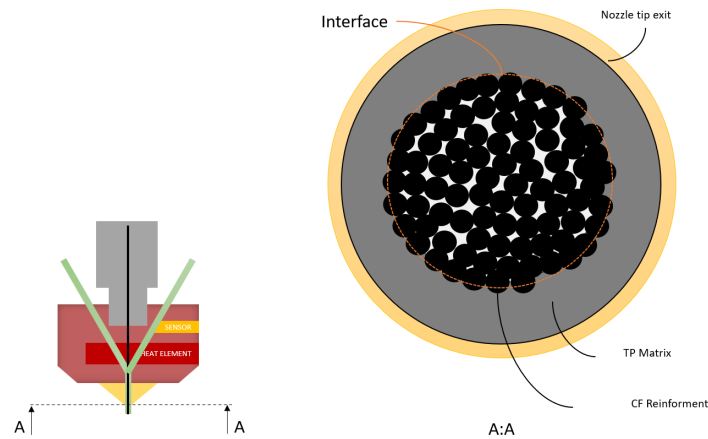


**Figure 6.1:** Schematic representation of the standard nozzle exit now utilized for C-FRTP 3D printing. Ideally, the CF is sitting concentrically in the matrix.

### 6.2.2. Reinforced thermoplastics

As previously discussed, C-FRP composites derive their strength from the bonding between the high-tensile-resistant fiber and the elastic matrix bonding agent. However, the melt impregnation process needs to be improved, resulting in incomplete permeability. Consequently, the bond is primarily based on weak mechanical interlocking and friction generated by the pressure applied by the matrix. In particular, tensile strength analysis experiments revealed that extended exposure time correlates with increased pull-out resistance. It is important to note that the fiber's strength is constrained when exposed, while complete encapsulation significantly reinforces the fiber.

The matrix's exertion of pressure enhances the composite's overall strength, particularly when the fiber is fully encapsulated. This difference in strength between exposed and encapsulated fibers indicates the importance of complete encapsulation for reliable test results. Therefore, it can be concluded that encapsulating the fiber with the matrix material yields considerable benefits. However, to maximize the effectiveness of this encapsulation, more research and experimentation should focus on improving the permeability of the TP matrix. This could improve the overall impregnation process and subsequently enhance the mechanical properties of the composite material.

Considering thick TP and impenetrable fiber, other parameters may contribute to an increase in IFSS and thus increase the contact surface. Increasing the interface contact surface could enhance the overall strength of the composite. Conceptual options without the need for other bonding agents or chemicals are listed below.

### 6.2.3. In nozzle pressure advantage

The dynamic mold experiment (see chapter 4) showed that external pressure and polymer overflow aided in smoother and faster melt flow around the interface, compared to the findings with the static experiment. The influence of pressure had a more significant impact on the formation of the interface. However, this also underscores the complexity of impregnation



dynamics, indicating that sustained pressure can positively aid impregnation and adversely affect the material's integrity over time. Due to short time and limited resources, a dynamic experiment must be performed to analyze the impact on the IFSS. The static experiment already shows a good impression but needs further experimental investigation.

Various C-FRTP FDM printing methods have been proposed by earlier researchers. However, the findings show that pressure is more a driving factor than time. However, as Darcy's law suggested, pressure does not thrive without time. Let's assume that 'ex-nozzle' and 'in-nozzle' have the exact available fusion times but differ in the location of the fusion. It is foreseen that the pressure building inside the nozzle is significantly higher than the pressure outside the nozzle, where the temperature is already decreased, and the pressure difference occurs quickly.

Analyzing the pressures in the nozzle and outside, there is an inevitable trade-off between pressure difference at the nozzle and the use of larger nozzle exit diameters. As seen, increased external pressure leads to increased melt flow around. Reduced pressure decreases the ability of the TP to flow smoothly around the fiber. In addition, challenges were observed in the alignment of dry CF threads that tend to delinearize and resist alignment through smaller diameter nozzles. Unless preliminary wetting is used, an investigation into optimal balance is advised. Initial research used 0.6mm and 0.8mm nozzles successfully.

The 'in-nozzle' impregnation benefits over in-nozzle impregnation since fiber must be added to the build volume with the matrix (prepreg) to achieve polymer sintering. If dry fiber is assumed to be pressured into the model, not enough pressure or temperature can be exerted to press fiber into the model. Thus, 'in-nozzle' benefits over 'ex-nozzle' composite strength, as polymer sintering is more effective polymer sintering.

## 6.3. Design improvements

### 6.3.1. Modifying nozzle shapes

Altering the shape of the nozzle used for the printing process could be a viable method. By redesigning the nozzle to facilitate better fiber-matrix interaction, it is possible to improve the impregnation process. The aim is to optimize the deposition and distribution of the matrix material around the fibers, ensuring maximum contact and bonding between the two. In figure 6.2, two basic suggestions have been schematically represented. However, the disadvantage of this is that the printheads need large modifications, such as rollers and extra matrix tubes.

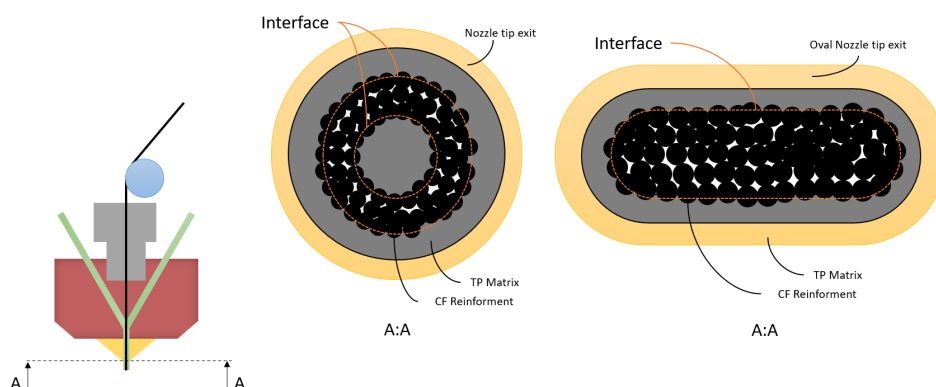


**Figure 6.2:** Concepts to increase the fiber-matrix contact surface. (Left) Central matrix; (Right) Oval nozzle exit

### 6.3.2. Adjusting fiber packing

Another option could be to investigate the applications of other types of fibers. For example, fiber constituents with lesser and more significant micro-filaments. During the experiments, it was observed that plain CF lacked strength since the TP matrix was not there to increase the mutual friction given by Coulomb's law. However, increasing the diameter of the fiber monofilaments is limited by the bend radius and flexibility.

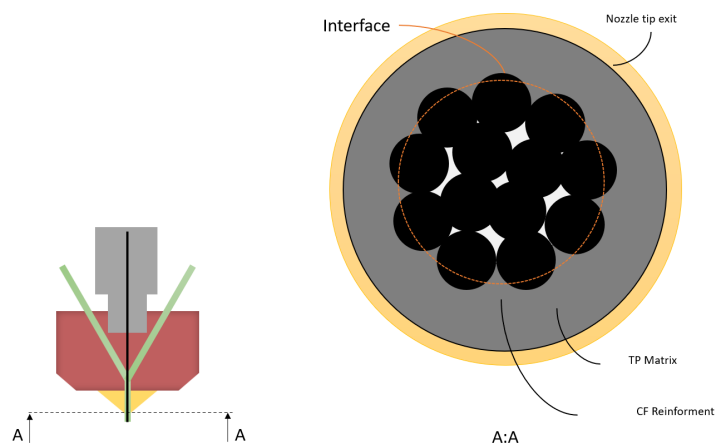


**Figure 6.3:** Concepts to increase the fiber-matrix contact surface. (Left) Central matrix; (Right) Oval nozzle exit

### 6.3.3. Pre-impregnation of fiber bundle

In this study, the feasibility of dry fiber impregnation was investigated. However, as red in Chapter 2, current production methods involve the impregnation of fiber sheets. This pre-impregnation gives a more stable permeability of even low viscous thermosets. In the future, an investigation on the impregnation of fiber thread before inserting into the fusion area may be performed.

# 7

## Recommendations

In this chapter, a selection of recommendations for future research is suggested.

### A. Materials:

- Explore the potential of employing thermoplastic materials with improved flow properties specifically customized for 'in-nozzle' impregnation techniques. Evaluate their compatibility with high-performance fibers to enhance the impregnation process in composite manufacturing.
- Explore alternative reinforcement fibers and investigate the influence of varying sizes and the number of microfilaments. Assess their compatibility with thermoplastic matrices to enhance adhesion and shear strength in composite materials.
- Explore and analyze the optimal fiber reinforcement and thermoplastic polymer combination. Establish a ranking system to assess their compatibility and effectiveness when used together.
- Explore innovative techniques for effectively blending lower-viscosity thermosets with thermoplastic polymers. Consider the impact on mechanical properties.

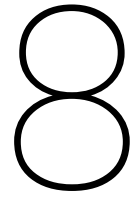
### B. Methodology:

- Explore the effects of altering printing parameters, such as nozzle diameter and temperature profiles, on impregnation quality and interfacial properties. This investigation aims to gain a comprehensive understanding of how these printing variables influence the impregnation process and the resultant properties of the interface in C-FRTP composites.
- Develop specialized test rigs or customized setups designed specifically to accurately evaluate melt impregnation and interfacial shear strength properties in C-FRTP composites. These setups should incorporate advanced capabilities such as pressure measurement tools and specialized molds capable of withstanding higher pressures. This enhancement in experimental apparatus would provide more precise and reliable assessments of interfacial properties, contributing to a deeper understanding of C-FRTP composite behavior under varying conditions.
- Standardize a method for testing single fibers for pull-out resistance using tensile test benches. Investigate the most accurate procedures for conducting tensile tests on individual microfilaments, considering their potential individual damage and low-friction characteristics, which could affect the test results.

- Investigate the C-FRTP printing process by numerical approximation. Use mathematical models and existing laws to define the relation between exposure time, pressure, temperature, melt impregnation, and IFSS

### C. Further C-FRTP Printing:

- Investigate the printing behavior of C-FRTP through in-nozzle impregnation using a real-time printing nozzle. Further, Investigate the influence of varying impregnation parameters such as pressure, temperature, and exposure time on the impregnation behavior. Additionally, analyze the interaction dynamics between the thermoplastic matrix and continuous fibers during the printing process. This investigation can provide valuable insights into optimizing impregnation conditions for enhanced C-FRTP printing quality.
- Develop a functional 'in-nozzle' print head designed explicitly for printing Carbon Continuous Fiber Reinforced Thermoplastic Polymer (C-FRTP) models.
- Creating a cutting mechanism to address the challenge of maintaining concentric alignment of fibers post-cutting remains a crucial development area.
- Explore research into printing paths or software applications designed for printing C-FRTP to control fiber orientation, enhance complexity, and improve scalability.
- Explore the utilities to modify nozzles to enhance pressure to melt impregnation. Involved in this study is the Fiber array and density of fiber packing



## Conclusion

The ever-growing demand for high-performance materials and more functional 3D printing has raised tremendous interest in using AM technologies to advance Multi-Material Additive Manufacturing (MMAM). Developing C-FRTP 3D printing opens new scalable FRP solutions. These components possess exceptional properties such as specific strength-to-weight, recyclability, impact/chemical resistance, and geometrical complexity. Researchers have successfully exploited FDM technology to 3D print C-FRTP composites but face significant challenges in extruding composition that exhibit high Interface bonding between high-performance fibers and thermoplastic polymer matrix. This is observed as porosities in the interface, which result in overall mechanical weakness.

Various Meso-level C-FRTP 3D printing methods and print heads have been developed and standardized, but more knowledge is needed of essential 'In-Nozzle' C-FRTP impregnation dynamics. During In-Nozzle impregnation, solid-dry high-performance fiber reinforcement and molten Thermoplastic polymer matrix bond inside the Print head and are deposited onto the build volume as a composite. This master thesis explores the challenges and potential solutions by conceptualizing a functional 'In-Nozzle' impregnation extruder capable of extruding proper C-FRTP composites using FDM printing.

exploring the feasibility and pushing the boundaries of C-FRTP fabrication through FDM printing. In pursuit of this, each chapter unfolded a specific aspect of this objective. Starting with Chapter 2, a detailed literature investigation delves into the fundamentals of FDM technology and C-FRTP 3D printing, including current limitations and opportunities in this domain. From this, the research objective was stated. Followed by a chapter 3 experimental research was initiated, and a methodology for approaching this research on in-nozzle C-FRTP 3D Printing. The research objective aimed to investigate the challenges posed by the limitations of dry fiber in the penetration of a thick TP melt. The analysis highlighted the need for the fiber to exit the fiber guide tube closely to the nozzle exit, limiting its exposure time in the fusion area with the TP melt. The investigation of melt impregnation dynamics began with Chapter 4. Chapter 4 explored the melt impregnation dynamics of the TP melt through CF bundles, revealing limited melt impregnation by microscopic analysis. Chapter 5 analyzes the interfacial shear strength by testing the pull-out resistance of the C-FRTP samples. The study of the interfacial shear strength revealed a strength peak at moderate exposure times. Furthermore, a strength advantage was observed between neat TP PLA (matrix) and C-FRTP composite. Chapter 4 and Chapter 5 start with an extensive theoretical framework followed by experiments as validation.

Based on the observations in Chapters 4 and 5, a discussion (see Chapter 6) underscored the potential of C-FRTP printing but also highlighted its limitations. The limitations identified

in this study require further investigation and development. Future research recommended was suggested in Chapter 7. Future research should address these limitations to enhance the feasibility and applicability of C-FRTP printing.

In conclusion, C-FRTP printing offers immense potential, providing reliability, controllability, scalability, and environmental benefits to various industries, particularly aerospace, military, renewable energy, and automotive. Despite the observed limitations, continued research and development in this field promise a more efficient and effective utilization of C-FRTP composites, contributing significantly to the advancement of composite manufacturing technologies.

This research highlights the current challenges and lays the foundation for future advancements in C-FRTP printing through 'in-nozzle' impregnation methods, offering insights into improving material compatibility, impregnation quality, and interfacial bonding.

# References

- [1] *3D Printhead for Composite Materials & 2013; Engineering Design Fair 2022 - engineeringdesignfair.ucalgary.ca*. 2023. URL: <https://engineeringdesignfair.ucalgary.ca/mechanical/3d-printhead-for-composite-materials/> (visited on 11/11/2023).
- [2] Don Adams. *Fiber-matrix interfacial bond test methods - compositesworld.com*. 2023. URL: <https://www.compositesworld.com/articles/fiber-matrix-interfacial-bond-test-methods> (visited on 10/31/2023).
- [3] Behnam Akhoundi, Amir Hossein Behraves, and Arvin Bagheri Saed. "An innovative design approach in three-dimensional printing of continuous fiber-reinforced thermoplastic composites via fused deposition modeling process: In-melt simultaneous impregnation". In: *Proceedings of the Institution of Mechanical Engineers, Part B: Journal of Engineering Manufacture* 234 (2019). ISSN: 2041-2975. DOI: 10.1177/0954405419843780. URL: <http://dx.doi.org/10.1177/0954405419843780>.
- [4] Alaa M. Almushaikeh et al. "Manufacturing of carbon fiber reinforced thermoplastics and its recovery of carbon fiber: A review". In: *Polymer Testing* 122 (2023). ISSN: 0142-9418. DOI: 10.1016/j.polymertesting.2023.108029. URL: <http://dx.doi.org/10.1016/j.polymertesting.2023.108029>.
- [5] V. Bheemreddy et al. "Modeling of fiber pull-out in continuous fiber reinforced ceramic composites using finite element method and artificial neural networks". In: *Computational Materials Science* 79 (Nov. 2013), pp. 663–673. ISSN: 0927-0256. DOI: 10.1016/j.commatsci.2013.07.026. URL: <http://dx.doi.org/10.1016/j.commatsci.2013.07.026>.
- [6] Jeppe Byskov and Nikolaj Vedel-Smith. *Additive Manufacturing*. Springer International Publishing, 2022. ISBN: 9783031154287. DOI: 10.1007/978-3-031-15428-7\_32. URL: [http://dx.doi.org/10.1007/978-3-031-15428-7\\_32](http://dx.doi.org/10.1007/978-3-031-15428-7_32).
- [7] Paola Carnevale. *Fibre-matrix interfaces in thermoplastic composites: A meso level approach*. TUDelft repository and printed in the Netherlands by Uitgeverij BOXPress, s-Hertogenboch, 2014. ISBN: 978-90-8891-810-0.
- [8] ASTM F48 Committee. *Standard Terminology for Additive Manufacturing F2792:(2013)*. 2013. URL: <https://www.astm.org/Standards.F2792.htm> (visited on 08/30/2023).
- [9] Andrew N. Dickson, Hisham M. Abourayana, and Denis P. Dowling. "3D Printing of Fibre-Reinforced Thermoplastic Composites Using Fused Filament Fabrication—A Review". In: *Polymers* 12 (2020). ISSN: 2073-4360. DOI: 10.3390/polym12102188. URL: <http://dx.doi.org/10.3390/polym12102188>.
- [10] Michael Dwamena. *3D Printer Feed Rate Vs Flow Rate - Same or Different? — 3dprinterly.com*. URL: <https://3dprinterly.com/3d-printer-feed-rate-vs-flow-rate-same-or-different/> (visited on 11/01/2023).
- [11] Shady Farah, Daniel G. Anderson, and Robert Langer. "Physical and mechanical properties of PLA, and their functions in widespread applications — A comprehensive review". In: *Advanced Drug Delivery Reviews* 107 (2016), pp. 367–392. ISSN: 0169-409X. DOI: 10.1016/j.addr.2016.06.012. URL: <http://dx.doi.org/10.1016/j.addr.2016.06.012>.

- [12] Ismail Fidan et al. "The trends and challenges of fiber reinforced additive manufacturing". In: *The International Journal of Advanced Manufacturing Technology* 102 (2019). ISSN: 1433-3015. DOI: 10.1007/s00170-018-03269-7. URL: <http://dx.doi.org/10.1007/s00170-018-03269-7>.
- [13] Johannes Karl Fink. "Unsaturated Polyester Resins". In: *Reactive Polymers Fundamentals and Applications*. Elsevier, 2013. DOI: 10.1016/b978-1-4557-3149-7.00001-2. URL: <http://dx.doi.org/10.1016/B978-1-4557-3149-7.00001-2>.
- [14] James Garofalo and Daniel Walczyk. "In situ impregnation of continuous thermoplastic composite prepreg for additive manufacturing and automated fiber placement". In: *Composites Part A: Applied Science and Manufacturing* 147 (2021). ISSN: 1359-835X. DOI: 10.1016/j.compositesa.2021.106446. URL: <http://dx.doi.org/10.1016/j.compositesa.2021.106446>.
- [15] *Goodfellow - Supplier of materials for research and development - goodfellow.com*. 2023. URL: <https://www.goodfellow.com/> (visited on 08/31/2023).
- [16] Jeffrey Gotro. *Characterization of Thermosets Part 21: Tensile Testing of Polymers; A Molecular Interpretation - Polymer Innovation Blog - polymerinnovationblog.com*. 2023. URL: <https://polymerinnovationblog.com/characterization-thermosets-part-21-tensile-testing-polymers-molecular-interpretation/> (visited on 11/21/2023).
- [17] Seymour Hasanov et al. "Review on Additive Manufacturing of Multi-Material Parts: Progress and Challenges". In: *Journal of Manufacturing and Materials Processing* 6 (2021). ISSN: 2504-4494. DOI: 10.3390/jmmp6010004. URL: <http://dx.doi.org/10.3390/jmmp6010004>.
- [18] *How to Manufacture Carbon Fiber Parts — formlabs.com*. 2023. URL: <https://formlabs.com/eu/blog/composite-materials-carbon-fiber-layup/> (visited on 10/10/2023).
- [19] *Industrial Additive Manufacturing Platform - markforged.com*. 2023. URL: [markforged.com](http://markforged.com) (visited on 10/09/2023).
- [20] *Introduction to Aerospace Materials*. Elsevier, 2012, pp. 303–337. DOI: 10.1533/9780857095152.303. URL: <http://dx.doi.org/10.1533/9780857095152.303>.
- [21] Khairul Izwan Ismail, Tze Chuen Yap, and Rehan Ahmed. "3D-Printed Fiber-Reinforced Polymer Composites by Fused Deposition Modelling (FDM): Fiber Length and Fiber Implementation Techniques". In: *Polymers* 14 (2022). ISSN: 2073-4360. DOI: 10.3390/polym14214659. URL: <http://dx.doi.org/10.3390/polym14214659>.
- [22] S M Fijul Kabir, Kavita Mathur, and Abdel-Fattah M. Seyam. "A critical review on 3D printed continuous fiber-reinforced composites: History, mechanism, materials and properties". In: *Composite Structures* 232 (2020). ISSN: 0263-8223. DOI: 10.1016/j.compstruct.2019.111476. URL: <http://dx.doi.org/10.1016/j.compstruct.2019.111476>.
- [23] Daniel Kaczmarek et al. "An investigation of in situ impregnation for additive manufacturing of thermoplastic composites". In: *Journal of Manufacturing Processes* 64 (2021). ISSN: 1526-6125. DOI: 10.1016/j.jmapro.2021.02.018. URL: <http://dx.doi.org/10.1016/j.jmapro.2021.02.018>.
- [24] Nanya Li, Yingguang Li, and Shuting Liu. "Rapid prototyping of continuous carbon fiber reinforced polylactic acid composites by 3D printing". In: *Journal of Materials Processing Technology* 238 (2016). ISSN: 0924-0136. DOI: 10.1016/j.jmatprotec.2016.07.025. URL: <http://dx.doi.org/10.1016/j.jmatprotec.2016.07.025>.



- [25] Federico Lupone et al. "Experimental Characterization and Modeling of 3D Printed Continuous Carbon Fibers Composites with Different Fiber Orientation Produced by FFF Process". In: *Polymers* 14.3 (2022). ISSN: 2073-4360. DOI: 10.3390/polym14030426. URL: <http://dx.doi.org/10.3390/polym14030426>.
- [26] Bo Madsen and Hans Lilholt. "Physical and mechanical properties of unidirectional plant fibre composites—an evaluation of the influence of porosity". In: *Composites Science and Technology* (2003). ISSN: 0266-3538. DOI: 10.1016/S0266-3538(03)00097-6. URL: [http://dx.doi.org/10.1016/S0266-3538\(03\)00097-6](http://dx.doi.org/10.1016/S0266-3538(03)00097-6).
- [27] P.K. Mallick. *Fiber-Reinforced Composites: Materials, Manufacturing and Design*. Third edition. CRC Press Taylor & Francis Group, LLC, 2007. ISBN: 978-0-8493-4205-9.
- [28] Hannah Mason and Ginger Gardiner. *3D printing with continuous fiber: A landscape — compositesworld.com*. 2023. URL: <https://www.compositesworld.com/articles/3d-printing-with-continuous-fiber-a-landscape> (visited on 09/09/2023).
- [29] Ryosuke Matsuzaki et al. "Three-dimensional printing of continuous-fiber composites by in-nozzle impregnation". In: *Scientific Reports* 6 (2016). ISSN: 2045-2322. DOI: 10.1038/srep23058. URL: <http://dx.doi.org/10.1038/srep23058>.
- [30] 3D moldex. *Viscosity Model for Thermoplastic*. 2023. URL: [https://support.moldex3d.com/2020/en/4-7-1-1\\_viscositymodelforthermoplastic.html](https://support.moldex3d.com/2020/en/4-7-1-1_viscositymodelforthermoplastic.html) (visited on 10/12/2023).
- [31] Miguel Ángel Molina-Moya et al. "Experimental Analysis and Application of a Multivariable Regression Technique to Define the Optimal Drilling Conditions for Carbon Fiber Reinforced Polymer (CFRP) Composites". In: *Polymers* (2023). DOI: 10.3390/polym15183710. URL: <http://dx.doi.org/10.3390/polym15183710>.
- [32] Benedict O'Neill. *3D print speed: What it is and why it matters — wevolver.com*. (Visited on 10/12/2023).
- [33] Heather J. O'Connor and Denis P. Dowling. "Low pressure additive manufacturing of continuous fiber reinforced polymer composites". In: *Polymer Composites* 40 (2019). ISSN: 1548-0569. DOI: 10.1002/pc.25294. URL: <http://dx.doi.org/10.1002/pc.25294>.
- [34] Michelle Oepping. *Differences in structure: The properties of plastic types — thermoplasticcomposites.de*. 2023. URL: <https://thermoplasticcomposites.de/en/2019/12/03/differences-in-structure-the-properties-of-plastic-types/> (visited on 10/02/2023).
- [35] Chrysoula Pandelidi et al. "The technology of continuous fibre-reinforced polymers: a review on extrusion additive manufacturing methods". In: *The International Journal of Advanced Manufacturing Technology* 113 (2021). ISSN: 1433-3015. DOI: 10.1007/s00170-021-06837-6. URL: <http://dx.doi.org/10.1007/s00170-021-06837-6>.
- [36] P. Peltonen and P. Järvelä. "Methodology for Determining the Degree of Impregnation from Continuous Glass Fibre prepreg". In: *Polymer Testing* 11 (1992) 215-224 (1991).
- [37] Pavan Kumar Penumakala, Jose Santo, and Alen Thomas. "A critical review on the fused deposition modeling of thermoplastic polymer composites". In: *Composites Part B: Engineering* 201 (2020). ISSN: 1359-8368. DOI: 10.1016/j.compositesb.2020.108336. URL: <http://dx.doi.org/10.1016/j.compositesb.2020.108336>.

- [38] Juan Pratama et al. "A Review on Reinforcement Methods for Polymeric Materials Processed Using Fused Filament Fabrication (FFF)". In: *Polymers* 13 (2021). ISSN: 2073-4360. DOI: 10.3390/polym13224022. URL: <http://dx.doi.org/10.3390/polym13224022>.
- [39] Hauke Prüß and Thomas Vietor. "Design for Fiber-Reinforced Additive Manufacturing". In: *Journal of Mechanical Design* 137.11 (2015). ISSN: 1528-9001. DOI: 10.1115/1.4030993. URL: <http://dx.doi.org/10.1115/1.4030993>.
- [40] João Pedro Reis, Marcelo de Moura, and Sylwester Samborski. "Thermoplastic Composites and Their Promising Applications in Joining and Repair Composites Structures: A Review". In: *Materials* 13 (2020). ISSN: 1996-1944. DOI: 10.3390/ma13245832. URL: <http://dx.doi.org/10.3390/ma13245832>.
- [41] Oswaldo Rivero-Romero, Ismael Barrera-Fajardo, and Jimy Unfried-Silgado. "Effects of printing parameters on fiber eccentricity and porosity level in a thermoplastic matrix composite reinforced with continuous banana fiber fabricated by FFF with in situ impregnation". In: *The International Journal of Advanced Manufacturing Technology* 125.3–4 (2023). ISSN: 1433-3015. DOI: 10.1007/s00170-022-10799-8. URL: <http://dx.doi.org/10.1007/s00170-022-10799-8>.
- [42] Marcin P. Serdeczny et al. "Experimental and analytical study of the polymer melt flow through the hot-end in material extrusion additive manufacturing". In: *Additive Manufacturing* 32 (2020). ISSN: 2214-8604. DOI: 10.1016/j.addma.2019.100997. URL: <http://dx.doi.org/10.1016/j.addma.2019.100997>.
- [43] Kubi Sertoglu. *Three unknown facts about continuous fiber 3D printing from Anisoprint CEO Fedor Antonov - 3dprintingindustry.com*. 2023. URL: <https://3dprintingindustry.com/news/three-unknown-facts-about-continuous-fiber-3d-printing-from-anisoprint-ceo-fedor-antonov-173555/> (visited on 08/13/2023).
- [44] Nor Aiman Sukindar et al. "ANALYZING THE EFFECT OF NOZZLE DIAMETER IN FUSED DEPOSITION MODELING FOR EXTRUDING POLYLACTIC ACID USING OPEN SOURCE 3D PRINTING". In: *Jurnal Teknologi* 78.10 (2016). ISSN: 0127-9696. DOI: 10.11113/jt.v78.6265. URL: <http://dx.doi.org/10.11113/jt.v78.6265>.
- [45] Fatiha Teklal et al. "A review of analytical models to describe pull-out behavior – Fiber/matrix adhesion". In: *Composite Structures* 201 (2018). ISSN: 0263-8223. DOI: 10.1016/j.compstruct.2018.06.091. URL: <http://dx.doi.org/10.1016/j.compstruct.2018.06.091>.
- [46] *Thermoplastics for AM: Semi-Crystalline vs Amorphous — aniwaa.com*. 2023. URL: <https://www.aniwaa.com/insight/am-materials/am-thermoplastics-semi-crystalline-vs-amorphous/> (visited on 11/15/2023).
- [47] J.L. Thomason et al. "Fibre cross-section determination and variability in sisal and flax and its effects on fibre performance characterisation". In: *Composites Science and Technology* 71.7 (2011). ISSN: 0266-3538. DOI: 10.1016/j.compscitech.2011.03.007. URL: <http://dx.doi.org/10.1016/j.compscitech.2011.03.007>.
- [48] James L. Thomason and Jose L. Rudeiros-Fernández. "Characterization of interfacial strength in natural fibre – polyolefin composites at different temperatures". In: *Composite Interfaces* 29.2 (2021). ISSN: 1568-5543. DOI: 10.1080/09276440.2021.1913901. URL: <http://dx.doi.org/10.1080/09276440.2021.1913901>.

- [49] James L. Thomason and Jose L. Rudeiros-Fernández. “Characterization of interfacial strength in natural fibre – polyolefin composites at different temperatures”. In: *Composite Interfaces* 29.2 (2021). ISSN: 1568-5543. DOI: 10.1080/09276440.2021.1913901. URL: <http://dx.doi.org/10.1080/09276440.2021.1913901>.
- [50] Xiaoyong Tian et al. “Interface and performance of 3D printed continuous carbon fiber reinforced PLA composites”. In: *Composites Part A: Applied Science and Manufacturing* 88 (2016). ISSN: 1359-835X. DOI: 10.1016/j.compositesa.2016.05.032. URL: <http://dx.doi.org/10.1016/j.compositesa.2016.05.032>.
- [51] Tomáš Tichý et al. “Mathematical Modelling of Temperature Distribution in Selected Parts of FFF Printer during 3D Printing Process”. In: *Polymers* 13.23 (2021). ISSN: 2073-4360. DOI: 10.3390/polym13234213. URL: <http://dx.doi.org/10.3390/polym13234213>.
- [52] Ida Tolen. *How to Calculate Thermal Stress - sciencing.com*. URL: <https://sciencing.com/calculate-thermal-stress-2770.html> (visited on 11/21/2023).
- [53] *Understanding Viscosity for Epoxy Adhesives, Potting Compounds and Sealants - MasterBond.com*. 2023. URL: <https://www.masterbond.com/techtips/understanding-viscosity-epoxy-adhesives-potting-compounds-and-sealants> (visited on 11/22/2023).
- [54] *Vacuum Bagging - entropyresins.com*. URL: <https://entropyresins.com/how-tos/vacuum-bagging/#:~:text=When%20the%20bag%20is%20sealed,envelope%20remain%20at%2014.7%20psi>. (visited on 10/04/2023).
- [55] Takahiro Wada et al. “Application of Glass Fiber and Carbon Fiber-Reinforced Thermoplastics in Face Guards”. In: *Polymers* 13 (2020). ISSN: 2073-4360. DOI: 10.3390/polym13010018. URL: <http://dx.doi.org/10.3390/polym13010018>.
- [56] Fuji Wang et al. “Fiber–matrix impregnation behavior during additive manufacturing of continuous carbon fiber reinforced polylactic acid composites”. In: *Additive Manufacturing* 37 (2021). ISSN: 2214-8604. DOI: 10.1016/j.addma.2020.101661. URL: <http://dx.doi.org/10.1016/j.addma.2020.101661>.
- [57] Hao Wang et al. “Pull-out method for direct measuring the interfacial shear strength between short plant fibers and thermoplastic polymer composites (TPC)”. In: *hfsfg* 68 (2013). ISSN: 0018-3830. DOI: 10.1515/hf-2013-0052. URL: <http://dx.doi.org/10.1515/hf-2013-0052>.
- [58] Anthonius Petrus Dignum Weustink. *Development of a rapid thermoplastic impregnation device*. TUDelft repository and Printed by PrintPartners Ipskamp, 2008. ISBN: 978-90-9022623-1.
- [59] *What is FDM (fused deposition modeling) 3D printing? - hubs.com*. 2023. URL: <https://www.hubs.com/knowledge-base/what-is-fdm-3d-printing/> (visited on 09/16/2023).
- [60] Chuncheng Yang et al. “3D printing for continuous fiber reinforced thermoplastic composites: mechanism and performance”. In: *Rapid Prototyping Journal* 23 (2017). ISSN: 1355-2546. DOI: 10.1108/rpj-08-2015-0098. URL: <http://dx.doi.org/10.1108/RPJ-08-2015-0098>.
- [61] Zhongsen Zhang et al. “An investigation into printing pressure of 3D printed continuous carbon fiber reinforced composites”. In: *Composites Part A: Applied Science and Manufacturing* 162 (2022). ISSN: 1359-835X. DOI: 10.1016/j.compositesa.2022.107162. URL: <http://dx.doi.org/10.1016/j.compositesa.2022.107162>.

# A

## Tables and figures

The supporting elements are presented here. This includes tables and figures

### A.1. Schematic representation of different AM technologies

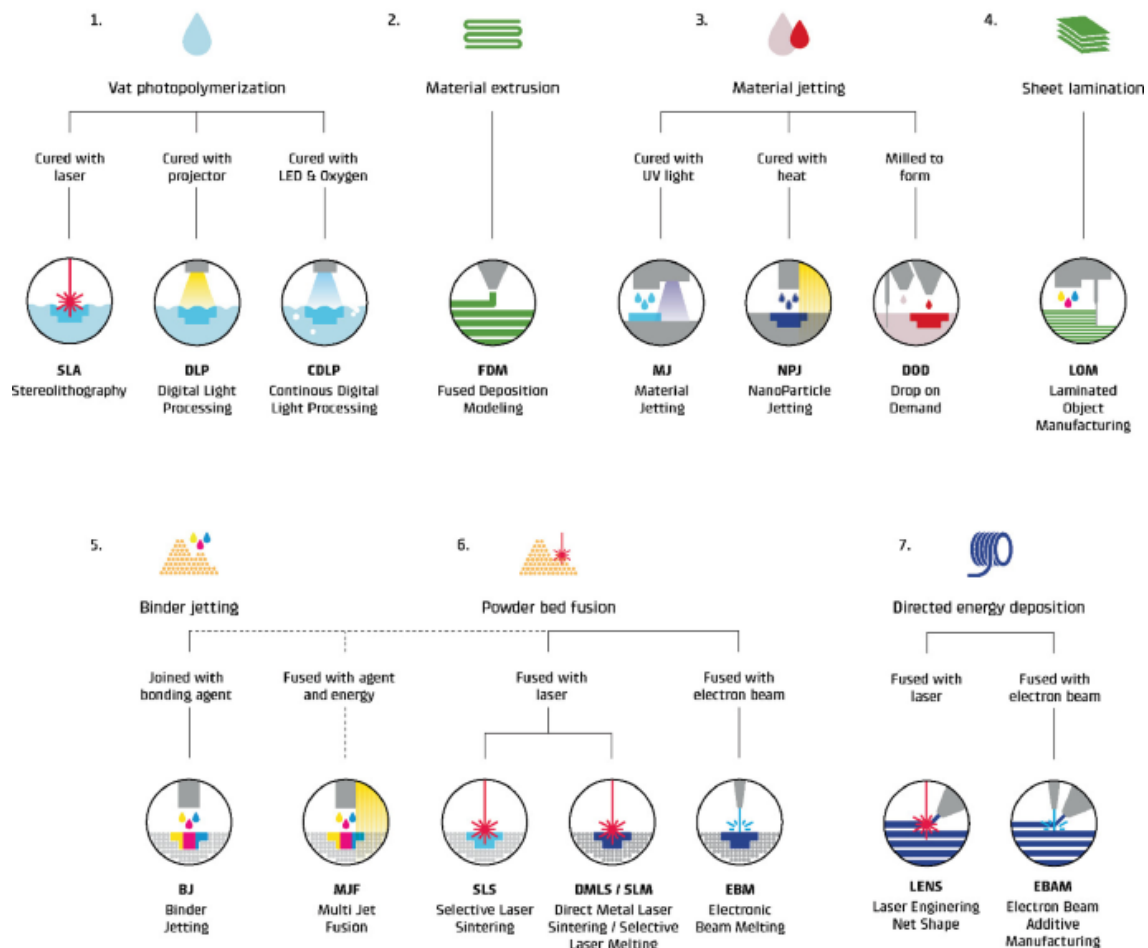


Figure A.1: Representation of different AM technologies. Adapted from [6]

## A.2. Overview of available thermoplastic polymers



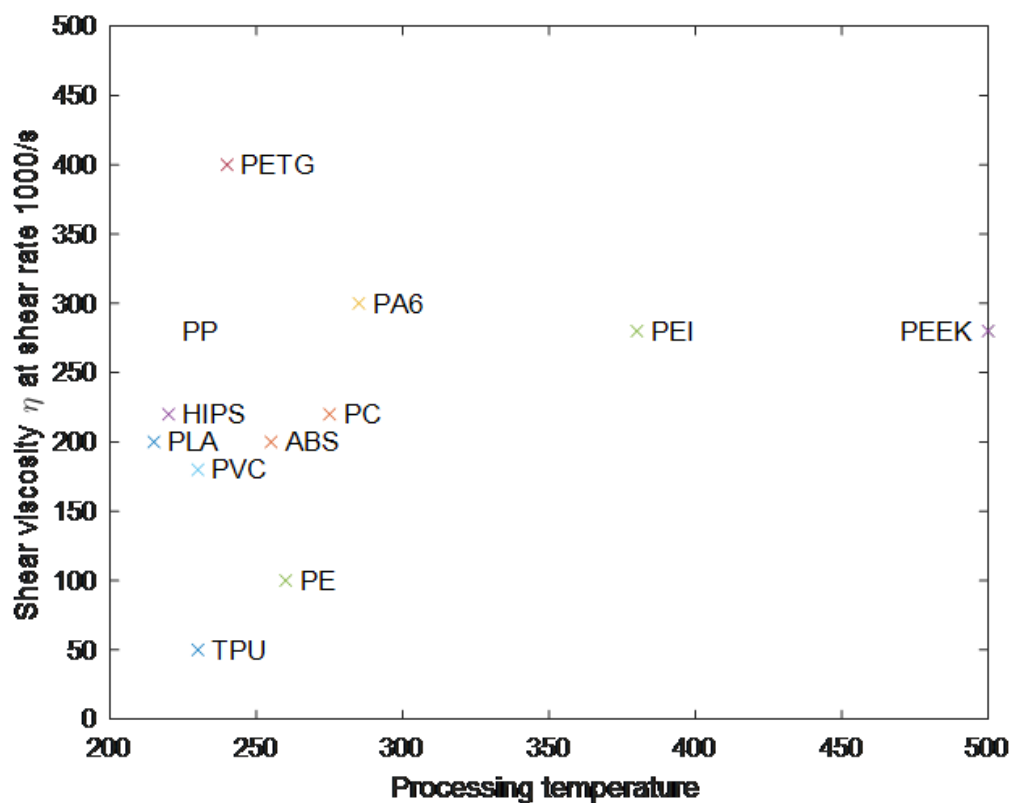
THERMOPLASTIC MATERIALS		
Primary group:	Semi Crystalline	Amorphous
		
<b>Standard</b> Good mouldability and easy to process but lack good strength, hardness and heat resistance. often used for packaging, toys and household.	PLA (Polylactic Acid):	ABS (Acrylonitrile Butadiene Styrene):
	PP (polypropylene)	HIPS (High Impact Polystyrene)
	PE (Polyethylene)	PVC (Polyvinyl chloride)
<b>Engineering</b> Utilized in applications needing strong and stiff properties, without the specific hardness or heat resistance.	PETG (Polyethylene Terephthalate Glycol):	PPE (Polyphenylene ether)
	TPU (Thermoplastic polyurethane)	PC (polycarbonate)
	PA 6 (Nylon) (Polyamide)	ASA (Acrylonitrile Styrene Acrylate)
<b>High-Performance</b> commonly applied in situations demanding high strength, impact resistance, hardness, and heat resistance.	PEEK (Polyether Ether Ketone):	PEI (ULTEM) (Polyetherimide)
	PTFE (Polytetrafluorethylene)	

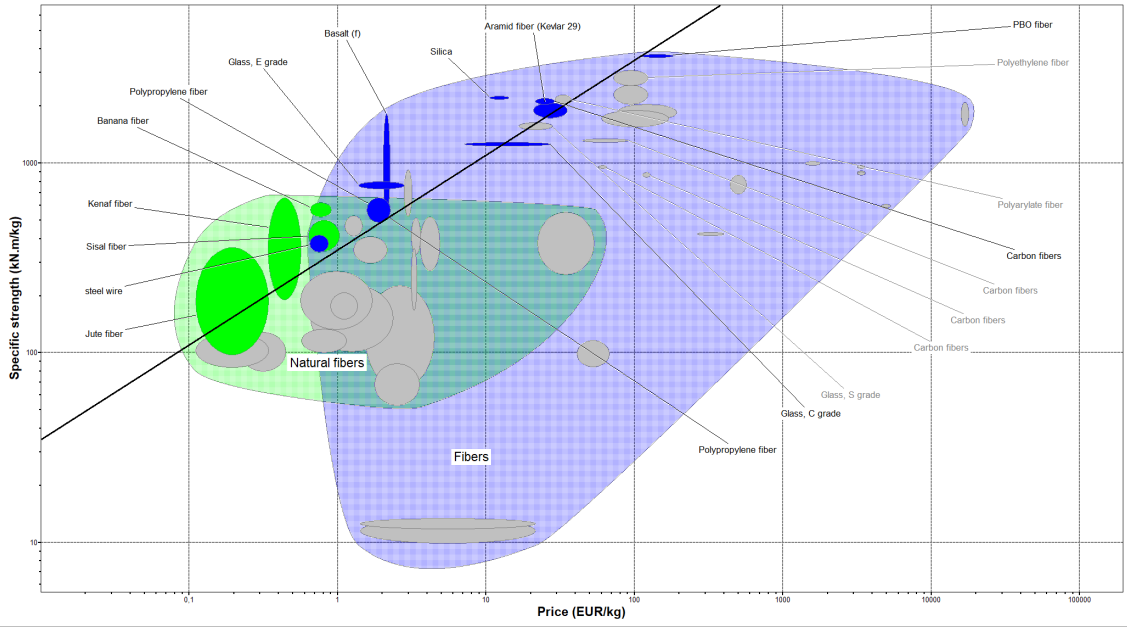
Table A.1: Partly adapted from [46], [59], [34]

## A.3. Thermoplastic Polymer rheology analysis

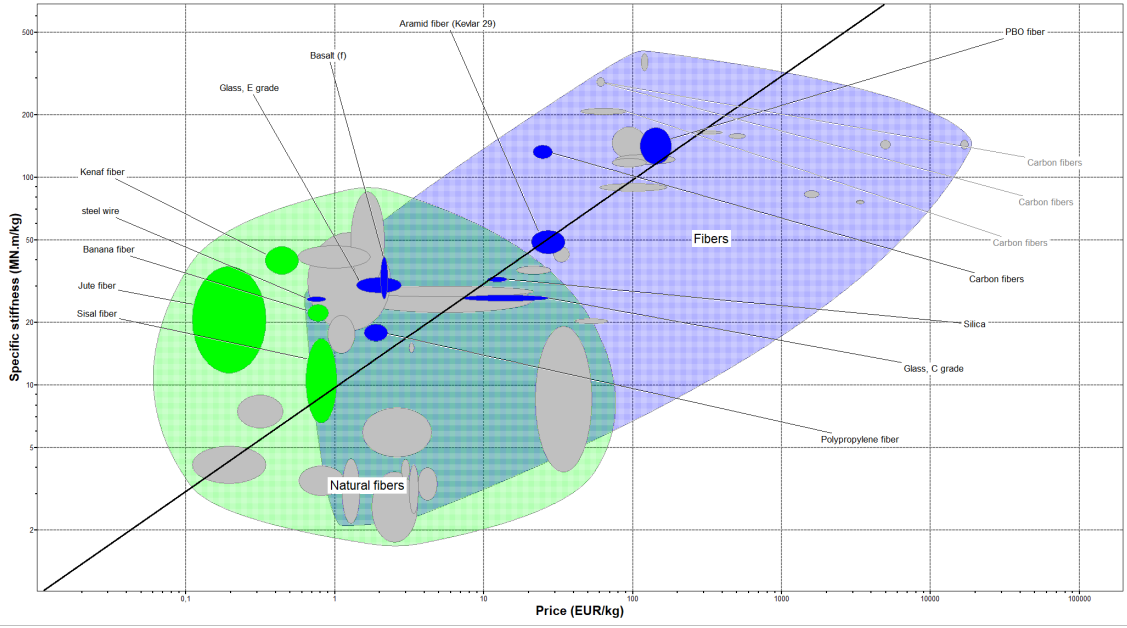


**Table A.2:** This graph shows the viscosity of different thermoplastic polymers measured at a shear rate of 1000/s. The x-axis represents the temperature (in  $C^\circ$ ) for being processed during 3D Printing and the y-axis represents the viscosity (in Pa.s)

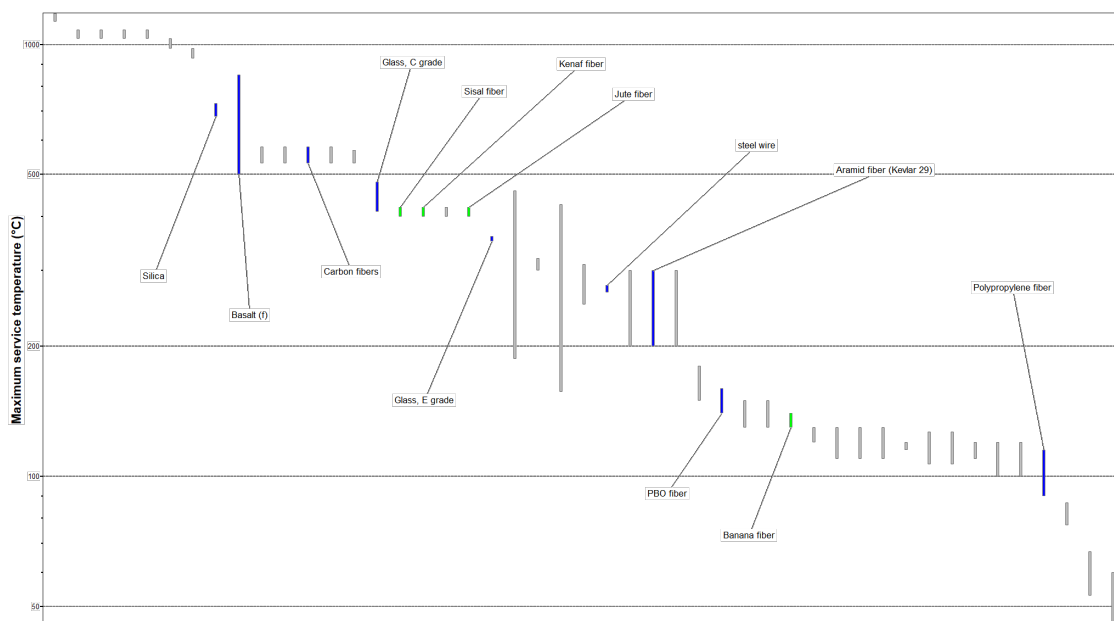
### A.4. Fiber selection criteria



(a)



(b)



(c)

**Figure A.2:** (a) Specific strength over price per kg with material index  $\frac{\sigma_f}{C_p}$ ; (b) Specific stiffness over price per kg with material index  $\frac{E_f}{C_p}$ ; (c) Maximum service temperature of materials ranked from high to low [Granta® Edupack 2022].

### A.5. C-CF catalogue from supplier

Carbon Fiber	Micro filament diameter [mm]	Fila- diame- ter	Number of fil- aments [-]	Tex number [gkm <sup>-1</sup> ]	Thread diam- eter [mm]
Tenax® UMS2526	0.0048		12K	400	0.526
HS40 carbon fiber thread	0.005		12K	430	0.548
Tenax® HTA 34-700	0.007		3K	200	0.383
Tenax® HTA	0.007		6K	400	0.542
34-700	0.007		12K	795	0.767
HS40	0.008		10K	900	0.800
F500	0.009		2K	280	0.402

**Table A.3:** Catalogue of available High performance Pan based Carbon Fibers by supplier Goodfellows.com. 3K Tenax ® HTA was selected since this CF has the lowest weight and thus overall diameter. [15]

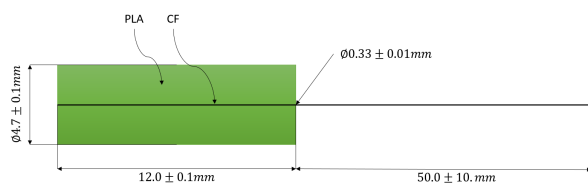


# B

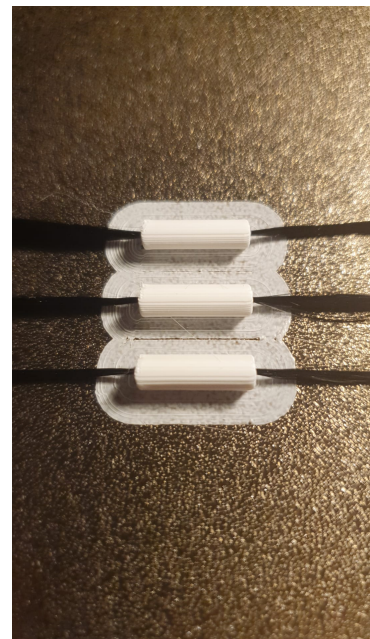
## Technical drawings and fabrication steps

### B.1. Technical drawing sample designs

#### B.1.1. Experiment 1 & melt impregnation



(a)



(b)

**Figure B.1:** (a) Technical drawing of samples used for IFSS experiment 1 & melt impregnation analysis, (b) Real Samples printer and prepared for packing

B.1.2. Experiment 2

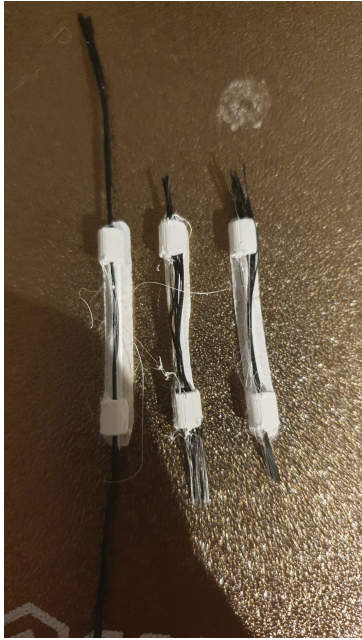
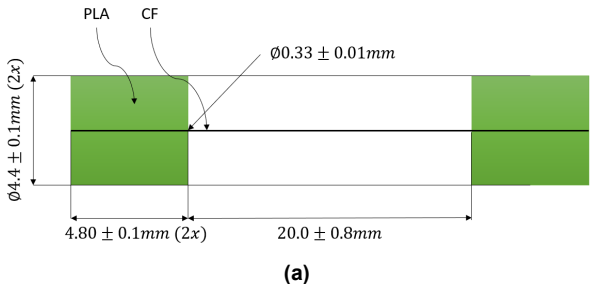


Figure B.2: (a) Technical drawing of samples used for IFSS experiment 2, (b) Real Samples printer and prepared for packing

B.1.3. Experiment 3

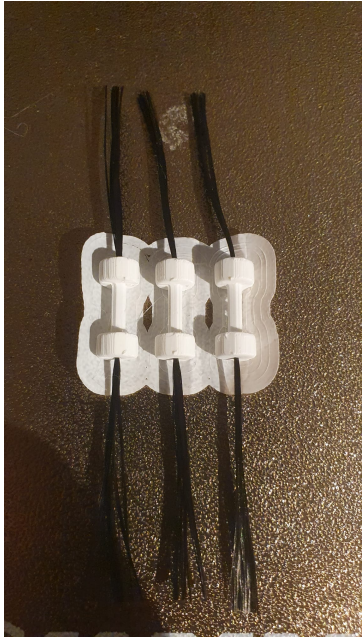
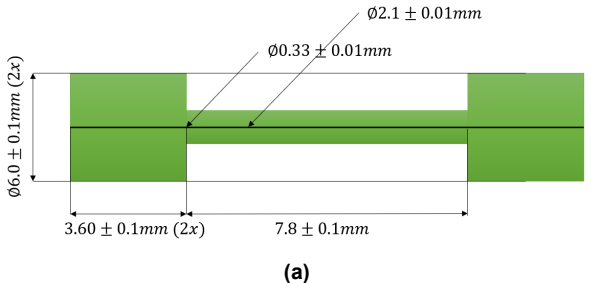


Figure B.3: (a) Technical drawing of sample used for IFSS experiment 3, (b) Real Samples printer and prepared for packing

## B.2. Step-by-step sample fabrication

Step 0 Prepare materials by cleaning, drying and heat treatment

Step 1 Designing the 3D Model and

- 1.1 Prepare a CAD model. SolidWorks© was utilized as Cad software for modelling sample designs.
- 1.2 Define the specific dimensions and parameters for the cavity, considering diameter, depth, and any additional features essential for the intended analysis.
- 1.3 Save as STL-file

Step 2 prepare for 3D printing with slicer software

- 2.1 Load the CAD models STL-file in the slicer software. Ultimaker's© slicing application CURA was utilized as Slicer software.
- 2.2 Place the samples on the virtual print bed. Three per print for quantity.
- 2.3 Add-in a pause moment at the last layer before the central cavity is closed.
- 2.4 Put in the correct settings, Temperature 215°C, Layer height 0.16mm, infill 100%, Print speed 30mm/s. (Some settings may vary according to 3D printer and material specifications.)

Step 3 FDM 3D printing process

- 3.1 Initiate the printing process, ensuring that the 3D printer is calibrated and set up correctly.
- 3.2 Monitor the printing progress (especially the first layer) and ensure the accurate fabrication of the sample.
- 3.3 When the printer head is intervened by the added-in pause. Place 50mm of CF thread in the cavity. Make sure the cavity is clean. For easier placing, slightly twist the Fiber to make it denser.
- 3.4 Check whether the CF Thread is fully in the cavity. sticking above the layer CF Thread may be caught by the printer head and disrupt the sample. Continue the 3D printer.

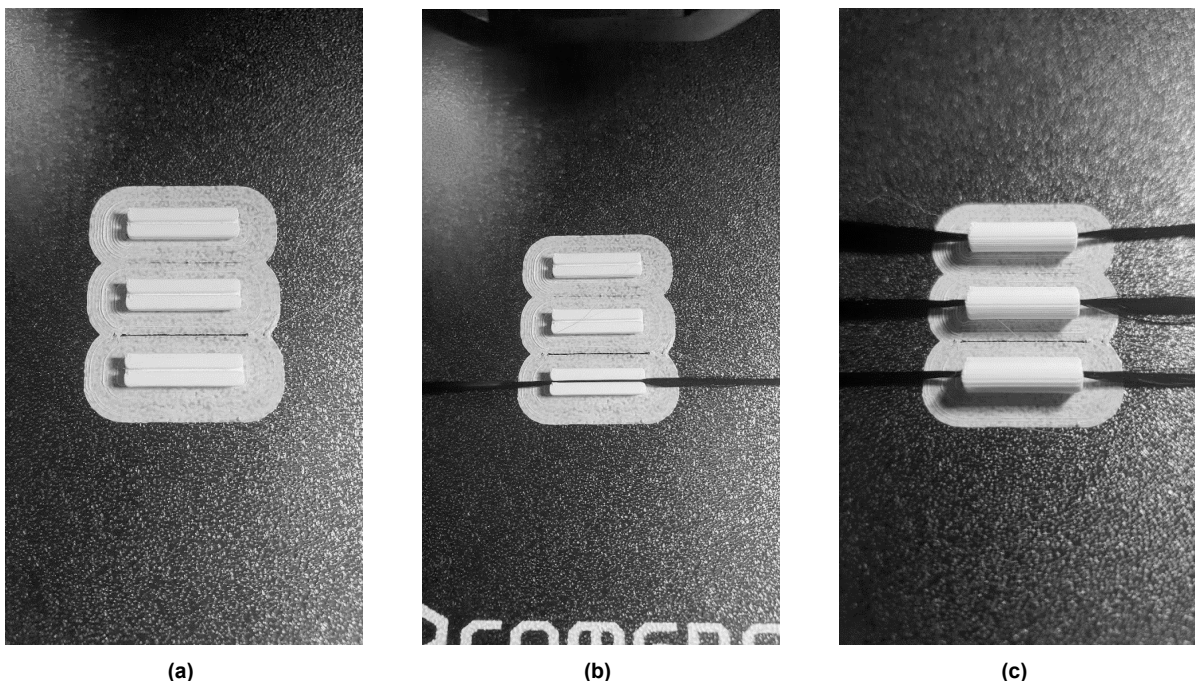


**Figure B.4:** Representation of CF thread laid in the cavity of printed PLA matrix. The printer is paused, CF thread laid in and resumed again.

#### Step 4 Post processing and packing.

- 4.1 Remove excess materials with cutting pliers.
- 4.2 Prepare small strips of aluminium (30x30mm). and wrap the samples tightly in the aluminium.
- 4.3 Store the samples in sealed bags and note the research group

### B.3. Step-by-step pressurized experiment

#### Step 0 Prepare materials by cleaning, drying and heat treatment

#### Step 1 Fabricate the aluminium mold

- 1.1 Use an regular counterbore to drill the 45° top section of the aluminium mold
- 1.2 Make two small slots at the bottom of the mold with a tiny triangular file.
- 1.3 Place the CF in slot and place a small piece of Kapton tape over the mold

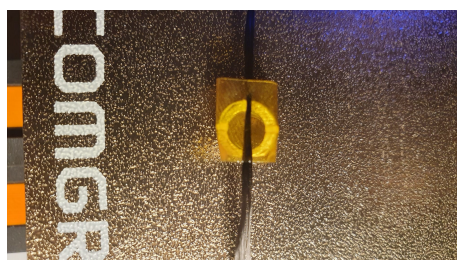
#### Step 2 prepare 3D printer

- 2.1 Remove the original 0.4mm nozzle and replace it by the 2.00mm drilled nozzle
- 2.2 Heat up the printer bed to 90°C (maximum reachable temperature) and heat up the nozzle to 215°C.
- 2.3 Place the mold with the counterdrilled side under the installed 3D printer nozzle and lower until touching. Check whether the heat bed (springed) is slightly pushed down.

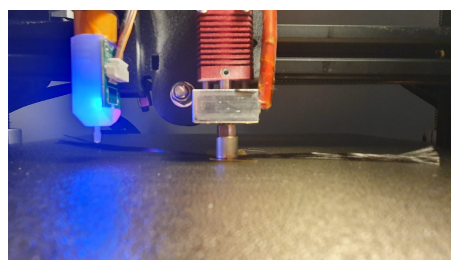
#### Step 3 Pressurization process

- 3.1 Start extruding TP by activating the extruder motor and fill up the mold. Approximate extruding 60mm (with the 0.4mm setting still active) fills up the mold. The mold is completely filled up when TP starts to pour out through the gaps
- 3.2 Keep extruding until the exposure time is reached. Every 30mm of extruded material represent 15 seconds of exerted pressure. Prepare, TP will flow from all sides outwards

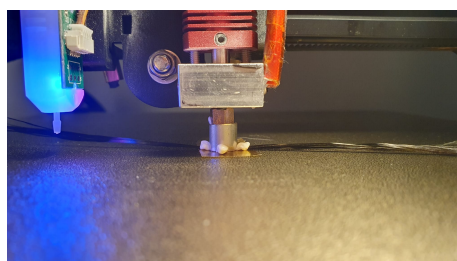
#### Step 4 After finishing remove the sample and clean off excess TP material.



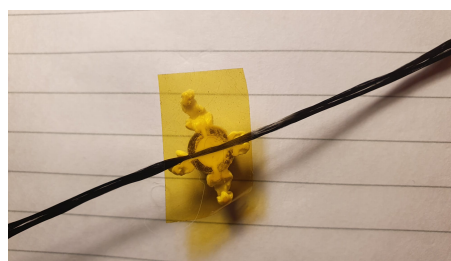
(a) Top view of sample



(b) Sample pressed down closing the mold



(c) Pressurization process



(d) Sample after pressurization

**Figure B.5:** Microscopic images of an CF bundle taken by Keyence®; (a) Full bundle section (M50x); (b) Single microfilament (M2000x); (c) Cutt CF (M2000x); (d) Straighten bundle of CF (Magnitude 50x)

## B.4. Keyence© VHX-6000 Digital microscope

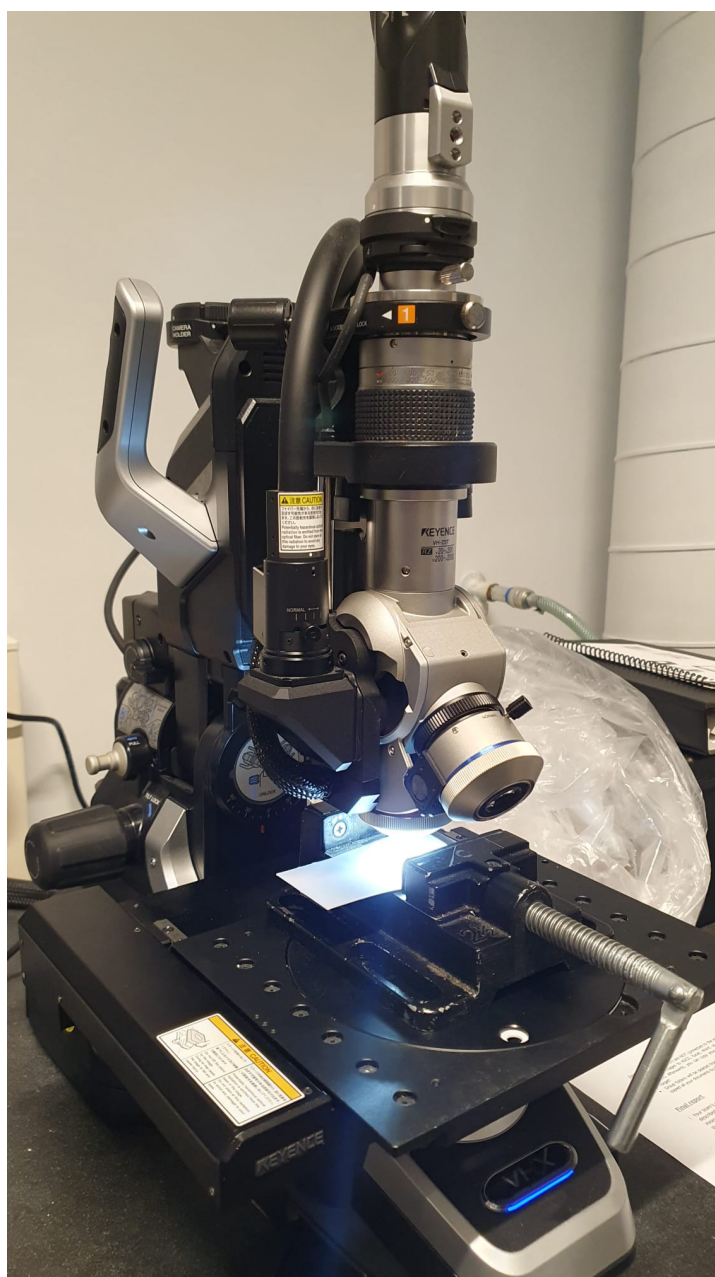


**Figure B.6:** The Keyence© VHX-6000 Digital microscope utilized for the melt impregnation analysis performed in chapter 4

### B.5. Tensile testbench

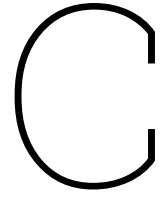


(a)



(b)

**Figure B.7:** (a) Tensile bench utilized for IFSS analysis (b) tensile bench including specially prepared L-shaped brackets utilized for IFSS experiments 1 & IFSS experiment 2



# Results

## C.1. Interfacial shear strength analysis

### C.1.1. Single fiber tensile test results

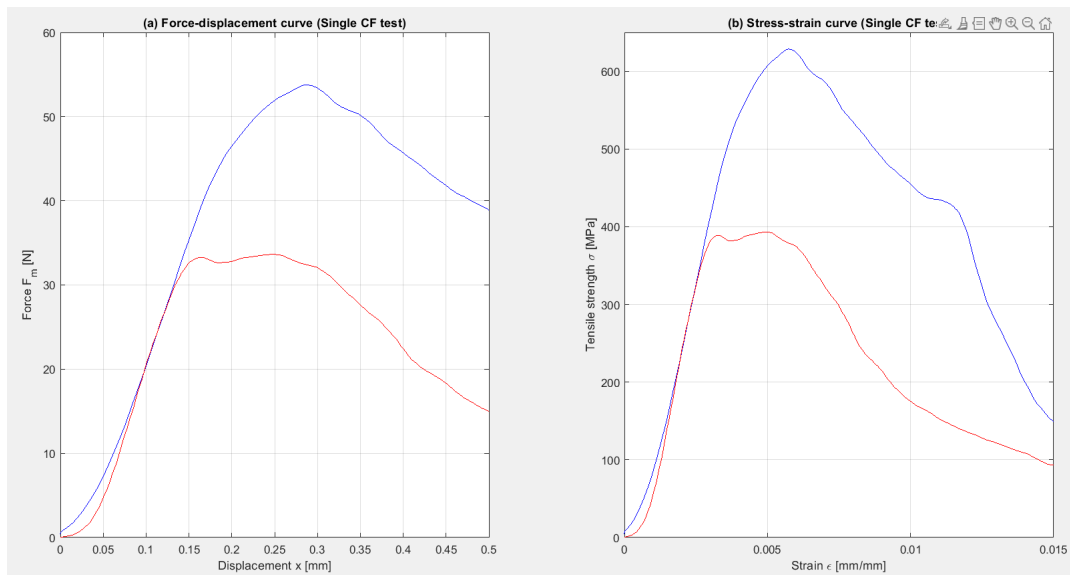


**Figure C.1:** Results from the tensile test performed by the testbench on single CF samples (a) Force-displacement curves (b) stress-strain curves

C.1.2. Neat thermoplastic tensile test results

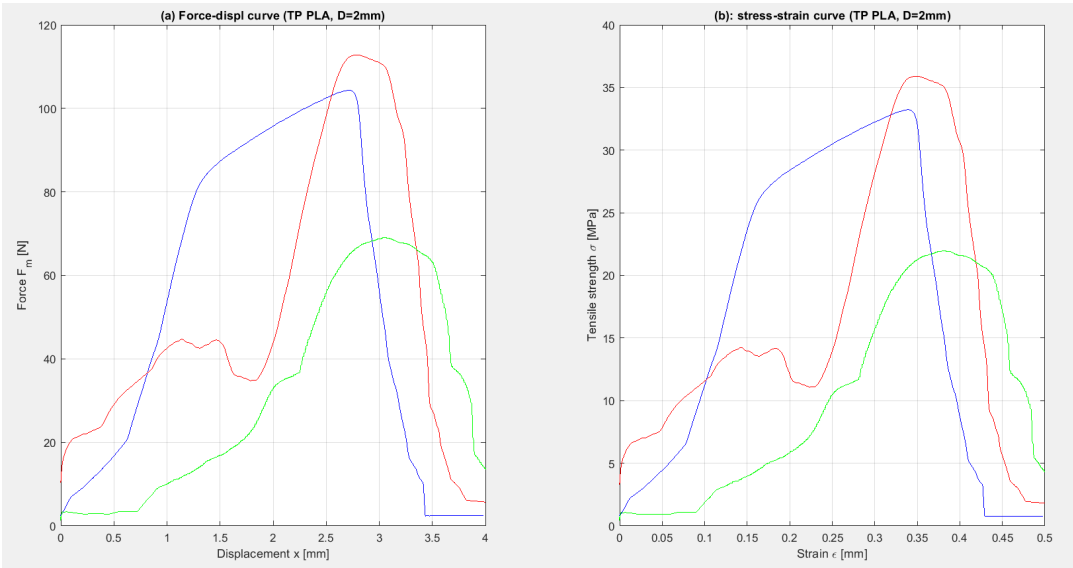


Figure C.2: Results from the tensile test performed by the testbench on neat Thermoplastic samples with an D = 2mm (a) Force-displacement curves (b) stress-strain curves



C.1.3. C-FRTP tensile test results (Experiment 1)

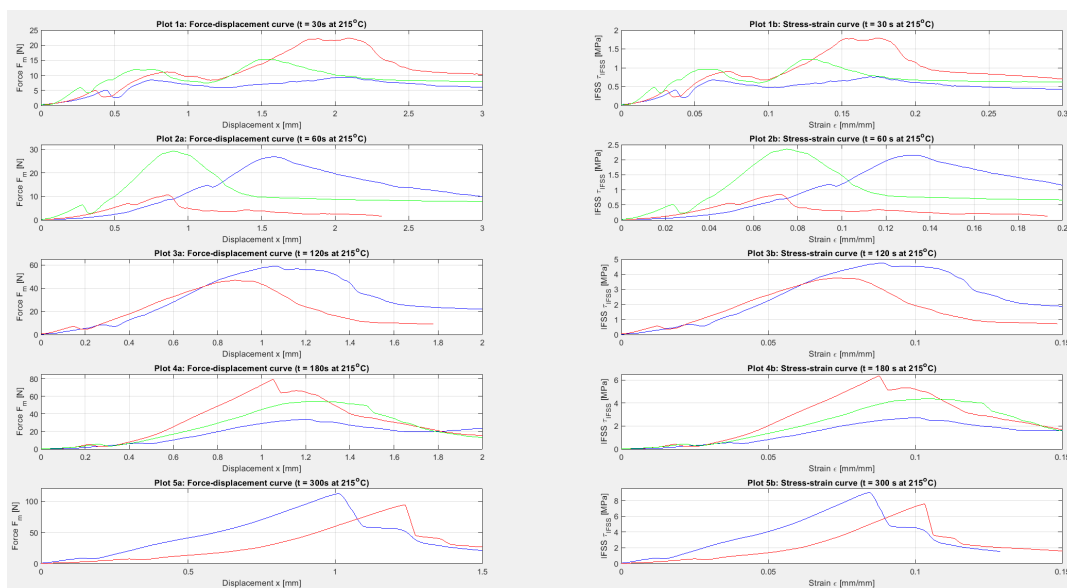


Figure C.3: Results from the tensile test (experiment 1) performed by the testbench on composite samples (a) Force-displacement curves (b) stress-strain curves

C.1.4. C-FRTP tensile test results (Experiment 2)

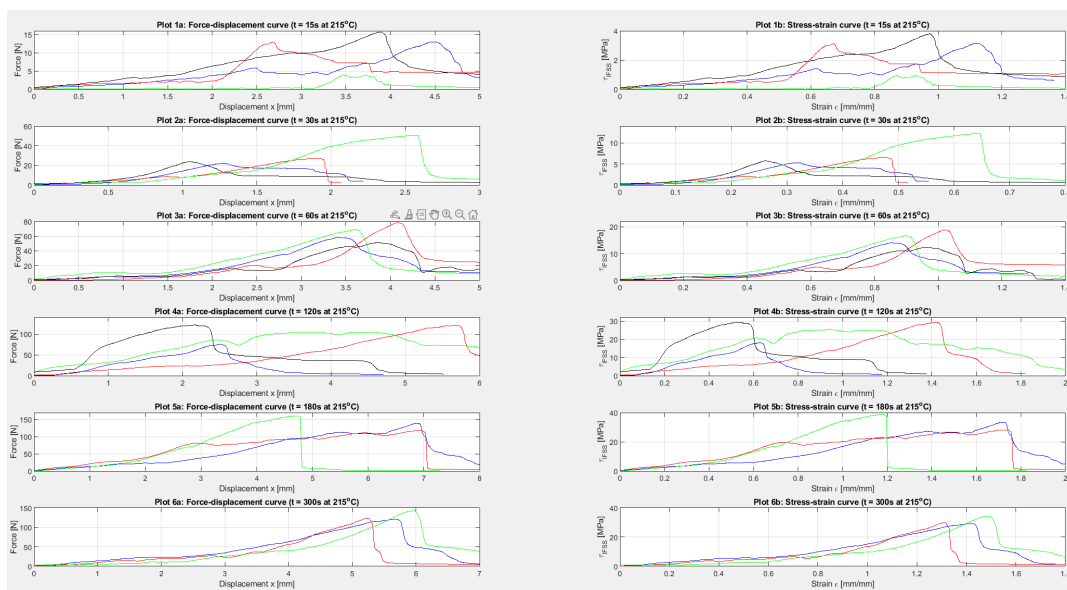


Figure C.4: Results from the tensile test (experiment 2) performed by the testbench on composite samples (a) Force-displacement curves (b) stress-strain curves

C.1.5. C-FRTP tensile test results (Experiment 3)

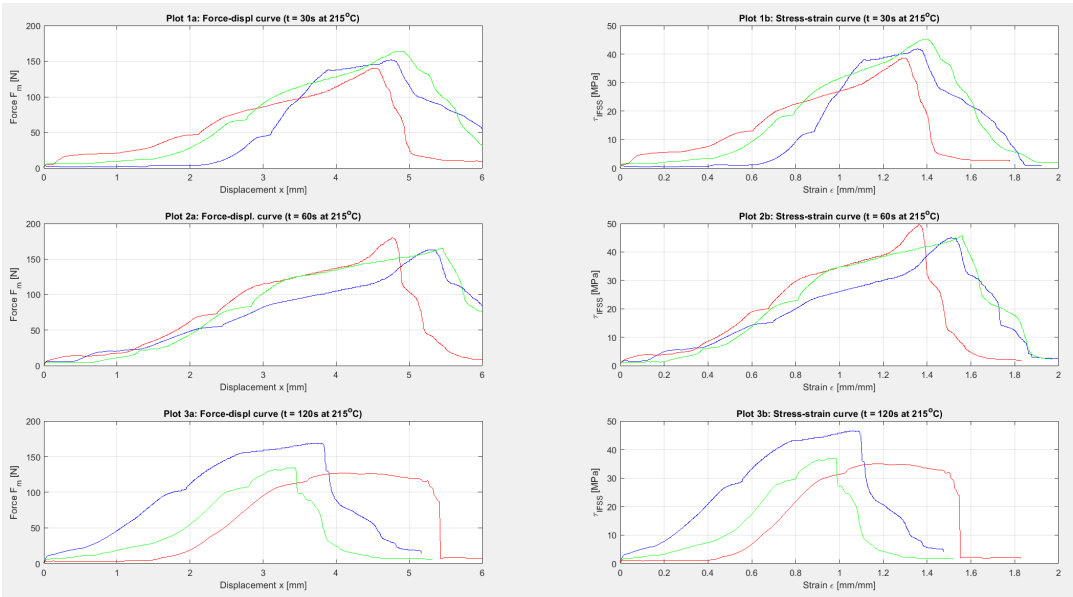


Figure C.5: Results from the tensile test (experiment 3) performed by the testbench on composite samples (a) Force-displacement curves (b) stress-strain curves